

USE OF SPATIALLY VARIABLE SUBGRADE MODULUS FOR IMPROVED
ACCURACY IN STRUCTURAL MODELING OF RAFT FOUNDATIONS

A THESIS SUBMITTED TO
THE GRADUATE SCHOOL OF NATURAL AND APPLIED SCIENCES
OF
MIDDLE EAST TECHNICAL UNIVERSITY

BY

GÖKHAN ÖZYURT

IN PARTIAL FULFILLMENT OF THE REQUIREMENTS
FOR
THE DEGREE OF DOCTOR OF PHILOSOPHY
IN
CIVIL ENGINEERING

JULY 2023

Approval of the thesis:

**USE OF SPATIALLY VARIABLE SUBGRADE MODULUS FOR
IMPROVED ACCURACY IN STRUCTURAL MODELING OF RAFT
FOUNDATIONS**

submitted by **GÖKHAN ÖZYURT** in partial fulfillment of the requirements for the degree of **Doctor of Philosophy in Civil Engineering, Middle East Technical University** by,

Prof. Dr. Halil Kalıpçılar
Dean, Graduate School of **Natural and Applied Sciences**

Prof. Dr. Erdem Canbay
Head of the Department, **Civil Engineering**

Assoc. Prof. Dr. Nabi Kartal Toker
Supervisor, **Civil Engineering, METU**

Examining Committee Members:

Prof. Dr. B. Sadık Bakır
Civil Engineering, METU

Assoc. Prof. Dr. Nabi Kartal Toker
Civil Engineering, METU

Prof. Dr. Erdal Çokça
Civil Engineering, METU

Asst. Prof. Dr. Salih Tileylioğlu
Civil Engineering, Kadir Has University

Assoc. Prof. Dr. Abdullah Sandıkkaya
Civil Engineering, Hacettepe University

Date: 26.07.2023

I hereby declare that all information in this document has been obtained and presented in accordance with academic rules and ethical conduct. I also declare that, as required by these rules and conduct, I have fully cited and referenced all material and results that are not original to this work.

Name, Last name: Gökhan Özyurt

Signature:

ABSTRACT

USE OF SPATIALLY VARIABLE SUBGRADE MODULUS FOR IMPROVED ACCURACY IN STRUCTURAL MODELING OF RAFT FOUNDATIONS

Özyurt, Gökhan

Doctor of Philosophy, Civil Engineering
Supervisor: Assoc. Prof. Dr. Nabi Kartal Toker

July 2023, 140 pages

While designing the foundations of buildings, soil-foundation interaction must also be considered, alongside the load distributions, sectional forces, and deformations in the soil layers due to the structural loads. In routine structural engineering practice, the Winkler (1867) spring idealization is commonly used to address this requirement. In the literature, although the simple Winkler method is distinctly asserted as insufficient in representing the contact pressure distribution beneath the foundation, in current commercial structural engineering software programs, Winkler models are frequently used for simulating soil behavior. PLAXIS 2D/3D and SAP2000, commonly used commercial software in geotechnical and structural analysis applications, are used to carry out a series of analyses for several cases to examine the behavior of shallow raft foundations on dry sands under static loading and thus, obtain more accurate distributions of subgrade modulus. The variables considered in the analyses are foundation thickness, structure width, soil stiffness, number of stories, and column positions. Distributions of subgrade modulus that accurately correspond to the PLAXIS results of bending moment and settlement are obtained through iterative processes conducted on springs in SAP2000. After all, relations are

proposed to comprehensively account for all parameters that significantly influence the distributions of subgrade modulus. Additionally, 3-D parametric studies are conducted to illustrate the extrapolation of findings from two-dimensional assessments to three-dimensional scenarios. The results indicate that the distribution of subgrade modulus significantly impacts the analysis of raft foundations. The findings provide insights into the usage of subgrade modulus and inform the design and optimization of foundation systems.

Keywords: Subgrade Modulus, Winkler Springs, Dry Sand, Soil-Structure Interaction, SAP2000 Spring Constant

ÖZ

KONUMSAL OLARAK DEĞİŞKEN YATAK KATSAYISININ RADYE TEMELLERİN YAPISAL TASARIMINDA İYİLEŞTİRİLMİŞ KULLANIMI

Özyurt, Gökhan
Doktora, İnşaat Mühendisliği
Tez Yöneticisi: Doç. Dr. Nabi Kartal Toker

Temmuz 2023, 140 sayfa

Bina temelleri tasarlanırken, yük dağılımları, kesit kuvvetleri ve yapısal yükler nedeniyle zemin tabakalarında meydana gelen deformasyonların yanı sıra zemin-temel etkileşimi de dikkate alınmalıdır. Rutin yapı mühendisliği uygulamalarında, bu gereksinimi karşılamak için Winkler (1867) yay idealizasyonu yaygın olarak kullanılmaktadır. Literatürde, basit Winkler yönteminin temel altındaki temas basıncı dağılımını temsil etmekte yetersiz olduğu açıkça öne sürülse de mevcut ticari yapı mühendisliği yazılım programlarında, Winkler modelleri hala zemin davranışını simüle etmek için sıklıkla kullanılmaktadır. Geoteknik ve yapısal analiz uygulamalarında yaygın olarak kullanılan PLAXIS 2D/3D ve SAP2000 programları, kuru kum üzerindeki sığ radye temellerin statik yükleme altındaki davranışlarını ve böylelikle temel altındaki yatak katsayısı dağılımını daha doğru bir şekilde elde etmek için farklı durumları içeren bir dizi analizi gerçekleştirmek üzere kullanılmıştır. Analizlerde dikkate alınan değişkenler, temel kalınlığı, yapı genişliği, zemin sertliği, kat sayısı ve kolon konumlarıdır. SAP2000'de yaylar üzerinde gerçekleştirilen iteratif süreçlerle, eğilme momenti ve oturmanın PLAXIS sonuçlarına tam olarak karşılık geldiği yatak katsayısı dağılımları elde edilmiştir.

Sonuçta, yatak katsayısı dağılımını önemli ölçüde etkileyen tüm parametreleri kapsayan ilişkiler önerilmiştir. Ek olarak, iki boyutlu değerlendirmelerden elde edilen sonuçların üç boyutlu senaryolarda nasıl sonuçlar ortaya koyacağını göstermek için 3 boyutlu parametrik çalışmalar da yürütülmüştür. Sonuçlar, yatak katsayısı dağılımının radye temellerinin analizini önemli ölçüde etkilediğini göstermektedir. Elde edilen bulgular ışığında bu çalışma, yatak katsayısının kullanımına ilişkin yeni öneriler getirerek sığ temel sistemlerinin güvenli ve ekonomik olarak tasarlanmasına katkı sağlamaktadır.

Anahtar Kelimeler: Yatak Katsayısı, Winkler Yayları, Kuru Kum, Zemin-Yapı Etkileşimi, SAP2000 Yay Sabiti

To My Family

ACKNOWLEDGMENTS

The author wishes to express his deepest gratitude to his supervisor Dr. N. Kartal Toker, for his theoretical support, guidance, criticism, and encouragement throughout all stages of the study.

The author also wishes to express his special thanks to thesis monitoring committee members Prof. Dr. B. Sadık Bakır and Dr. Salih Tileyliođlu for their valuable advices and guidance from the beginning of this research.

The author expresses sincere gratitude to his family for providing unwavering support and encouragement throughout his academic journey. The unwavering love and faith shown by the family have been pivotal in motivating and guiding the author towards the successful completion of this thesis.

The author would like to express his gratitude to all former colleagues from the company who played a role in the initiation of this endeavor.

The author also acknowledges the invaluable support of close friends, namely Ezgi Yıldırım, Y. Tolga Mutlu and Ođuz Palabıyık. Their encouragement and companionship have been cherished throughout this academic endeavor. Additionally, special gratitude is extended to Seđkin Aydın for his assistance and guidance in the utilization of software tools.

Finally, the author wishes to extend a heartfelt paragraph of appreciation to Z. Gzde Kara, a true-life friend. Her unwavering support, genuine friendship, and shared experiences have illuminated this academic journey. Her role as a cherished has enriched not only the study but also the author's life as a whole.

TABLE OF CONTENTS

| | |
|--|-----|
| ABSTRACT..... | v |
| ÖZ | vii |
| ACKNOWLEDGMENTS | x |
| TABLE OF CONTENTS..... | xi |
| LIST OF TABLES | xiv |
| LIST OF FIGURES | xv |
| LIST OF ABBREVIATIONS | xix |
| LIST OF SYMBOLS | xx |
| CHAPTERS | |
| 1 INTRODUCTION | 1 |
| 1.1 Research Motivation | 3 |
| 1.2 Purpose and Scope | 5 |
| 1.3 Outline..... | 7 |
| 2 LITERATURE REVIEW | 9 |
| 2.1 Rigid Method..... | 9 |
| 2.2 Non-Rigid Method | 11 |
| 2.2.1 Subgrade Modulus & Basic Winkler Model..... | 12 |
| 2.2.2 Coupled Method..... | 16 |
| 2.2.3 Pseudo-Coupled Method..... | 17 |
| 2.2.4 Multiple-Parameter Methods | 19 |
| 2.3 Finite Element Method (FEM)..... | 22 |
| 2.3.1 Soil-Structure Interaction (SSI) Modeling..... | 24 |

| | | |
|-------|---|-----|
| 2.3.2 | SAP2000..... | 27 |
| 2.3.3 | PLAXIS 2D/3D | 27 |
| 2.3.4 | Common Material Models..... | 30 |
| 2.3.5 | Choice of the Constitutive Model..... | 31 |
| 3 | METHODOLOGY | 33 |
| 3.1 | Effects of Foundation Thickness | 36 |
| 3.2 | Effects of Staged Construction | 41 |
| 3.3 | Effects of Number of Stories | 44 |
| 3.4 | Effects of Foundation (Structure) Width | 47 |
| 3.5 | Effects of Soil Stiffness | 51 |
| 3.6 | Effects of Relative Stiffness of the Soil-Raft System..... | 53 |
| 3.7 | Replacement of Superstructure with a Thicker Foundation | 57 |
| 3.8 | The Case of Structure Width Less Than Foundation Width..... | 59 |
| 3.9 | Effects of Column (Loading) Positions | 62 |
| 4 | RELATIONSHIP BETWEEN SPRING CONSTANTS AND PROBLEM VARIABLES..... | 67 |
| 4.1 | Correlating the Subgrade Modulus Distribution to Problem Parameters . | 67 |
| 4.2 | Proposed Methodology | 75 |
| 4.3 | Validation and Comparative Analysis of Proposed Approach | 76 |
| 5 | EXPLORING 3-D TRIALS: EXAMPLE ANALYSES | 81 |
| 6 | CONCLUSION | 97 |
| 6.1 | Summary of Work | 97 |
| 6.2 | Conclusions..... | 98 |
| 6.3 | Recommendations for Future Researches..... | 100 |

| | |
|---|-----|
| REFERENCES | 103 |
| APPENDICES | |
| A. Material Properties of the Structural Concrete Elements (rafts, columns, beams) for PLAXIS 2D and SAP2000 | 107 |
| B. Single Thicker Foundation Calculations for Superstructure Replacement | 108 |
| C. Summary of Analyses | 110 |
| D. Spring Constant Distribution Results for 53 Analyses - Including Iteration (Continuum), Excel Solver Findings, and Proposed Relations..... | 115 |
| E. Views of Excel Program for Spring Constant Analysis..... | 133 |
| CURRICULUM VITAE | 139 |

LIST OF TABLES

TABLES

| | |
|--|----|
| Table 2.1 Range of modulus of subgrade reaction (Bowles, 1996) | 16 |
| Table 2.2 Compiling of multi-parameter models | 22 |
| Table 5.1 Comparison of settlement and moment results of the first trial 3D analysis | 89 |
| Table 5.2 Comparison of settlement and moment results of the second trial 3D analysis | 96 |

LIST OF FIGURES

FIGURES

| | |
|---|----|
| Figure 1.1 Soil pressure distribution in the rigid and flexible methods of analysis. (a) Rigid foundation. (b) Flexible foundation..... | 2 |
| Figure 2.1 Assumed subgrade reaction in the rigid body method | 10 |
| Figure 2.2 Computational model of the Winkler spring analysis approach | 14 |
| Figure 2.3 The non-linear σ - δ relationship and idealized k_s linear function..... | 14 |
| Figure 2.4 Modeling of soil-structure interaction using coupled springs | 17 |
| Figure 2.5 Division of mat into zones with the different modulus of subgrade reaction values for pseudo-coupled analysis..... | 18 |
| Figure 2.6 Surface displacement profiles of Filonenko-Borodich model (1940): (a) basic model, (b) concentrated load, (c) rigid load, and (d) uniform flexible load .. | 20 |
| Figure 2.7 Visualization of Kerr model (1964)..... | 21 |
| Figure 2.8 Typical Mat Foundation Problem..... | 24 |
| Figure 2.9 'Structural' component analysis | 25 |
| Figure 2.10 Problem Components: 'Ideal' Analysis..... | 26 |
| Figure 2.11 Example of PLAXIS 2D problems: a) plane strain, and b) axisymmetric (PLAXIS, 2011) | 28 |
| Figure 2.12 (a) 15-node and 12-stress point soil element in PLAXIS 2D, (b) 6-node and 3-stress point soil element in PLAXIS 2D, (c) Typical 3D soil element (10- node tetrahedron with 4 stress points) in PLAXIS 3D..... | 29 |
| Figure 3.1 Geometry and boundary conditions in PLAXIS 2D models | 34 |
| Figure 3.2 An example structural view of the 2-dimensional analysis (a) PLAXIS 2D v-8.6 (b) SAP2000 v-21.1. | 35 |
| Figure 3.3 General appearance of the PLAXIS 2D model for the 'Effects of Foundation Thickness' case..... | 37 |
| Figure 3.4 Comparison of (a) settlement and (b) bending moment results of 0.5 m thick and 2.0 m thick rafts..... | 38 |

| | |
|---|----|
| Figure 3.5 Comparison of (a) settlement, (b) bending moment, and (c) shear force results obtained from PLAXIS 2D and SAP2000 software for the 2.0 m raft thickness case | 39 |
| Figure 3.6 Distribution of spring constant values for 0.5 m and 2.0 m thick rafts.. | 40 |
| Figure 3.7 General model views of the two 'Staged Construction' cases in PLAXIS: (a) four-story five-span model and (b) five-story four-span model | 41 |
| Figure 3.8 Settlement and bending moment results of the foundations for the staged construction method and the linear static normal (non-staged) method..... | 42 |
| Figure 3.9 Distribution of spring constant values for the staged and non-staged analyses (a) Four-Story, (b) Five-Story | 43 |
| Figure 3.10 Bending moment diagrams of the first-floor slab at the end of the second stage and the fifth-floor slab at the end of the sixth stage..... | 44 |
| Figure 3.11 SAP2000 appearance of the 16-Story Structure - Final Case | 45 |
| Figure 3.12 Representation of spring constant distributions for the 'Increasing Number of Stories' case | 46 |
| Figure 3.13 Superimposed appearance of spring constant distributions for the 'Increasing Number of Stories' case..... | 46 |
| Figure 3.14 General appearance of the first and second PLAXIS 2D models used for the 'Increasing Foundation (Structure) Width' case | 48 |
| Figure 3.15 Settlement and bending moment results of the foundations for the 'Increasing Foundation (Structure) Width' case..... | 49 |
| Figure 3.16 Representation of spring constant distributions for the 'Increasing Structure Width' case on a single graph | 50 |
| Figure 3.17 General appearance of the first PLAXIS 2D model used for the 'Increasing Soil Stiffness' case..... | 51 |
| Figure 3.18 Representation of spring constant distributions for the 'Increasing Soil Stiffness' case on a single graph | 52 |
| Figure 3.19 Superimposed view of spring constant distributions of the 'Increasing Soil Stiffness' case | 53 |

| | |
|---|----|
| Figure 3.20 General view and properties of the models for the 'Relative Stiffness Changes in Soil-Raft System' case..... | 54 |
| Figure 3.21 Settlement, bending moment, and the linked spring constant distribution results for the 'Stiffness Changes in Soil-Raft System' case | 55 |
| Figure 3.22 Scaled appearance of superimposed spring constant distributions of 'Relative Stiffness Changes in Soil-Raft System' case..... | 56 |
| Figure 3.23 General appearance of the five-story four-span and four-story five-span superstructure models, as well as their replacement with thicker foundations..... | 58 |
| Figure 3.24 Distribution of spring constant values for the 'Superstructure Rigidity Reflected by a Single Thicker Foundation' case | 59 |
| Figure 3.25 General view of the first, second, fourth, and seventh models for the 'Structure Width Less Than Foundation Width' case..... | 60 |
| Figure 3.26 Superimposed appearance of settlement and spring constant distributions of the models for the 'Structure Width Less Than Foundation Width' case..... | 62 |
| Figure 3.27 General appearance of the two PLAXIS 2D models used for the 'Column (Loading) Positions' case..... | 63 |
| Figure 3.28 Settlement, bending moment diagrams, and variation of spring constant distributions according to column positions | 64 |
| Figure 3.29 Sample view of the resultant force positions of the column loads acting on the foundation | 66 |
| Figure 4.1 Functional representation of the distribution of spring constants | 68 |
| Figure 4.2 Scatter plot of calculated and grouped coefficient 'a' values versus relative rigidity | 72 |
| Figure 4.3 Scatter plot of quadratic function length versus foundation width..... | 73 |
| Figure 4.4 Scatter plot of the ratio of spring coefficient values at the points; end of quadratic function and edge of the foundation versus relative rigidity..... | 74 |
| Figure 4.5 Spring constant distribution of different approaches and the corresponding settlement and bending moment results (Analysis No: 49) | 78 |

| | |
|---|----|
| Figure 4.6 Spring constant distribution of different approaches and the corresponding settlement and bending moment results (Analysis No: 40)..... | 80 |
| Figure 5.1 General view of the first trial 3D analysis | 82 |
| Figure 5.2 Spring coefficient distribution calculated for the first trial 3D analysis | 83 |
| Figure 5.3 Settlement results of the first trial 3D analysis; (a) PLAXIS 3D, (b) Proposed approach, (c) Constant spring approach | 85 |
| Figure 5.4 First 3-D analysis bending moment results; comparison in x-direction: (a) PLAXIS 3D, (b) Proposed approach, (c) Constant spring approach | 86 |
| Figure 5.5 First 3-D analysis bending moment results; comparison in y-direction: (a) PLAXIS 3D, (b) Proposed approach, (c) Constant spring approach | 87 |
| Figure 5.6 General view of the second trial 3D analysis..... | 90 |
| Figure 5.7 Spring coefficient distribution calculated for the second trial 3D analysis | 90 |
| Figure 5.8 Settlement results of the second trial 3D analysis; (a) PLAXIS 3D, (b) Proposed approach, (c) Constant spring approach | 93 |
| Figure 5.9 Second 3-D analysis bending moment results; comparison in x-direction: (a) PLAXIS 3D, (b) Proposed approach, (c) Constant spring approach. | 94 |
| Figure 5.10 Second 3-D analysis bending moment results; comparison in y-direction: (a) PLAXIS 3D, (b) Proposed approach, (c) Constant spring approach. | 95 |

LIST OF ABBREVIATIONS

ABBREVIATIONS

| | |
|----------|---|
| 2D | Two-dimensional |
| 3D | Three-dimensional |
| ACI | American Concrete Institute |
| CSI | Computers and Structures, Inc. |
| DIN | Deutsches Institut für Normung (German Institute for Standardization) |
| ECP | Egyptian Code of Practice |
| EI | Flexural rigidity |
| FEM | Finite Element Method |
| LCR | Load Concentration Ratio |
| MS | Microsoft |
| MS Excel | Microsoft Excel |
| MPa | Megapascal |
| PLAXIS | Geotechnical analysis software program |
| RR | Relative Rigidity |
| SAP2000 | Structural Analysis Program 2000 |
| SSI | Soil-Structure Interaction |
| SPT | Standard Penetration Test |

LIST OF SYMBOLS

SYMBOLS

| | |
|-----------------------|---|
| B | Width of foundation |
| E_b | Young modulus of foundation material |
| E_{50}^{Ref} | Secant stiffness of the supporting soil |
| E_{oed} | Oedometer loading stiffness |
| E_s | Young modulus of soil |
| E_{ur} | Triaxial unloading stiffness |
| γ | Unit weight of soil |
| k_s | Modulus of subgrade reaction |
| L | Length of foundation |
| R_{inter} | Interface strength reduction factor |
| c | Cohesion of soil |
| δ | Displacement or deformation |
| ν | Poisson's ratio of soil |
| σ | Normal stress |
| τ | Shear stress |
| ϕ | Angle of internal friction |

CHAPTER 1

INTRODUCTION

A mat foundation, also known as a raft, is a type of shallow foundation consisting of a relatively thick slab that rests on a large area of soil. It is designed to support and transfer loads from the structure to the underlying soil. Mat foundations are commonly used when shallow soil layers have low bearing capacity, as they act as a single foundation element and distribute the loads from the superstructure over a larger area. This helps to reduce differential and total settlements and provides a cost-effective and watertight solution. However, like any shallow foundation, a mat foundation needs to be evaluated for excessive settlements and bearing capacity failure. It also requires a structural design to resist the bending and shear forces caused by differential settlements in the soil. From a structural perspective, the soil-bearing pressure influences the distribution of internal bending moments and shear forces within the mat. Therefore, soil-foundation interaction, one of the challenging problems in civil engineering, has a critical role in foundation analysis and design.

Several methods have been proposed in the literature for analyzing mat foundations, which can be categorized into two main approaches: the rigid method (1) and the flexible method (2). In the rigid method, the mat is assumed to behave as an infinitely rigid plate; hence, the contact pressure has a planar distribution under the mat, as shown in Figure 1(a). Because the rigid method does not consider this redistribution of bearing pressure, it does not produce reliable estimates of the shears, moments, and deformations in the mat. While the rigid mat method is simple to use, experience has shown that it often overestimates both the mat thickness and the steel reinforcement (Bowles, 1997).

In the flexible mat method, the foundation is assumed to be non-rigid, and soil behavior is incorporated into the model, resulting in a non-linear distribution of soil-

bearing pressure underneath the foundation, as shown in Figure 1(b). Flexible methods produce more accurate foundation deformations and stress values. Unfortunately, non-rigid analyses are also more challenging to implement because they require consideration of soil-structure interaction (SSI), and the bearing pressure distribution is not as simple (Coduto, 2001). Various non-rigid methods are available for the structural analysis of mat foundations, ranging from the classical Winkler (1867) approach to elaborate three-dimensional finite element analysis. The most common method in current design practice is the Winkler spring approach, in which the soil is represented as independent elastic vertical springs supporting the mat. Despite being a rather rough idealization of reality and the emergence of more accurate methods, the Winkler spring approach still constitutes the state of practice because it can be easily applied in most commercial structural analysis computer programs.

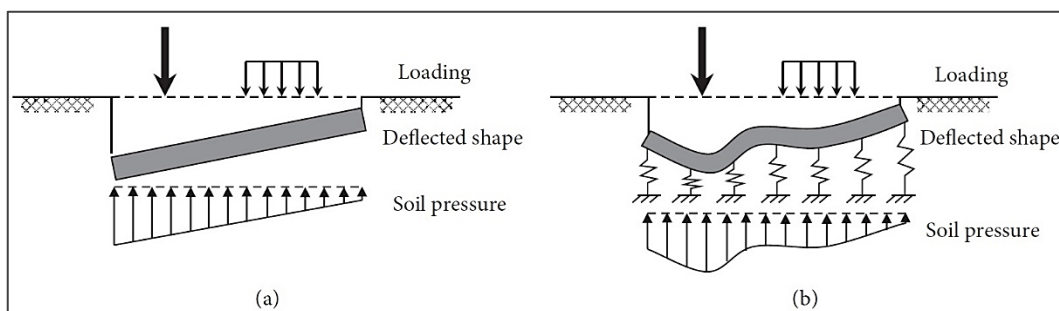


Figure 1.1 Soil pressure distribution in the rigid and flexible methods of analysis.

(a) Rigid foundation. (b) Flexible foundation.

Many studies have pointed out the shortcomings of the original basic Winkler spring approach, which assumes that the modulus of subgrade reaction has the same value everywhere under the mat, and have proposed alternative methods of various degrees of complexity (e.g., pseudo-coupled, multiple-parameter). In recent years, the finite element method is usually employed as a tool to execute the solution of the flexible raft approach. In this method, the mat is modeled by subdividing the concrete slab into small rectangular or triangular plate or shell elements. The soil behavior is tried

to be represented simply by springs lumped (Winkler model) at the nodes (in structural analysis programs) or by half-space medium (continuum model) (in geotechnical analysis programs).

Ideally, foundation design should account for soil stiffness, mat stiffness, and their interaction by selecting the appropriate subgrade modulus value. In addition to the need for correctly evaluating soil-mat interaction, it is also necessary to consider how the superstructure affects this interaction. Especially in recent decades, computer power has increased by orders of magnitude. However, this interdisciplinary soil-mat-superstructure relationship could not be fully and properly integrated into commercial analysis programs, and yet there is still an unfortunate but widespread persistence with the Winkler spring concept because of its convenience and simplicity. The price of this simplicity is high, given the potential for unreliable and unrealistic results and the enduring problem of assessing an appropriate modulus of subgrade reaction (Poulos, 2000).

1.1 Research Motivation

The subgrade modulus is a stiffness parameter typically used in defining the support conditions of mat foundations and can be described as a bridge between geotechnical and structural engineers if it is necessary to make an analogy. Physically, it is defined as the contact pressure of the foundation against the soil that causes unit deformation of the foundation. In practice, the parameter is often recommended by the geotechnical engineer and used by the structural engineer to analyze the structure. Unfortunately, as a parameter that spans the geotechnical and structural realms, the subgrade modulus has been misused and abused in practice to a point where engineers tend to forget the physical meaning and implications of using the parameter (Aristorenas & Gómez, 2014).

In the design of structures, it is common to find structural engineers who are uncertain about the form of subgrade modulus values provided by the geotechnical engineer and likewise, common to find geotechnical engineers who are uncertain about how subgrade modulus values are being applied by the structural designers (French et al., 2006). In addition, some engineers are unclear about using these values in developing foundation springs in most structural design methods, as implemented through packaged structural engineering computer software. In light of this widespread lack of understanding, it is fortunate that most simple designs are relatively insensitive to the value of the subgrade modulus.

Hence, there is a need to clarify for geotechnical engineers how their subgrade modulus value recommendations will be utilized in structural design methodologies. Simultaneously, the study aims to clarify the intent of subgrade modulus recommendations for structural engineers and present the distribution of spring coefficient values beneath the mat.

Moreover, the utilization of a constant spring or the pseudo-coupled approach is widespread in the current landscape of engineering practice. This tendency is rooted in the convenience of rapid analysis, as such approaches are often encoded into structural analysis software programs. As a result, the application of a constant spring or the pseudo-coupled methods has become the go-to approach almost for every project, enabling swift analyses. However, the potential hazards inherent in these approaches have motivated the exploration of a more nuanced perspective. Recognizing the inherent risks associated with such widespread practices and aiming to offer a sound analytical methodology, this study delves into the subject matter to shed light on the dangers associated with prevalent practices and to provide a viable and accurate analysis approach.

1.2 Purpose and Scope

Soil-structure interaction is a very broad subject and cannot practically be covered by a single study. Therefore, this study is intended to be one of the several that discusses various aspects of SSI.

The research objectives of this study can be summarized as follows:

- Obtaining more insight into the interaction between shallow raft foundations and soil.
- Discussing the wide range of SSI applications to illustrate where various subgrade models have been or might be used.
- Investigating the influence of different parameters on the subgrade modulus and its impact on foundation stresses and deformations.
- Exploring an optimal approach for geotechnical and structural engineers to design safe, reliable, and cost-effective foundation structures within a project framework.

As a result of these objectives, this study aims to identify the spatial distribution of spring coefficient values under a raft foundation that would help obtain the best possible accuracy regarding settlement and bending moments with a quick and straightforward analysis method. In the first step, this is accomplished by performing a series of 2D finite element analyses using the two common finite element software, PLAXIS 2D and SAP2000. The PLAXIS models have been expanded to incorporate the superstructure along with the conventional soil continuum, providing a comprehensive representation of the problem. This expansion assumes the validity of the chosen non-linear soil model and linearly elastic structural elements, allowing for an accurate depiction of the system's behavior.

Distributions of subgrade modulus beneath the mats are determined by making iterative processes between PLAXIS 2D and SAP2000. The iteration process in the spring coefficient values in SAP2000 is continued until the same settlement and

bending moment values found in the PLAXIS analyses are obtained. The resulting spring value distributions beneath the mats are then grouped, evaluated, and relations for possible spring value distributions for different cases are proposed. Studies are conducted on non-cohesive soils by changing soil properties, foundation and structure (building) dimensions, and loading conditions in different combinations.

Furthermore, two three-dimensional analyses are conducted to compare the performance of the proposed relations for calculating equivalent spring stiffness values at any point of a rectangular mat foundation with existing approaches. The results of this study and the proposed relationships can be used in the future as a basis for developing more rigorous subgrade modulus distributions that consider the complex soil-foundation-structure interaction behavior.

It is important to note that this study is explicitly focused on dry sands, a vital detail that refines the scope of this investigation. This strategic focus on dry sands allows for more targeted and relevant conclusions. This decision to concentrate on dry sands is driven by a combination of practical relevance, unique geotechnical characteristics, and the desire to provide specialized insights that can inform engineering practices in scenarios involving this specific soil type.

In contrast, other soil types, particularly those influenced by factors such as varying moisture conditions and water levels, introduce a multitude of uncertainties that can significantly complicate the analysis and design of foundation systems. The deliberate focus on dry sands in this study provides a controlled and targeted environment for a systematic investigation into the interaction between foundations and this specific soil type.

1.3 Outline

After this introduction of Chapter 1, in Chapter 2, information in the existing literature, methods used for foundation design, and approaches used to simulate soil behavior are reviewed. In Chapter 3, detailed information about PLAXIS 2D and SAP2000 analyses performed within the scope of this thesis study is presented. In addition, the evaluations of the variables considered and applied in the analyses are explained individually. In the fourth chapter, explanations are made about the inferences reached as a result of these analyses and the methods of their use. How the methodology proposed for 2D analyses produce results in 3-dimensional problems are presented with examples in Chapter 5. These examples also include the methods used in current commercial structural analysis software and comparatively present the results. In Chapter 6, comments and conclusions are presented as the final stage. Additionally, recommendations and solutions to various issues about designing foundations are presented to help geotechnical and structural engineers avoid frequent problems.

CHAPTER 2

LITERATURE REVIEW

Mat foundation, or radier, as it is called in the Turkish engineering community with its French name, is a large, composite shallow foundation that interacts with the ground like a slab it sits on or in. It is a heavily steel-reinforced flat concrete slab that bears the moments and shear forces of the individual columns and walls and transfers the upper loads to the underlying soil. A raft foundation may be used where the sub-soil has a low bearing capacity and/or the column loads are so large that conventional spread footings cover more than 50 percent of the area. The resulting mat load per unit area is small in magnitude and is distributed over the entire area, tending to reduce the differential settlement.

The general approach to designing an adequate foundation structure is to create a model that accurately represents reality. Extensive research has been conducted and published over the past decades. Different analysis methods have been developed to design raft foundations, ranging from conventional manual calculation methods to most modern computer-based methods. These methods can broadly be categorized into two main groups: the rigid method and the non-rigid methods.

2.1 Rigid Method

The simplest approach to the structural design of foundations is the rigid method (also known as the conventional method) (Teng, 1962). This method assumes that the foundation is much more rigid than the underlying soils, meaning that any distortions in the foundation are too small to significantly affect the distribution of bearing pressure. Consequently, the magnitude and distribution of bearing pressure depend solely on the applied loads and the weight of the foundation. The bearing

pressure is either uniform across the bottom of the foundation (if the normal load acts through the centroid and no moment load is present) or varies linearly across the foundation (if eccentric or moment loads are present) (Figure 2.1).

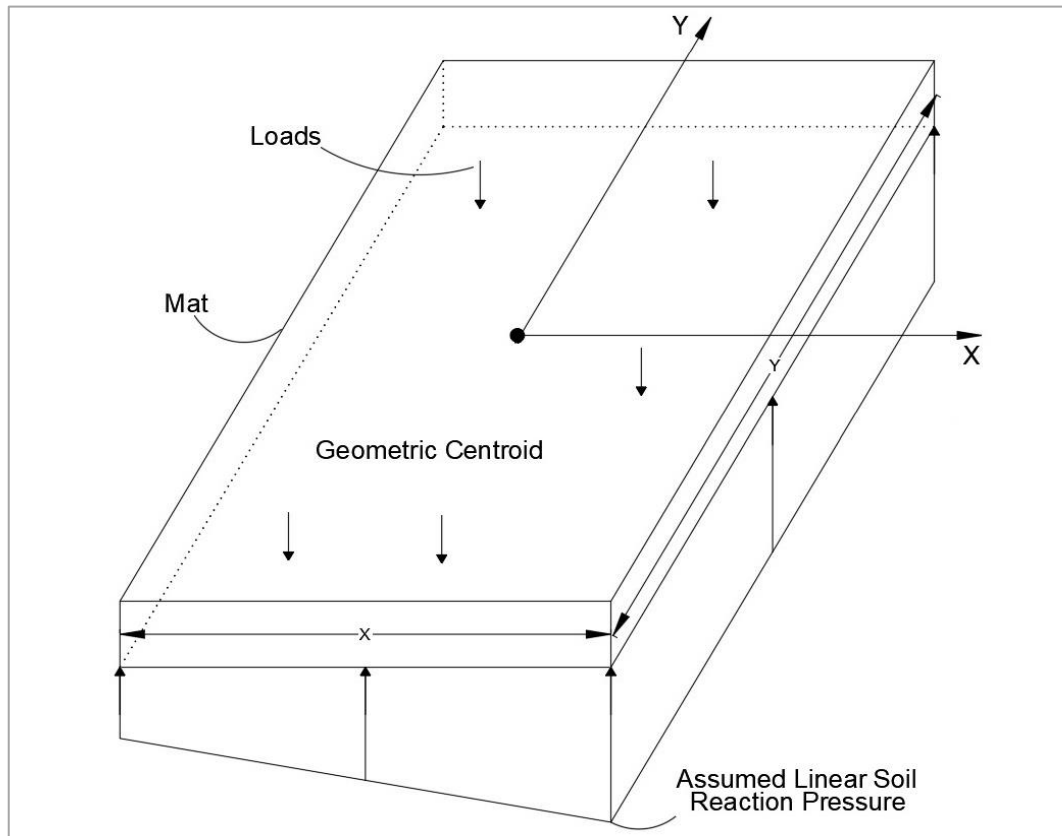


Figure 2.1 Assumed subgrade reaction in the rigid body method

Equation 2.1 provides the subgrade reaction pressure at any location along the mat's base. The mat is divided into strips after determining the response pressure, and the shear forces and bending moments are calculated for each strip using the fundamentals of statics.

$$\sigma_i = \frac{F_v}{xy} \pm \frac{M_x y_i}{I_x} \pm \frac{M_y x_i}{I_y} \quad (2.1)$$

where:

σ_i is the reaction pressure,

F_v is the total vertical loads on the mat,

x and y are the length and width of the mat, respectively,

M_x and M_y are the moments about the x and y axes, respectively, induced by the resultant load eccentricities,

I_x and I_y are the moments of inertia about the x and y axes, respectively, and

x_i and y_i are the distances to a point (i).

This simple distribution makes it easy to compute the flexural stresses and deflections (differential settlements) in the foundation. While this type of analysis is appropriate for pad footings, it is not convenient for mat foundations because in mat foundations width-to-thickness ratio is high, and the stiffness assumption considered in footings is no longer valid. The portions under the columns or the load-bearing walls settle more with respect to the unloaded sections, meaning higher bearing pressure values are observed under heavily loaded areas. Since the rigid method does not account for this redistribution of bearing pressure, it does not reliably estimate moments, shear forces, and settlements in the raft.

2.2 Non-Rigid Method

In order to overcome the inaccuracies of the rigid method, analysis that considers deformations in the foundation and their influence on the bearing pressure distribution is used. These are called non-rigid methods and produce more accurate values of foundation deformations and stresses. Unfortunately, non-rigid analyses are also more challenging to implement because they require consideration of soil-structure interaction (SSI), and the bearing pressure distribution is not as simple (Coduto, 2001).

2.2.1 Subgrade Modulus & Basic Winkler Model

Because non-rigid methods consider the effects of local deformations on the distribution of bearing pressure, it is necessary to define the relationship between settlement and bearing pressure. This is usually done by using the subgrade modulus, k_s (also known as the coefficient of subgrade reaction):

$$k_s = \frac{\sigma}{\delta} \quad (2.2)$$

where σ is the foundation pressure exerted on the soil, and δ is the resulting settlement.

It is simply the ratio of the applied vertical normal stress (subgrade reaction) to subgrade settlement at a point. In its basic form, this hypothesis assumes that the settlement, δ_i , at an arbitrary point i on the subgrade surface is caused only by the applied vertical normal stress (subgrade reaction) at that point, σ_i . This parameter is often referred to as the 'soil spring constant' or a similar term because one physical interpretation of the abstract behavior defined by Equation 2.2 is a spring (not necessarily linear or elastic but usually assumed so) oriented perpendicularly to the subgrade surface.

By positioning these perpendicularly oriented springs under the foundation, the interaction between the foundation and the underlying ground can be represented as a 'bed of springs,' each with a stiffness of k_s per unit area. The sum of these spring forces must equal the applied structural loads plus the mat's weight. The earliest use of these 'springs' to represent the interaction between soil and foundations has been attributed to Winkler (1867), so the analytical model is sometimes called a Winkler foundation or the Winkler method (Coduto et al., 2016). The Winkler spring method assumes that the mat foundation sits on vertical, discrete, and linearly elastic springs, acting independently from the others, representing the deformable soil (Figure 2.2).

This representation has the desired effect of increasing the bearing pressure beneath the columns, and this is a significant improvement over the rigid method. However, it is still only a coarse representation of the true interaction between foundation and soil (Hain & Lee, 1974; Horvath, 1983) and suffers from many problems, including the following:

1. The load-settlement behavior of soil is non-linear, so the k_s value must represent some equivalent linear function, as shown in Figure 2.3.
2. A uniformly loaded foundation underlain by perfectly uniform array of springs will settle uniformly into the soil (i.e., there will be no differential settlement), and all of the 'springs' will be equally compressed. In reality, the settlement of different parts of the mat foundation would be variable.
3. Primarily because of items 1 and 2, there is no single value of k_s for the entire area that genuinely represents the interaction between soil and a foundation.

The primary source of these problems is using single value and independent springs in the Winkler model. In reality, a load at one point on the foundation induces settlement both at that point and in the adjacent parts of the foundation, which is why a uniformly loaded foundation exhibits a concave-shaped settlement, not the uniform settlement as predicted by Winkler (Coduto, 2001).

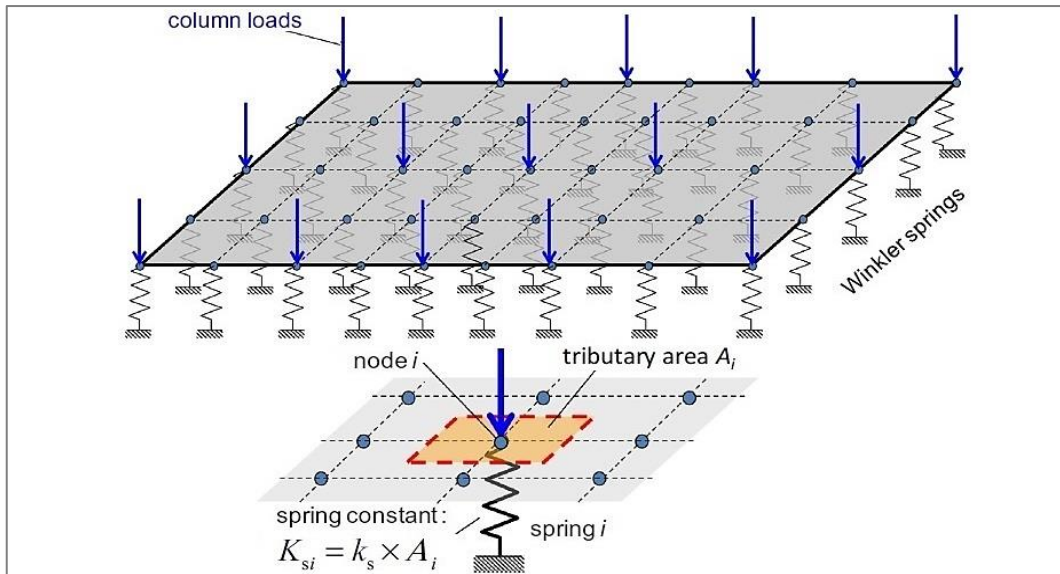


Figure 2.2 Computational model of the Winkler spring analysis approach

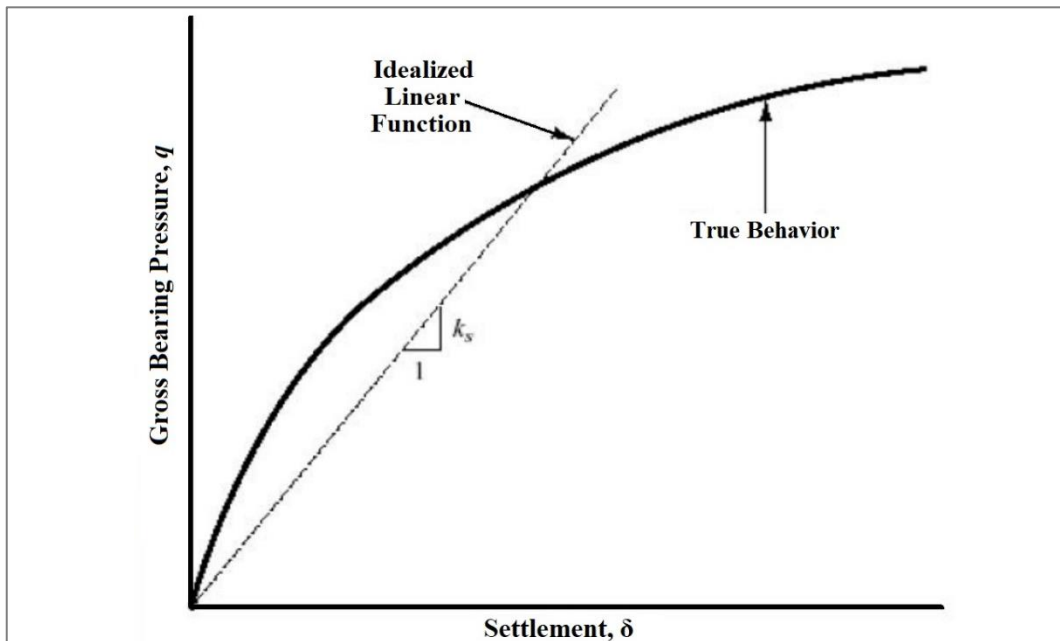


Figure 2.3 The non-linear σ - δ relationship and idealized k_s linear function

The coefficient of subgrade reaction has traditionally been determined from plate loading tests at the site and is affected by factors such as size, shape, and embedded depth of the plate. Terzaghi (1955) proposed that k_s for footings of width B could be obtained from plate load test data using the following equations:

For footings on clay;

$$k_s = k_1 \frac{B_1}{B} \quad (2.3)$$

For footings on sand;

$$k_s = k_1 \left(\frac{B + B_1}{2B} \right)^2 \quad (2.4)$$

where:

k_s is the desired value of modulus of subgrade reaction for full-size foundation,

k_1 is the value obtained from a plate-load test,

B_1 is the side dimension of the square base used in the load test.

In most cases, $B_1=0.3$ m, but whatever B_1 dimension was used should be input. Also, Equation 2.4 is not calibrated beyond $B/B_1 > 3$.

Since plate load testing is time-consuming and expensive, it is generally not widely used in practice. Only in large projects may building a test section and performing tests be considered feasible. It should also be noted that the applicability of plate load tests is highly controversial since a loaded plate has a limited impact depth and would not induce stresses in the deeper soil layers as a shallow mat foundation would. Also, since the size of the test plate is smaller than the actual foundation, the consequences of the scale effect are debatable.

Many attempts have also been made to derive the singular coefficient of subgrade reaction from empirical correlations besides the plate load test. Scott (1981) suggested a proper correlation for sandy soils between the subgrade reaction coefficient (k) and the corrected SPT number $(N_1)_{60}$, which is:

$$k_1 = 1.8 (N_1)_{60} \text{ (MN/m}^3\text{)} \quad (2.5)$$

Bowles (1996) suggested another correlation to approximate k_s using ultimate bearing capacity q_{ult} . The equation can be expressed as:

$$k_s = 40 q_{ult} \text{ (kN/m}^3\text{)} \quad (2.6)$$

where q_{ult} is furnished in kPa. This equation is based on the ultimate soil pressure causing a settlement of $\Delta H=0.0254$ m, and k_s is $q_{ult} / \Delta H$. Table 2.1 may be used as a guide and for comparing approximate equations.

Table 2.1 Range of modulus of subgrade reaction (Bowles, 1996)

| Type of Soil | k_s (kN/m ³) |
|--|----------------------------|
| Loose sand | 4,800–16,000 |
| Medium dense sand | 9,600–80,000 |
| Dense sand | 64,000–128,000 |
| Clayey medium dense sand | 32,000–80,000 |
| Silty medium dense sand | 24,000–48,000 |
| Clayey soil: | |
| $q_u \leq 200$ N/mm ² | 12,000–24,000 |
| $200 < q_u \leq 400$ N/mm ² | 24,000–48,000 |
| $q_u > 800$ N/mm ² | > 48,000 |

2.2.2 Coupled Method

The coupled method, using additional cross springs, can be described as the next step from the Winkler analysis. (Figure 2.4). Unlike the Winkler method, where vertical springs move independently, the coupled method considers the interdependence of these springs. In principle, this approach is more accurate than the Winkler method, but it is not clear how to select the k_s values for the coupling springs (Coduto et al., 2016). In practice, the coupled method is not used in widespread software applications, and developing custom structural analysis software may be necessary to perform this method effectively.

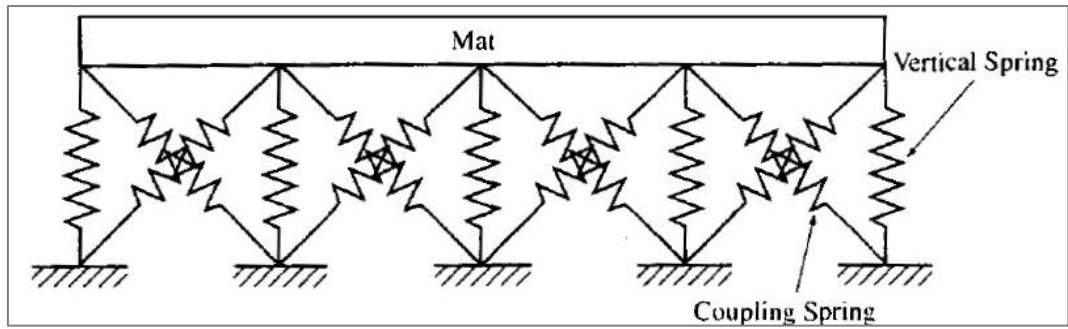


Figure 2.4 Modeling of soil-structure interaction using coupled springs

2.2.3 Pseudo-Coupled Method

The pseudo-coupled method, introduced by Bowles (1986), Liao (1991), Horvath (1993), and ACI Committee 336, aims to address the lack of coupling in the Winkler method while avoiding the complexities of the fully coupled method. This method uses 'springs' that act independently but have different k_s values depending on their location on the foundation (Figure 2.5). In reality, while nothing fundamentally new, the pseudo-coupled concept can be described as a repackaged version of the single-parameter Winkler Hypothesis. In essence, in the pseudo-coupled concept, Winkler's subsoil reaction coefficient is allowed to vary below the foundation element. Thus, as a subgrade model, it attempts to mimic the actual variable subsoil reaction that develops under the foundation, as outlined in Section 2.2.1.

The generic variations suggested to date developed with mat foundations assume an increase in k_s values near the edges of the foundation element. This method requires that the mat plan be divided into three or more concentric zones. The innermost (center) zone should be approximately one-half the mat's width and length. Then, k_s values shall be assigned to each zone using softer springs in the innermost zone and transitioning to the outermost (exterior). Typically, the k_s in the outermost zone is nearly twice as large as in the innermost zone. The products of each zone's area and its k_s should equal the sum of the product of the mat area and the average modulus of subgrade reaction, $k_{s, av}$, provided by the geotechnical consultant.

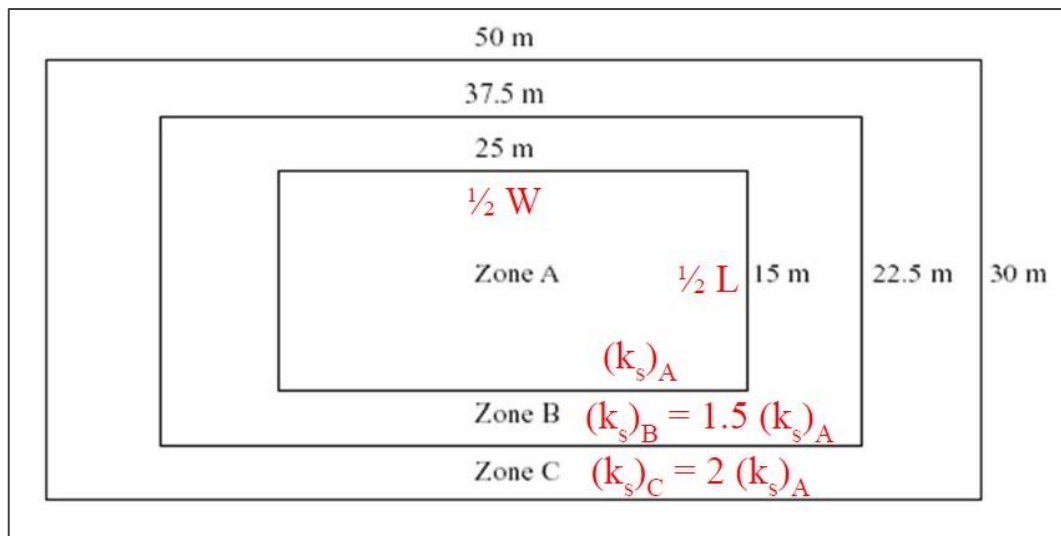


Figure 2.5 Division of mat into zones with the different modulus of subgrade reaction values for pseudo-coupled analysis

American Concrete Institute (ACI, 1993) found that the pseudo-coupled method produced computed moments 18 to 25 percent higher than those determined from the simple Winkler method, indicating how non-conservative Winkler can be. Most commercial foundation design software uses the Winkler method to represent the soil-structure interaction, and these software packages usually can accommodate the pseudo-coupled method.

While the pseudo-coupled concept appears to be the long-sought improvement to the traditional use of Winkler's Hypothesis with a constant Winkler coefficient of subgrade reaction, the actual improvement in a given problem is subject to significant variability that can be difficult to assess (Horvath, 1995). Despite the allure of potential improvement, utility of the pseudo-coupled method as an improved subgrade model is questionable because each application is a unique combination of geotechnical components and structural elements. For example, it cannot be expected to be the same distribution of subgrade reactions in two applications with different soil properties or dissimilar structural element layouts but mats with the same dimensions.

2.2.4 Multiple-Parameter Methods

The multiple-parameter methods offer an alternative approach to modeling soil behavior. In these subgrade model methods, Winkler's vertically and independently acting linear springs are replaced with springs and other mechanical elements. These additional interacting elements couple the independent springs and try to include load transfer in the transverse direction. The interaction elements can be pre-tensioned membranes, flexural elements, springs, and shear layers. Presented next are enhanced renditions of Winkler's original model that focused on introducing additional parameters to aid in modeling the coupling effect among soil springs.

Filonenko-Borodich (1940) model tries to provide the interaction between the springs by adding a new, thin elastic layer with tension force 'T' (pretensioned) on the surface of the springs of the Winkler model. This thin, flexible layer simulates the coupling effect of individual springs without extensively complicating the mathematical formulation and the corresponding analytical solutions. The basic view of the model and its deformation characteristics under various load conditions are shown in Figure 2.6. The governing equations of this model with two distinct expressions for strip foundations and rectangular/circular footings are presented below;

Strip foundations:

$$p = kw - T \frac{d^2w}{dx^2} \quad (2.7)$$

Rectangular or circular footings:

$$p = kw - T \nabla^2 w \quad (2.8)$$

where $\nabla^2 = \text{Laplace operator} \equiv d^2/dx^2 + d^2/dy^2$ and (T) is the tensile force.

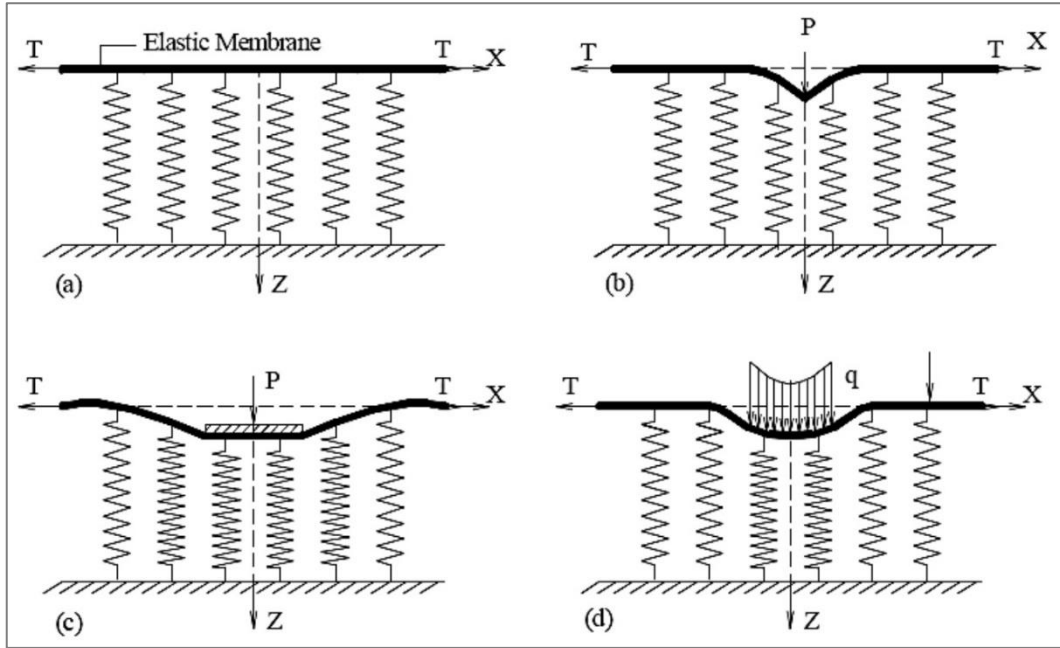


Figure 2.6 Surface displacement profiles of Filonenko-Borodich model (1940): (a) basic model, (b) concentrated load, (c) rigid load, and (d) uniform flexible load

Another improved ground behavior approach of Winkler's original model that tries to achieve deformation continuity among soil springs is proposed by Pasternak (1954). This subgrade model assumes the existence of shear interaction between the spring elements by connecting them to a thin layer of incompressible vertical elements with a defined thickness that undergo transverse shear deformations only. The pressure-deflection equation is expressed as follows;

$$p = kw - G \frac{d^2w}{dx^2} \quad (2.9)$$

where G is the shear layer constant.

As a generalization of the Pasternak concept, Kerr (1964) proposed a higher-order (three-parameter) foundation model by incorporating another Winkler medium over the shear layer of the Pasternak model endowed above. This model consists of two layers of elastic springs interconnected by an elastic shear layer (Figure 2.7). The differential equation governing the response of this model is as follows:

$$\left(1 + \frac{k_2}{k_1}\right)p = \frac{G}{k_1} \nabla^2 p + k_2 w - G \nabla^2 w \quad (2.10)$$

where k_1 and k_2 are the axial springs constants in the first and second layers, respectively, and w is the deflection of the first layer only.

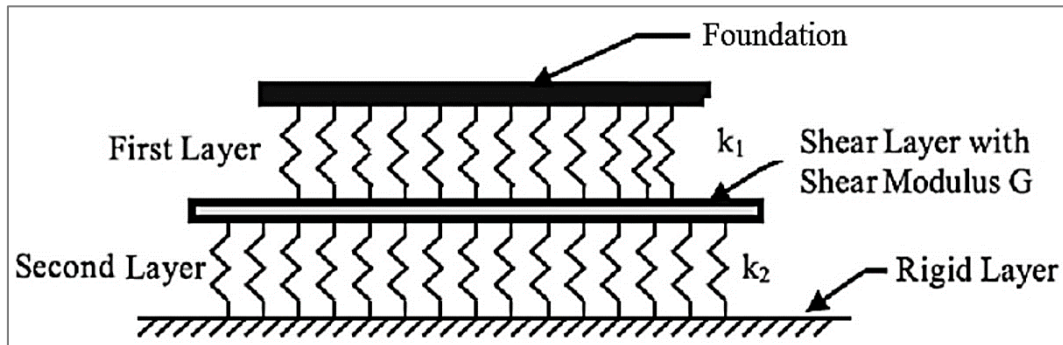


Figure 2.7 Visualization of Kerr model (1964)

It can be seen that adding a mechanical element in a kind of building-block approach results in a higher-order model, as reflected in the Kerr model. Table 2.2 summarizes the composition of several other subgrade models, including those mentioned above, in the order of their increasing mathematical complexity.

Table 2.2 Compiling of multi-parameter models

| Subgrade model | Physical elements used to visualize model |
|-------------------------------|--|
| Winkler's Hypothesis (1867) | springs |
| Filonenko-Borodich (1940) | pretensioned membrane + springs |
| Pasternak's Hypothesis (1954) | shear layer + springs |
| Kerr model (1964) | springs + shear layer + springs |
| Hetenyi (1946) | springs + plate + springs |
| Rhines (1969) | springs + plate + shear layer + springs |

The main disadvantage of multiple parameter models lies in their applicability in real design cases. Depending on the particular model used, there is a need to determine the two or more model coefficients (shear layers, deformed, pre-tensioned membranes, beams/plates), which turns out to be a significant problem. As to be in coupled-method, this time, it is not clear to accurately determine the characteristic and mechanical properties of additional elements. Also, these methods have yet to be incorporated into readily-available software packages, limiting their utilization in routine engineering projects.

2.3 Finite Element Method (FEM)

The finite element method (FEM) subdivides a domain or complex space into several small, countable, and finite pieces whose behavior can be described with comparatively simple equations. The accuracy of the element behavior approximations determines how closely the resulting simulated behavior resembles the actual continuum. While the method was initially developed for engineering analysis to model and analyze complex systems in mechanical and aerospace engineering, typical areas of interest covered by this method include analyses for civil engineering.

All the methods discussed so far aim to model and analyze three-dimensional soil using a series of one-dimensional springs and additional elements. This is done to simplify the issue sufficiently for structural analysis. FEM has the potential to eliminate the need for oversimplification and provide an accurate representation of the soil, foundation, and structure system, encompassing all components of a mechanical problem. In the sense of soil-foundation analysis, the method divides the soil and foundation into a network of rectangular or triangular small elements, each connected to adjacent segments in a certain way. All these elements in this network have defined engineering properties. Structural and gravitational loads are then applied, and the elements are stressed and deformed accordingly. Instead of solving the entire body in one equation, FEM allows us to create equations for each element and then combine them to come up with the solution for the whole body. In general, the solution to structural problems refers to determining the displacement at each node in the element and the stress within each element throughout the structure that experiences the applied loads.

In principle, this method accurately represents the soil and foundation and should facilitate an accurate and economical design. However, FEM software mainly focuses on one type of analysis (e.g., structural or geotechnical). And it is unable to accommodate a detailed and realistic analysis of the 'other' half of the problem, with the exception of a few custom-made research-grade programs.

In structural FEM software, the foundation and the superstructure are divided into hundreds or perhaps thousands of elements; each has certain defined dimensions, specified stiffnesses and strength, and is connected to the adjacent element in a specified way. Even so, the foundation is still supported by 'springs,' which do not fully reflect the behavior of the soil. From the geotechnical side, the soil can be modeled by the most superior soil mechanics models that best describe soil behavior; the foundation can be modeled by realistic element properties, but this time the stiffness of the superstructure and structural loading conditions are outside the estimation.

Principally, for more accurate models and, thus, more economical designs, the finite element analysis should be extended to include the underlying soil, the mat, and the superstructure in a single three-dimensional finite element model. Nevertheless, these extended finite element analyses are rarely performed in practice, which appears to be this method's most substantial disadvantage. A traditional design scenario in which finite element analysis methods of geotechnical and structural areas are jointly assigned is explained below.

2.3.1 Soil-Structure Interaction (SSI) Modeling

The typical scenario where a mat supports a superstructure is conceptually represented in Figure 2.8 to highlight key concepts of mat foundation behavior. Note that the subgrade, mat, and superstructure are the problem's three main components. A mat-supported structure represents a circumstance where SSI is significant. In such a case, the load-displacement behavior of any one component (mat, subgrade, or superstructure) is physically connected to and thus dependent upon the behavior of the other two via equilibrium and compatibility.

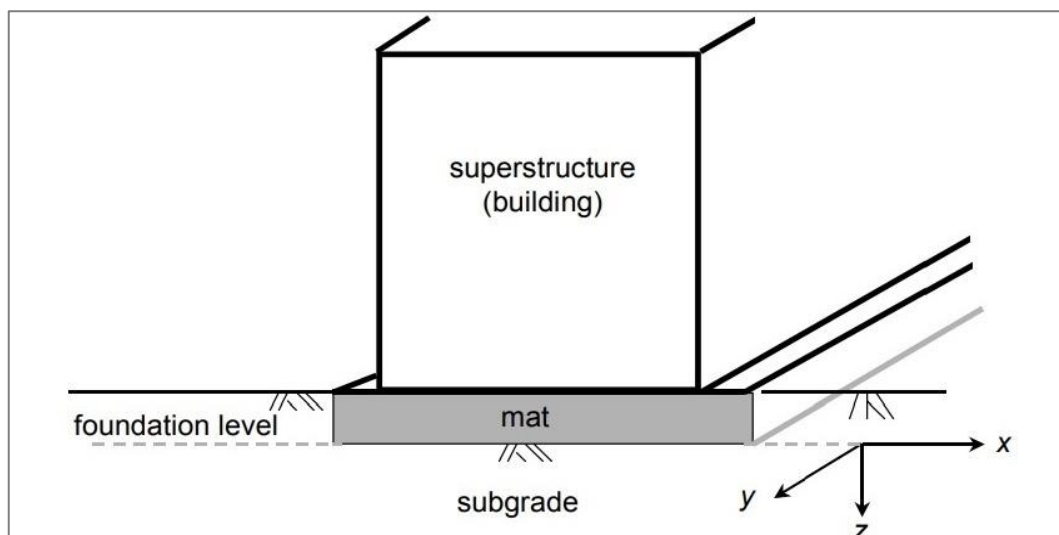


Figure 2.8 Typical Mat Foundation Problem

Therefore, to maximize the accuracy of the results, analyzing a single problem for the mat-subgrade-superstructure system is ideal, as depicted in Figure 2.8. Although the structural and geotechnical components can be found in various commercial and research forms, no such software that model and analyze the system as a whole is in widespread use.

Even with the current wide availability of digital computers in routine civil engineering practice, the traditional approach is to decompose a mat foundation problem into two separate analytical components. The superstructure and mat are integrated into a single model (megastructure) in the 'structural' analytical component, as described in Figure 2.9. This captures the ideal behavior of the structural components. Analysis of the megastructure can be accomplished easily, even in three dimensions if desired, with the structural analysis computer software that is commercially available and currently used routinely worldwide (Horvath, 2002). Nevertheless, the primary shortcoming of the structural component is the subgrade reaction, $p(x,y)$.

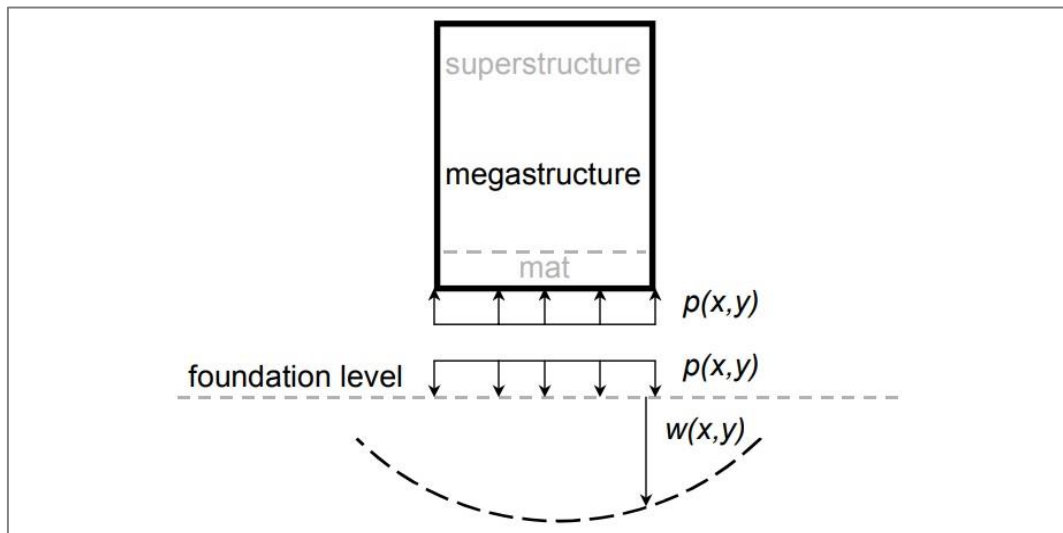


Figure 2.9 'Structural' component analysis

The 'geotechnical' component is to model the subgrade in one rigorous analysis. The problem is that computer software that can evaluate a three-dimensional continuum representing the subsurface beneath a foundation is not widely available in routine practice (only two-dimensional software is). Another drawback of the 'geotechnical' component is the lack of ability to model the superstructure interaction effects.

Consequently, the key item between the two analytical components is the subgrade reaction, $p(x,y)$. For this reason, it is vital to determine the amount and distribution of the sub-reaction correctly. Even though the 'ideal' solution delineated in Figure 2.10 will undoubtedly become a reality in the future, it will be many years before it is practical for everyday practice.

Below, some basic information is given about the two well-known finite element programs, SAP2000 and PLAXIS 2D/3D, used in this study as the structural and geotechnical components, respectively.

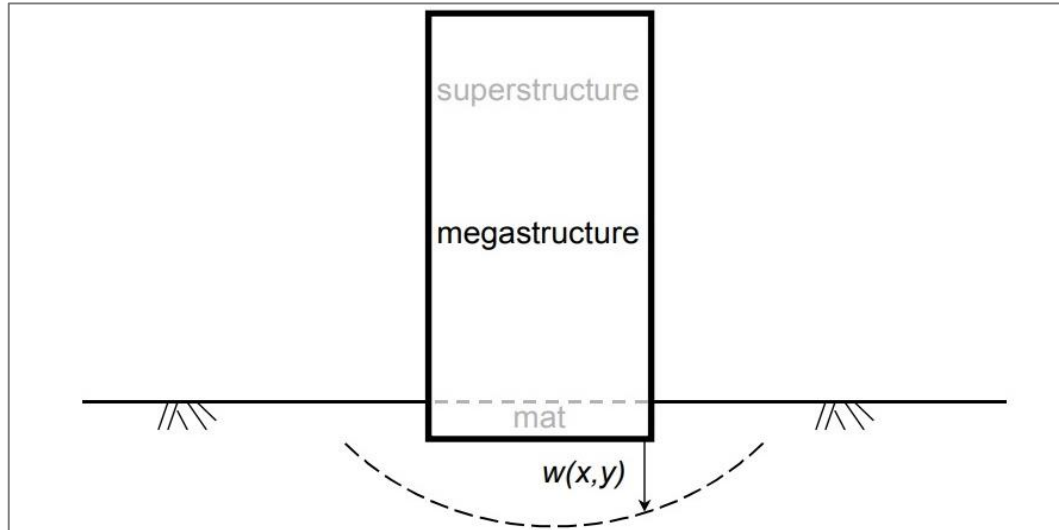


Figure 2.10 Problem Components: 'Ideal' Analysis

2.3.2 SAP2000

SAP2000 (Structural Analysis Program) is a general-purpose civil-engineering software ideal for analyzing and designing any type of structural system, developed by Computers and Structures, Inc., based in Berkeley, California. It enables to model, analyze, design, and optimize the basic and advanced structural systems ranging from 2D to 3D, from simple geometry to complex.

It offers different analysis options: linear, non-linear, static, and dynamic analysis. The design codes are integrated into this software, and this feature can automatically calculate wind, bridge, and seismic loads. It also offers comprehensive automatic code checks for international steel and concrete design standards (CSI, 2014).

2.3.3 PLAXIS 2D/3D

PLAXIS 2D/3D program is a two/three-dimensional finite element program used to make stability and deformation analyses for geotechnical applications. The PLAXIS 2D program can model plane strain or axisymmetric problems. The plane strain model can be utilized with a uniform cross-section, and the assumption that stresses in the z-direction (i.e., perpendicular to the cross-section) are zero. An axisymmetric model is used when stress and strain are considered identical in all radial directions for circular structures (Figure 2.11).

In PLAXIS 2D, there are two different triangle elements that can be employed to simulate soil layers and structures: 6-node and 15-node. As shown in Figure 2.12(a), the 15-node element provides fourth-order interpolation for displacement, and the numerical integration uses twelve Gauss points (stress points). A second-order interpolation for displacement is provided by the 6-node element, as shown in Figure 2.12(b), and the numerical integration uses three Gauss points. Compared to a 6-node element, a 15-node element produces more accurate findings but uses more memory and slows down calculating performance. In PLAXIS 3D, 10-node

tetrahedral elements are used to simulate the soil volume (Figure 2.12(c)), and 6-node triangular elements are used for area and surfaces.

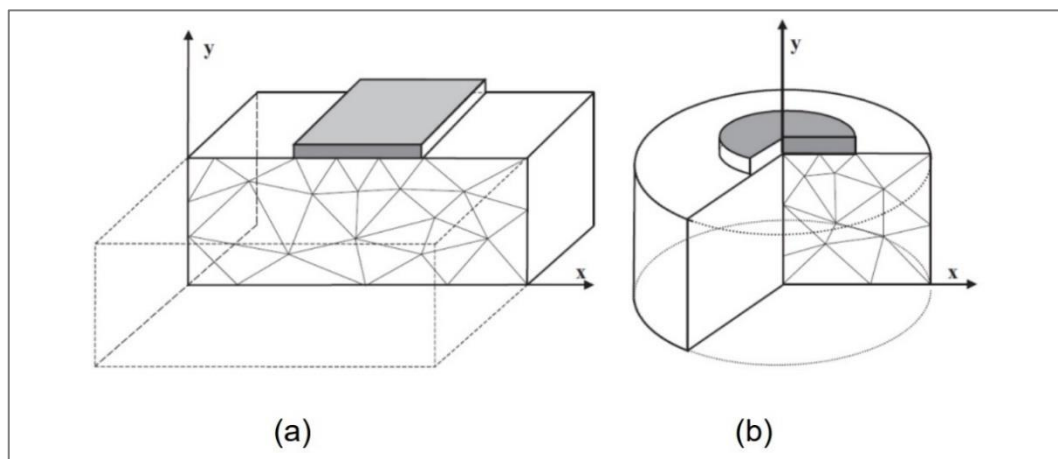


Figure 2.11 Example of PLAXIS 2D problems: a) plane strain, and b) axisymmetric (PLAXIS, 2011)

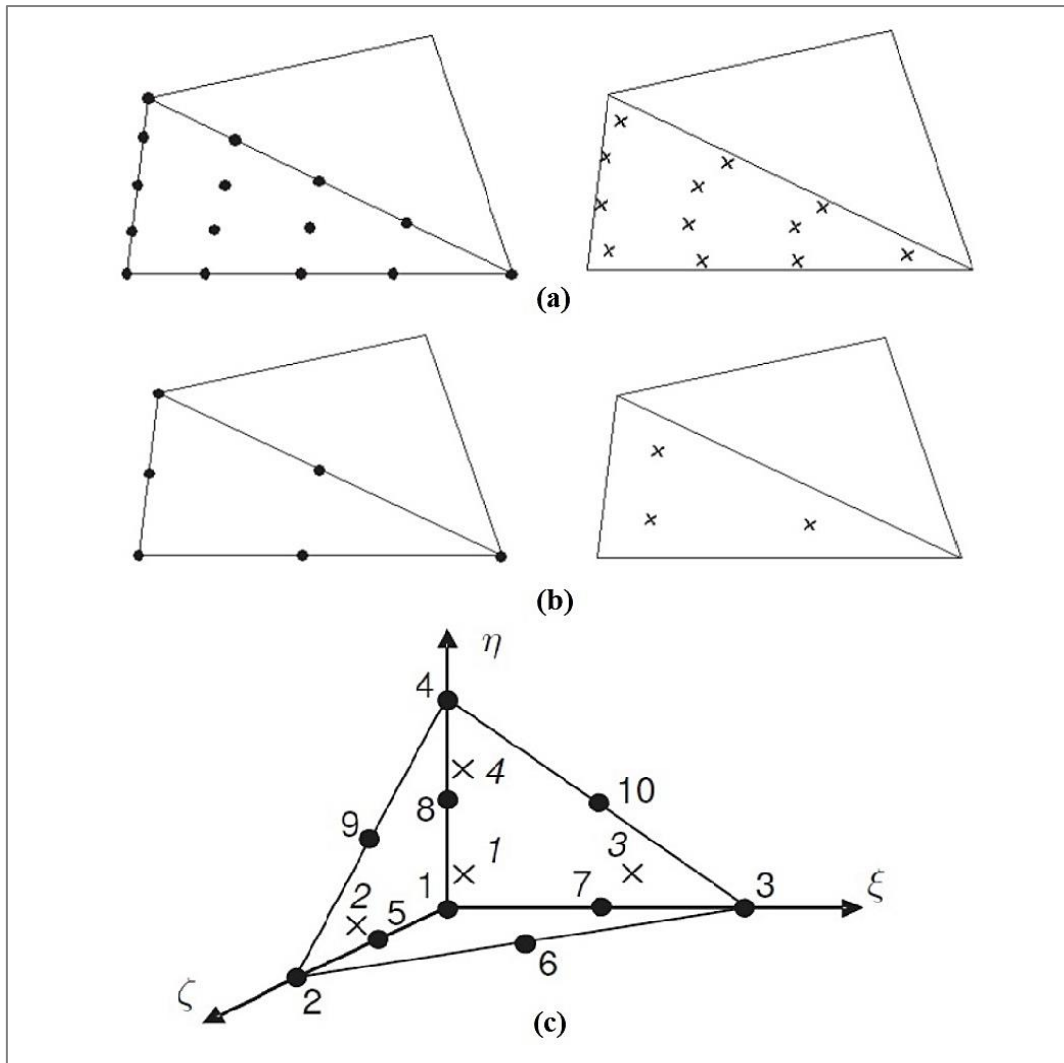


Figure 2.12 (a) 15-node and 12-stress point soil element in PLAXIS 2D, (b) 6-node and 3-stress point soil element in PLAXIS 2D, (c) Typical 3D soil element (10-node tetrahedron with 4 stress points) in PLAXIS 3D

Following the creation of the geometry model, a constitutive model must be selected, and material parameters must be assigned to the respective geometry clusters or layers.

2.3.4 Common Material Models

In PLAXIS 2D/3D, there are eight different material models available. Below their brief descriptions are provided.

- Linear elastic model uses Hook's law of isotropic linear elasticity to model stiff structures in the soil.
- Mohr-Coulomb model: This linearly elastic-perfectly plastic model is generally used as a first approximation of soil behavior. The model predicts either a constant average stiffness for each soil layer or a stiffness that increases linearly with depth. Due to this constant stiffness, it offers a first estimate of deformations, and computations tend to be relatively fast.
- Hardening Soil model: The Hardening Soil model is an advanced model for the simulation of soil behavior. As for the Mohr-Coulomb model, limiting states of stress are described by means of the friction angle, ϕ , the cohesion, c , and the dilatancy angle, ψ . However, soil stiffness is described much more accurately using three different input stiffnesses: the triaxial loading stiffness, E_{50} , the triaxial unloading stiffness, E_{ur} , and the oedometer loading stiffness, E_{oed} . As average values for various soil types, $E_{ur} \approx 3E_{50}$ and $E_{oed} \approx E_{50}$ are suggested as default settings. In contrast to the Mohr-Coulomb model, the Hardening Soil model also accounts for the stress-dependency of stiffness moduli. This means that all stiffnesses increase with pressure. This second-order model involves compression hardening, which is suitable for simulating the behavior of sands, gravels, and over-consolidated clays (Gouw, 2001).
- Hardening Soil model with small-strain stiffness: The Hardening Soil model with small-strain stiffness is a modification of the above Hardening Soil model that accounts for the increased stiffness of soils at small strains. Most soils exhibit a higher stiffness at low strain levels than at engineering strain levels, and this stiffness varies non-linearly with strain.

- **Soft Soil model:** This model is a Cam-Clay type model that can be used to simulate the behavior of soft soils such as normally consolidated clays and peat. This model assumes that the soil is isotropic, elastoplastic and is not affected by creep.
- **Soft Soil creep model:** This is a second-order model formulated in the framework of viscoplasticity. The model can be used to simulate the time-dependent behavior of soft soils, such as normally consolidated clays and peat.
- **Joined Rock model:** The Joined Rock model is an anisotropic elastic-plastic model specially meant to simulate the behavior of rock layers involving stratification and particular fault directions.
- **Modified Cam-Clay model:** This model assumes a logarithmic relationship between the volumetric strain and the mean effective stress and can be used to simulate the behavior of normally consolidated soft soils.

2.3.5 Choice of the Constitutive Model

The choice of a suitable constitutive model is a pivotal aspect in the analysis of soil-structure interaction for foundation design, with significant implications for the accuracy of results. The chosen model must accurately represent the mechanical behavior of the soil under the specific loading and boundary conditions relevant to the problem at hand. In this study, the Hardening Soil Model was selected as the most appropriate choice for analyzing raft foundations on non-cohesive soils without any water level.

Several factors guided the selection of the hardening soil model, aligning with the research objectives and scope. This non-linear soil model offers a balanced representation of soil behavior, encompassing both elastic and plastic deformations, which is vital for realistically portraying soil deformation in the context of shallow raft foundations. Soil behavior for a given stress level is considered to be truly elastic in the range of small strains. In this strain range, the soil may exhibit a non-linear stress-strain relationship; however, its stiffness is nearly fully recoverable during

unloading conditions. Beyond the pre-failure non-linearities of soil behavior, where foundations are assessed against serviceability limit and ultimate limit state analyses, a notable variation of stiffness is observed starting from very small shear strains. This phenomenon cannot be replicated by models such as the linear-elastic Mohr-Coulomb model (Obrzud & Truty, 2020).

The transition from these very small strains to engineering strains marks the domain where the hardening soil model excels. Its notable advantage is the ability to capture stress-strain behavior in soils under sequential loading, a common scenario for foundation systems subjected to staged and long-term loads, making it suitable for studying the long-term performance of foundations—a crucial aspect in practical engineering applications. Additionally, the hardening soil model is a better fit compared to models developed for soft soils, as rafts on such soils are less likely to be designed without ground improvement or foundation piles.

The choice of the hardening soil model is also motivated by its compatibility with the commonly used finite element software PLAXIS. This ensures consistency between the modeling approach and the capabilities of the software, enhancing the reliability and relevance of findings.

Overall, the selection of the hardening soil model aligns with the need for a comprehensive, realistic, and practically applicable representation of soil behavior in the context of shallow raft foundations. This choice enables the exploration of intricate soil-structure interaction and provides valuable insights into the design and optimization of foundation systems within the scope of this research.

CHAPTER 3

METHODOLOGY

In this study, commonly used commercial software programs, PLAXIS 2D/3D and SAP2000, were employed to investigate the behavior of shallow raft foundations under static loading and analyze the distribution of subgrade modulus beneath the foundation. A total of fifty-three analysis sets were conducted with PLAXIS 2D and SAP2000 across various cases, considering variables such as foundation thickness, width, soil stiffness, number of floors, building width, and column positions. Each analysis set begins with a PLAXIS 2D model that simulates the soil and structure together and is assumed to be the most accurate estimate of the combined behavior. This is followed by iterations in SAP2000, where the spring constants are varied until the results (settlement profile and bending moment diagram in the raft) match those obtained from PLAXIS 2D. It is important to mention that other studies in the past have also looked into this kind of research, where PLAXIS was employed to model both the foundation and the building structure. Gragnano et al. (2014) found an overall very good match, as such highlighting the possibility to use the code PLAXIS to perform both structural and geotechnical calculations in soil-structure interaction problems.

The studies first started by analyzing multistory buildings with raft foundations resting on single-layered non-cohesive soils with PLAXIS 2D software. The boundary conditions in PLAXIS 2D were defined as 1.5 times the foundation width from both ends and two times the foundation width below the foundation level. The purpose of selecting these boundary dimensions, which is commonly employed in practice, is to strike a balance between capturing significant effects and ensuring computational efficiency.

Mat foundations were directly placed on top of the ground as the first stage, and the columns and slabs of the upper levels were added sequentially, one story at a time to represent the staged construction. Air is defined as a material with zero strength and weight for the empty frame spaces formed between the columns and slabs of the superstructure. The range of parameters considered in the analyses included raft thickness (0.7-1.50 meters), raft width (20-60 m), soil secant stiffness (E_{50}^{Ref}) (20-65 MPa), slab thickness (0.20-0.30 m), number of floors (4-20), column side dimension (0.40-0.60 m), and center-to-center column spacing (2-10 m). Structural concrete elements (rafts, columns, and slabs) were modeled as plates with elastic material type. Input material parameters of structural elements are listed in Appendix A. The hardening soil model was used in the analyses to model the supporting soil under the foundations.

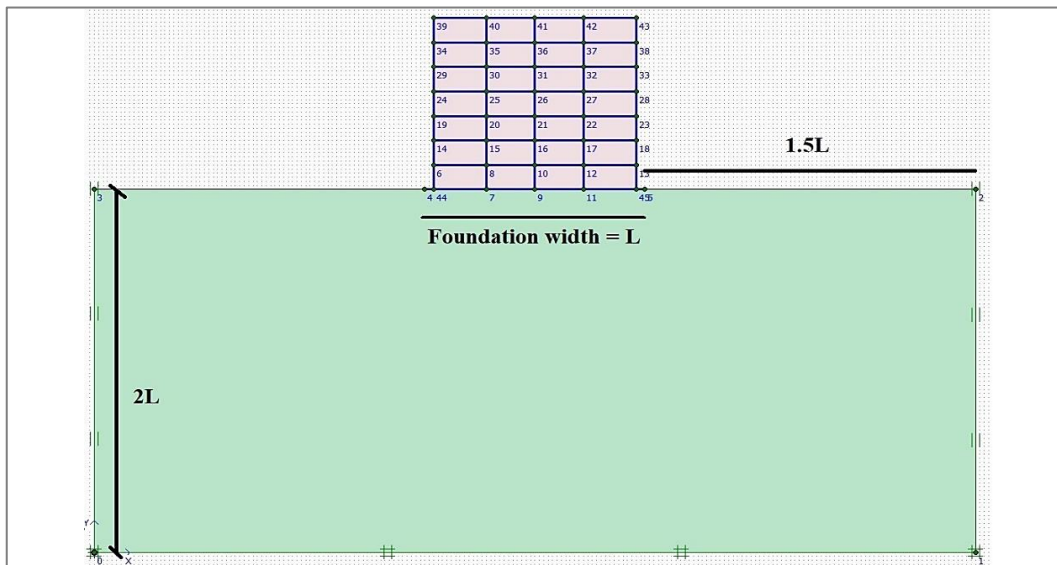


Figure 3.1 Geometry and boundary conditions in PLAXIS 2D models

The models created in PLAXIS 2D were replicated in SAP2000, ensuring they had the same shape, dimensions, and structural material properties. Frame elements were used to model all columns and beams. A linear-elastic constitutive law was adopted for these elements, whose parameters were selected consistently with the assumed

non-reinforced concrete material. Four-node, thick shell elements were used to model the raft (plate-bending behavior) behavior in three-dimensional analyses. The frame elements (columns, slabs) and the shell elements (raft) were connected without any constraints at the joints. The bottom of the models was supported by the line or area springs for translation in the direction of gravity. The springs were placed at an interval of 0.5 m, which balances the computational time against the accuracy of the results. An example view of the 2-dimensional analyses created in both software is shown in Figure 3.2.

An iterative process was implemented, adjusting the spring constants in SAP2000 until the settlement and bending moment results converged and aligned with the corresponding results from the PLAXIS 2D analysis. Convergence was considered achieved when the settlement and bending moment values of the SAP2000 analyses were within ± 5 percent at all nodes compared to the PLAXIS 2D results. The outcome of each analysis set is the determination of the distribution of spring constants (k) that aligns with the results obtained from the continuum analysis, which is deemed more realistic. The analyses carried out within this study's scope are detailed below, with the variables grouped within themselves.

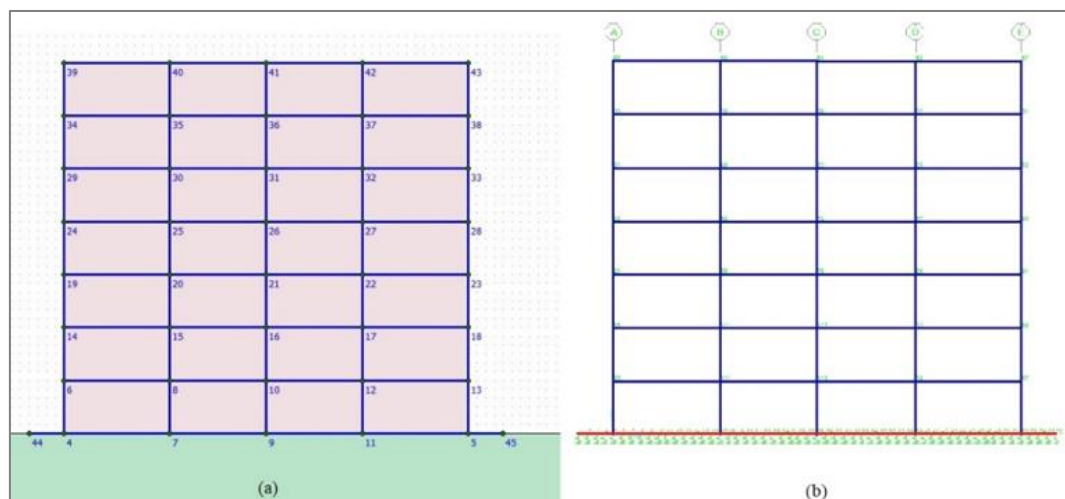


Figure 3.2 An example structural view of the 2-dimensional analysis (a) PLAXIS 2D v-8.6 (b) SAP2000 v-21.1.

In the calculation and presentation of the spring constants, the tributary area of each spring node was taken into account. For the two-dimensional analyses, the nodes located at the edges had half the area compared to the inner nodes of the beam. Similarly, for the three-dimensional analyses, the nodes at the plate corners had one-fourth, and those at the edges had half the area. This condition is visually represented in Figure 2.2.

3.1 Effects of Foundation Thickness

Before conducting the series of 53 analyses mentioned above, to establish the iteration process and observe the effects of system variables, two preliminary analyses were performed. In these analyses, the objective was also to explore how the variation in foundation thickness impacts the soil reaction. Specifically, two raft foundations with different thicknesses (0.5 m and 2.0 m) were analyzed using PLAXIS 2D. Both foundations were placed on a 40-meter thick layer of sand, modeled as hardening soil with a unit weight of 18 kN/m³. The soil properties were kept the same for both models, and no water level was considered. An interface strength reduction factor (R_{inter}) of 0.67 was assigned between the soil and foundation. The raft foundations were modeled as elastic beam elements, and distributed column loads were applied at four locations along the raft. (Figure 3.3).

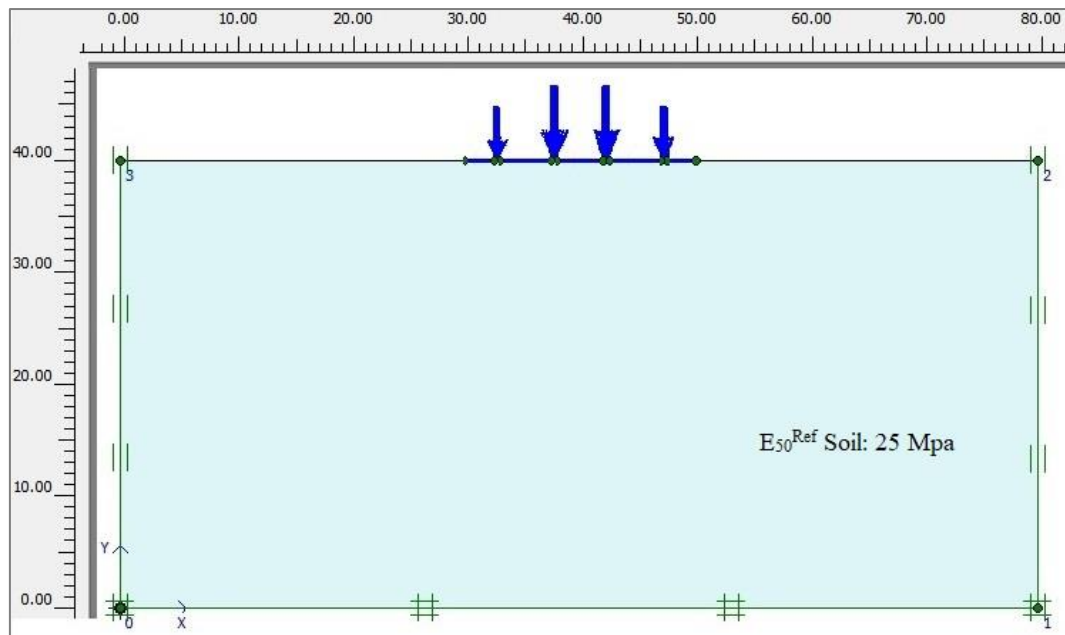


Figure 3.3 General appearance of the PLAXIS 2D model for the 'Effects of Foundation Thickness' case

By analyzing the two different foundation thicknesses and observing the corresponding soil reactions in the preliminary analyses, valuable insights were gained regarding the influence of foundation thickness on the behavior of the raft foundation system. These findings served as a basis for further investigations in the subsequent series of analyses, allowing for a comprehensive exploration of the effects of various system variables on the performance of the foundation.

The settlement and bending moment results obtained from the two PLAXIS 2D analyses are compared. It is observed that the thicker foundation settled uniformly with a settlement of approximately 6 cm. On the other hand, the thinner foundation experienced maximum settlements of 4 cm at the center and 2.5 cm at the edges. The increased settlement in the thicker foundation can be attributed to its higher self-weight compared to the thinner foundation. It settles uniformly due to its higher rigidity resulting from the increased thickness. As the raft thickness increases, the differential settlement decreases, leading to higher foundation bending moments (Figure 3.4).

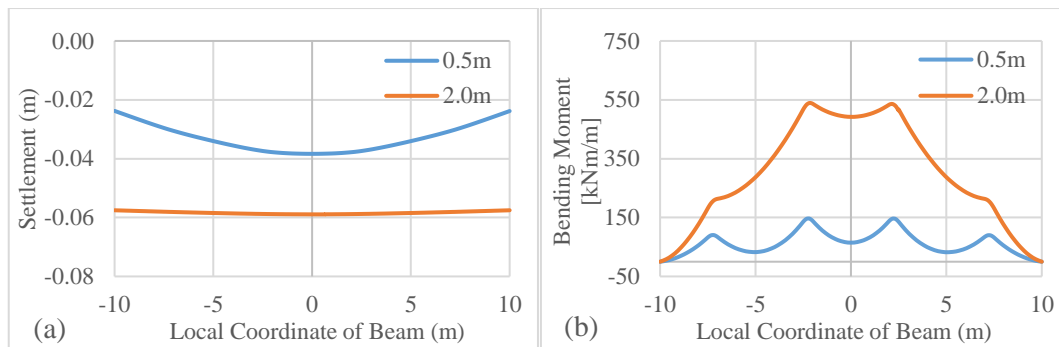


Figure 3.4 Comparison of (a) settlement and (b) bending moment results of 0.5 m thick and 2.0 m thick rafts

As mentioned above, in order to determine the distribution of soil reaction beneath the foundation, modeling studies were also conducted in SAP2000, using the same raft properties and loading conditions. The trial-error method was employed to determine Winkler's spring coefficients in SAP2000 that closely matched the settlement and moment results obtained from PLAXIS 2D. Figure 3.5 illustrates the settlement, bending moment, and shear force results of the 2.0 m thick foundation obtained from both software programs. It can be observed that the results are almost perfectly overlapping. Additionally, Figure 3.5 also includes the SAP2000 results obtained by the constant spring approach. The overlapping settlement and bending moment results obtained from PLAXIS 2D and SAP2000 using the trial-error method demonstrate the limitations and discrepancies introduced by the constant spring approach.

It is worth noting that SAP2000 assigns nodes on each spring defined at 0.5 m intervals; it has a regular and intermittent node distribution, whereas PLAXIS defines irregular but frequent nodes. These intermittent nodes are the cause of the discontinuous results appearing on the diagrams.

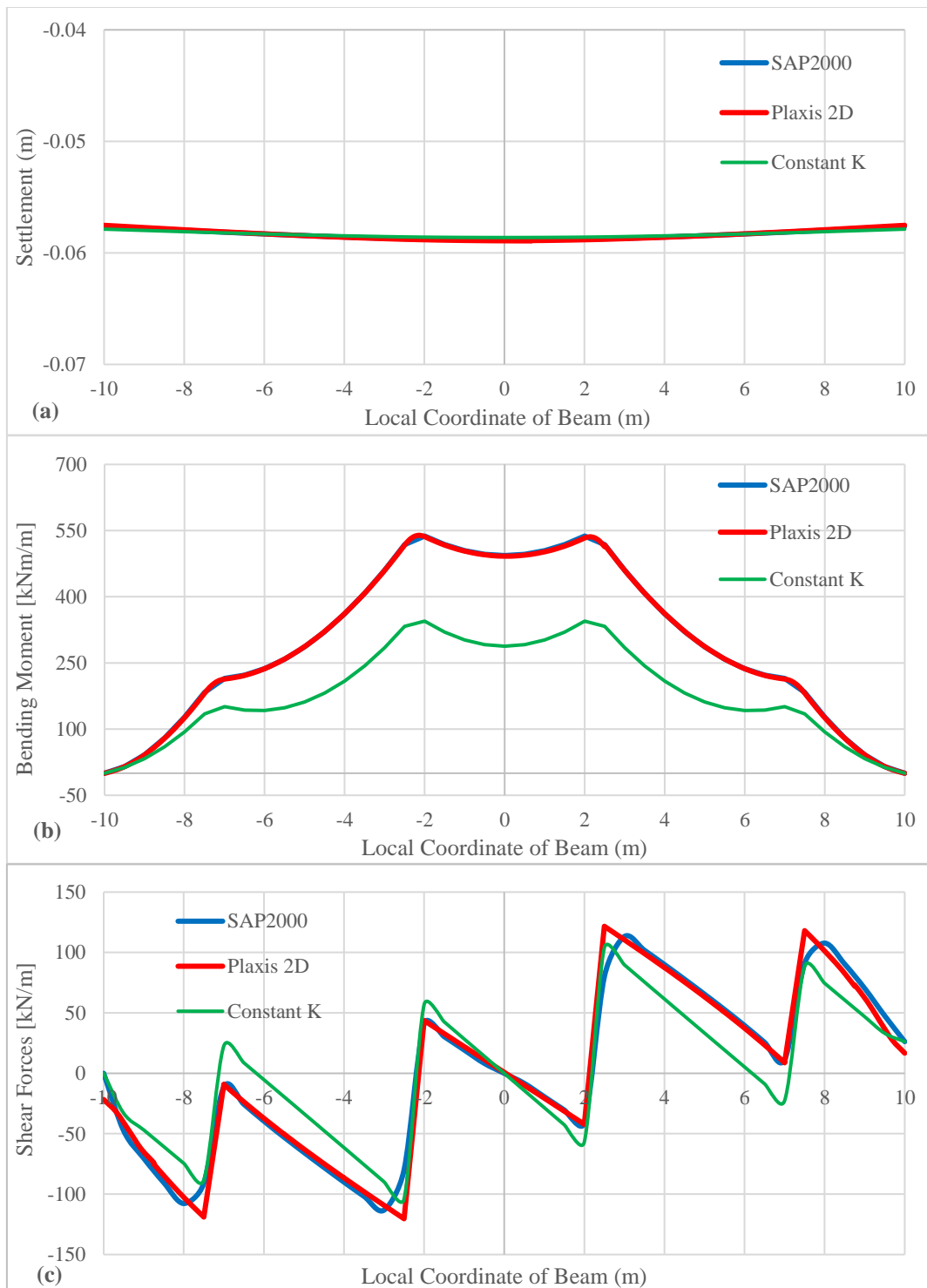


Figure 3.5 Comparison of (a) settlement, (b) bending moment, and (c) shear force results obtained from PLAXIS 2D and SAP2000 software for the 2.0 m raft thickness case

In the case of a 2.0-meter raft thickness, an overall trend of a U shape can be observed in the distribution of spring constants, with higher values closer to the edges of the foundation. However, as the rigidity of the foundation decreases (underlying soil properties unchanged), the spring coefficients concave downwards, especially at the midsection. (Figure 3.6). Notably, both distributions exhibit a significant and steep upward increase towards the edges of the foundation.

It should be noted that the term "spring constant" used in the context of this study is not equivalent to the subgrade modulus. It is essential to clarify to the readers that the spring constants derived from the analysis represent the subgrade response but are not the actual subgrade modulus values. In the context of the study, the spring constants can be considered as a representation of the subgrade modulus, but they should be scaled appropriately. Specifically, the spring constants at the edges should be multiplied by 2 to account for the half-tributary area. Additionally, considering the 0.5-meter spacing of the springs, the spring constants can be doubled to represent the subgrade modulus in the analysis.

To summarize, the distribution of spring constants (k) was determined through the analysis using PLAXIS 2D and SAP2000. The calculated spring constants should be adjusted by doubling the values at the edges to account for the half-tributary area and by doubling all values considering the 0.5-meter spring spacing. These adjustments ensure a more accurate representation of the subgrade modulus in the analysis.

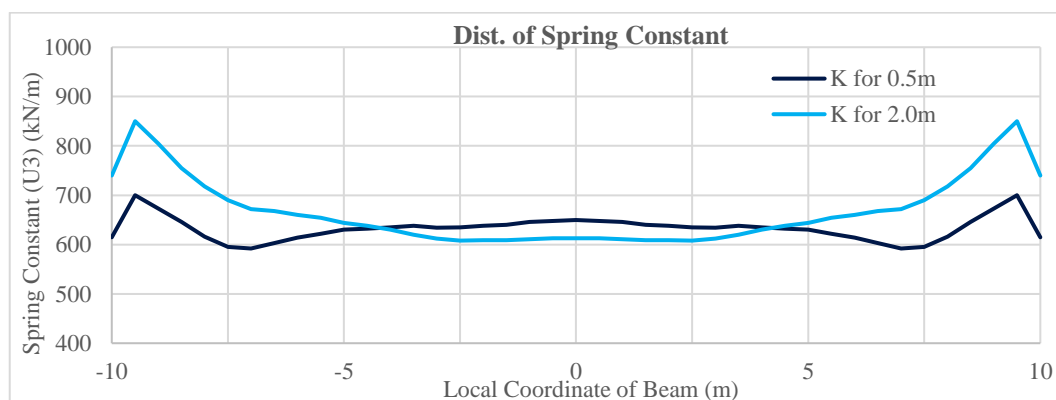


Figure 3.6 Distribution of spring constant values for 0.5 m and 2.0 m thick rafts

3.2 Effects of Staged Construction

In order to gain insight into the implementation of staged construction modeling and analyze the interaction between two different finite element software programs, modeling studies were conducted. Two of these model studies, four-story five-span and five-story four-span models, are shown in Figure 3.7. In staged construction models, the raft foundation construction was identified as the first stage, and the columns and the slabs of the upper levels were added in a sequential manner of one story at a time to represent the following stages of construction. Consequently, there are five construction phases for the four-story case and six phases for the five-story case. In the last phases, roof forces were defined at the top of the column locations.

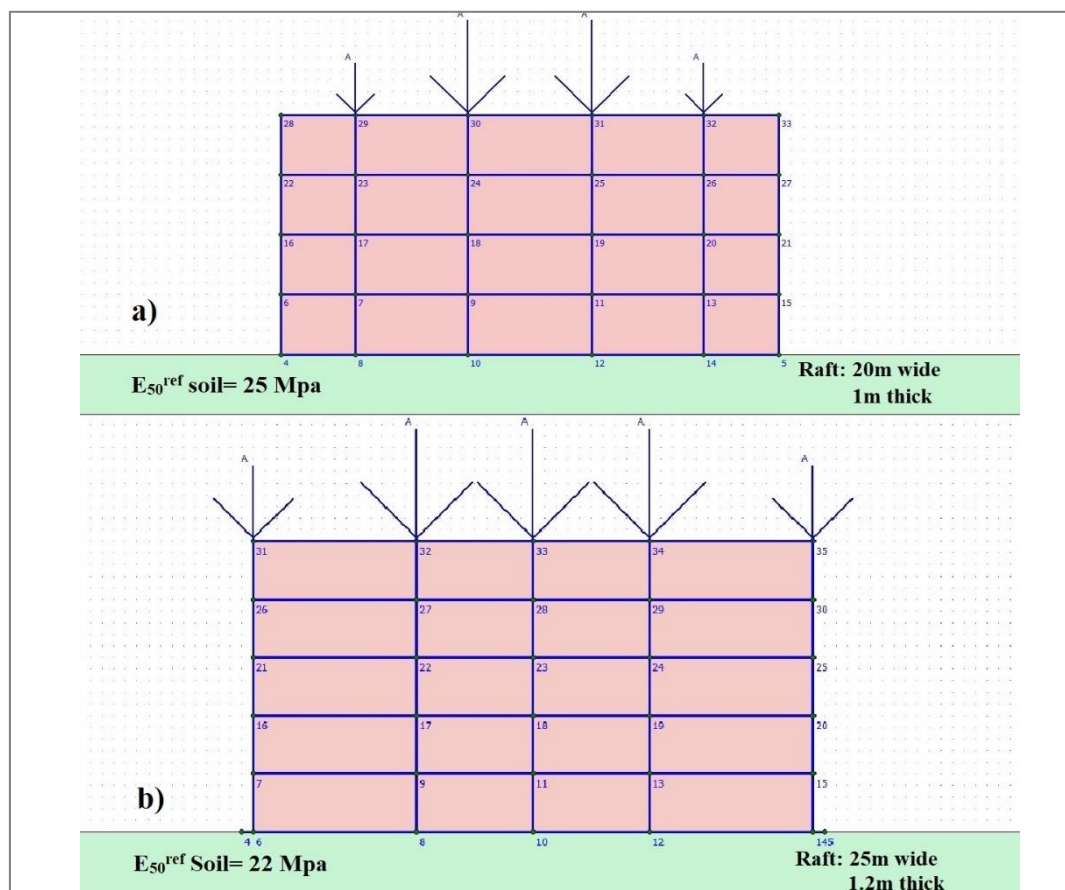


Figure 3.7 General model views of the two 'Staged Construction' cases in PLAXIS:
(a) four-story five-span model and (b) five-story four-span model

A comparative analysis between the results obtained from the staged construction method and the linear static normal analysis (non-staged) approach reveals notable differences in settlement values, settlement response, and internal stress distribution within the raft (refer to Figure 3.8). Specifically, in the staged construction scenario, a reduction of approximately 5 percent in settlement values is observed, primarily concentrated at the edges of the foundation. This decrease can be attributed to the progressive hardening mechanism of the soil during each construction stage. The gradual settlement process compacts the soil, particularly at the foundation edges, resulting in reduced settlement but increased bending moments. The interaction between structural elements during the construction phases may further contribute to this phenomenon. Moreover, the maximum bending moment values show an approximate increase of 50 percent and 30 percent for the respective cases.

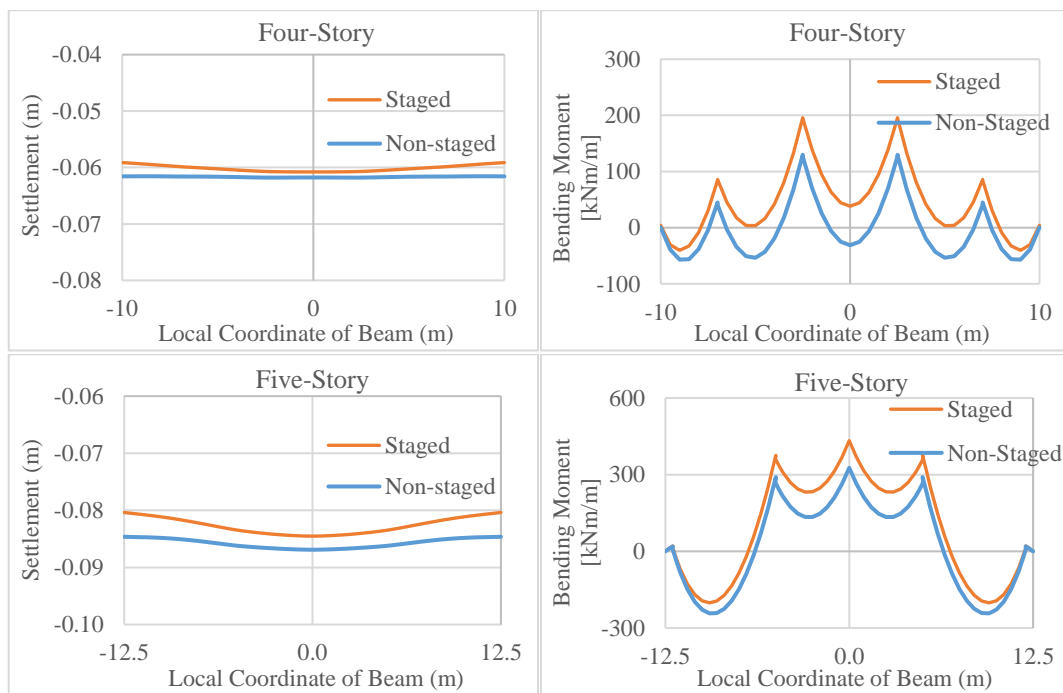


Figure 3.8 Settlement and bending moment results of the foundations for the staged construction method and the linear static normal (non-staged) method

As stated before, the spring constants were also investigated by trial and error so that the settlement and moment values of the raft in SAP2000 were the same as those of PLAXIS 2D. Figure 3.9 shows the spring coefficient distributions obtained for staged and non-staged construction methods. In the staged construction method, the spring constants are almost the same in the middle sections and only get higher values at the foundation edges than those of the linear static (non-staged) method. These increases are in the order of 10 percent and are mainly concentrated on the foundation edges with a length of 5 percent of the foundation width.

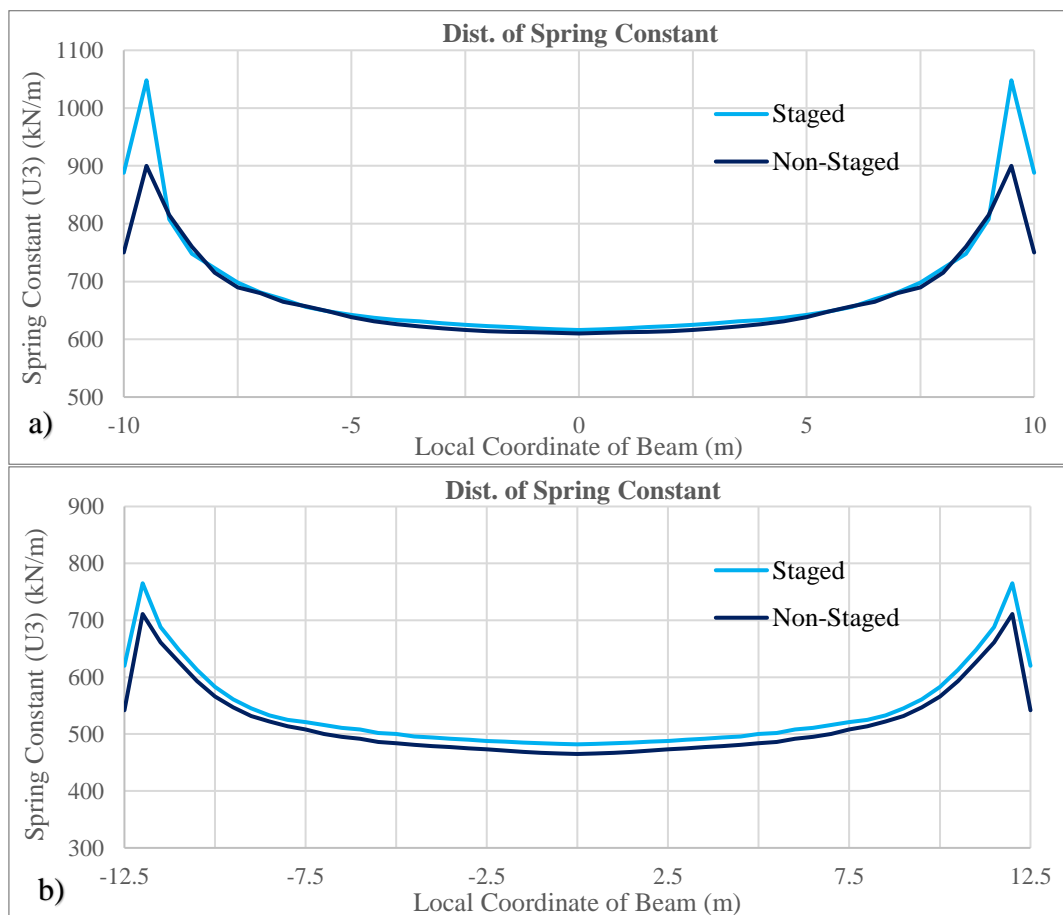


Figure 3.9 Distribution of spring constant values for the staged and non-staged analyses (a) Four-Story, (b) Five-Story

Precise results obtained not only for the raft but also for other superstructure frame elements would show that both software solutions are compatible. In this context, the bending moment values of the slab elements for the five-story case, obtained from both software, were compared (Figure 3.10). The errors for the results of the first slab at the end of the second construction stage and the fifth slab at the end of the sixth stage are at most 5 percent, as was the case in the raft foundation.

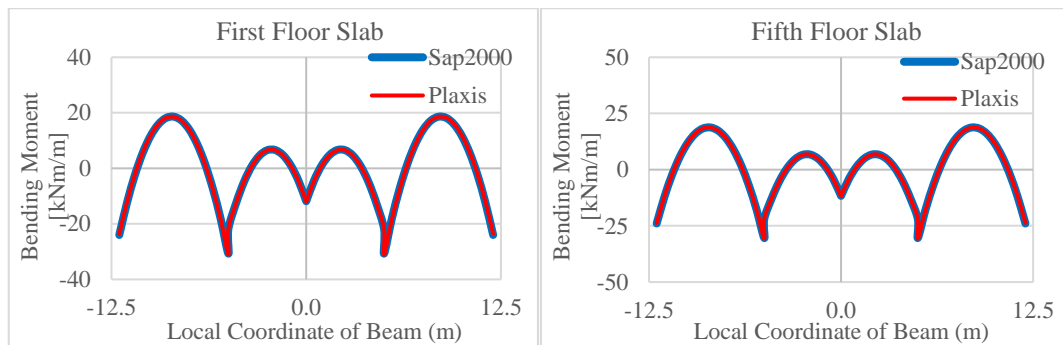


Figure 3.10 Bending moment diagrams of the first-floor slab at the end of the second stage and the fifth-floor slab at the end of the sixth stage

Consideration of stage construction analysis can offer a more realistic calculation of reactions and stresses. It also has effects on soil response, and these effects may be crucial in high-rise buildings with a large number of construction phases. Thus, the staged construction analysis method is used in this study, and its effects are assessed.

3.3 Effects of Number of Stories

In this section, studies were carried out to see how the soil response beneath the foundation would change with the increasing number of structure stories. The initial model had a four-story building with a foundation width of 40 meters and a foundation thickness of 1 meter. The soil properties under the foundations were consistently set as $E_{50}^{Ref} = 25000 \text{ kN/m}^2$ and $\phi = 32^\circ$ across all three models in this section. Subsequently, the number of stories was doubled in each successive model,

with the final model featuring a 16-story structure. For each story, the slab thickness was 200 mm, and the column height was 3 meters. The SAP2000 view of the 16-story structure, which corresponds to the final case, is presented in Figure 3.11.

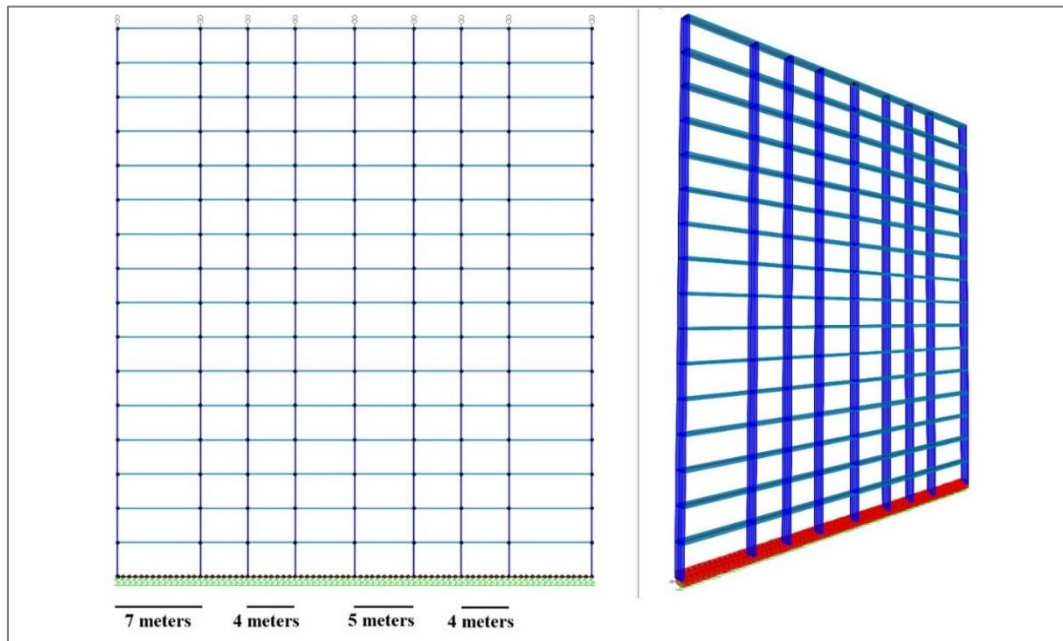


Figure 3.11 SAP2000 appearance of the 16-Story Structure - Final Case

In order to see the changes occurring in subgrade reactions due to the increasing number of structure floors, the results obtained from 3 different models are collected on a graph and examined (Figure 3.12). Upon individual analysis of the results, it is evident that the distribution of subsoil reactions adheres to the general principle of higher reactions at the ends and lower reactions at the center. The maximum spring coefficient value is approximately 1.8 times greater at the ends compared to the center. The variation in subgrade modulus between these two points exhibits a well-correlated second-degree parabolic distribution. With an increase in the number of stories and, consequently, the system's overall weight, there is a slight overall increase in the distribution of spring coefficients. However, no discernible changes are observed in the parabolic shapes in the mid-section of the U form.

In order to better understand the differences between the distributions, the results are examined on a superimposed graph, and it is observed that almost the same distribution occurs beneath the foundations (Figure 3.13). This study shows that the increase in the building's number of stories does not substantially affect the spring coefficient distribution while the values are affected only slightly.

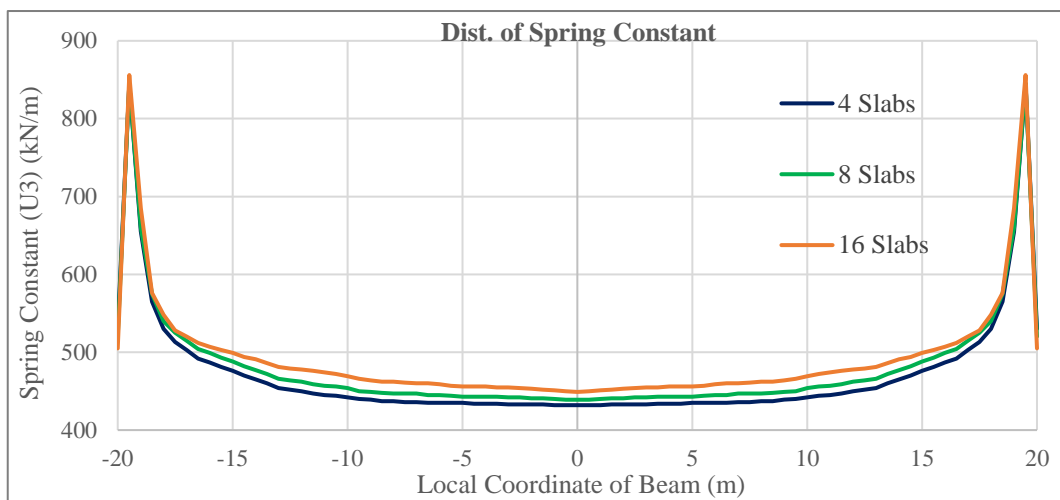


Figure 3.12 Representation of spring constant distributions for the 'Increasing Number of Stories' case

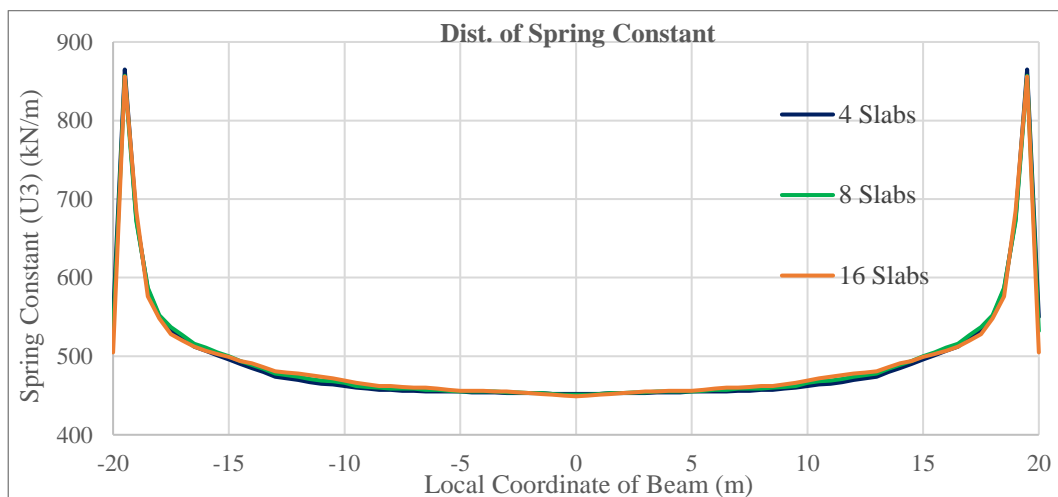


Figure 3.13 Superimposed appearance of spring constant distributions for the 'Increasing Number of Stories' case

3.4 Effects of Foundation (Structure) Width

In order to observe the changes that would be formed in the ground response by the enlargement of the foundation (& structure), five different models were studied. An initial analysis was done by a six-story building having a 20-meter width and 0.8 m thick raft. Modeling continued up to a structure and foundation width of 60 meters by increasing the width by 10 meters at each step. These 10-meter increments were done symmetrically by adding new axes of columns. The slab thickness was 200 mm, and the column height was 3 meters in all analyses.

PLAXIS 2D views of the first and second cases are provided in Figure 3.14, showcasing the general appearance of these models. The analyses were conducted using the dead load and staged construction method without any additional loads applied to the structures. The soil used in these five models can be defined as loose sand, and its properties were; $E_{50}^{\text{Ref}} = 20000 \text{ kN/m}^2$ and $\phi = 31^\circ$ in all the models.

The settlement and bending moment results of the rafts obtained from PLAXIS 2D and SAP2000 software are shown in Figure 3.15. As always, a 5 percent error limit was not exceeded in both the settlement or bending moment results for any of the nodes on the rafts.

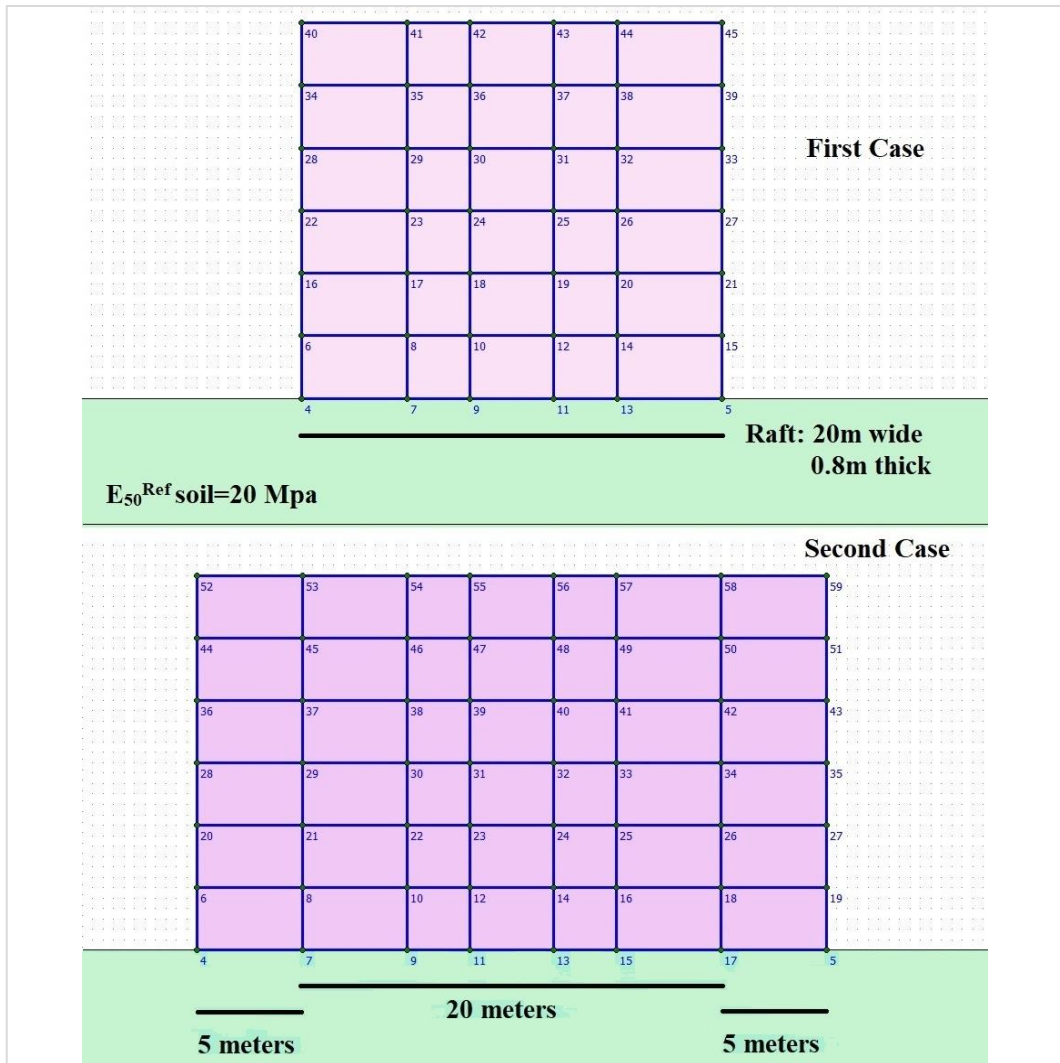


Figure 3.14 General appearance of the first and second PLAXIS 2D models used for the 'Increasing Foundation (Structure) Width' case

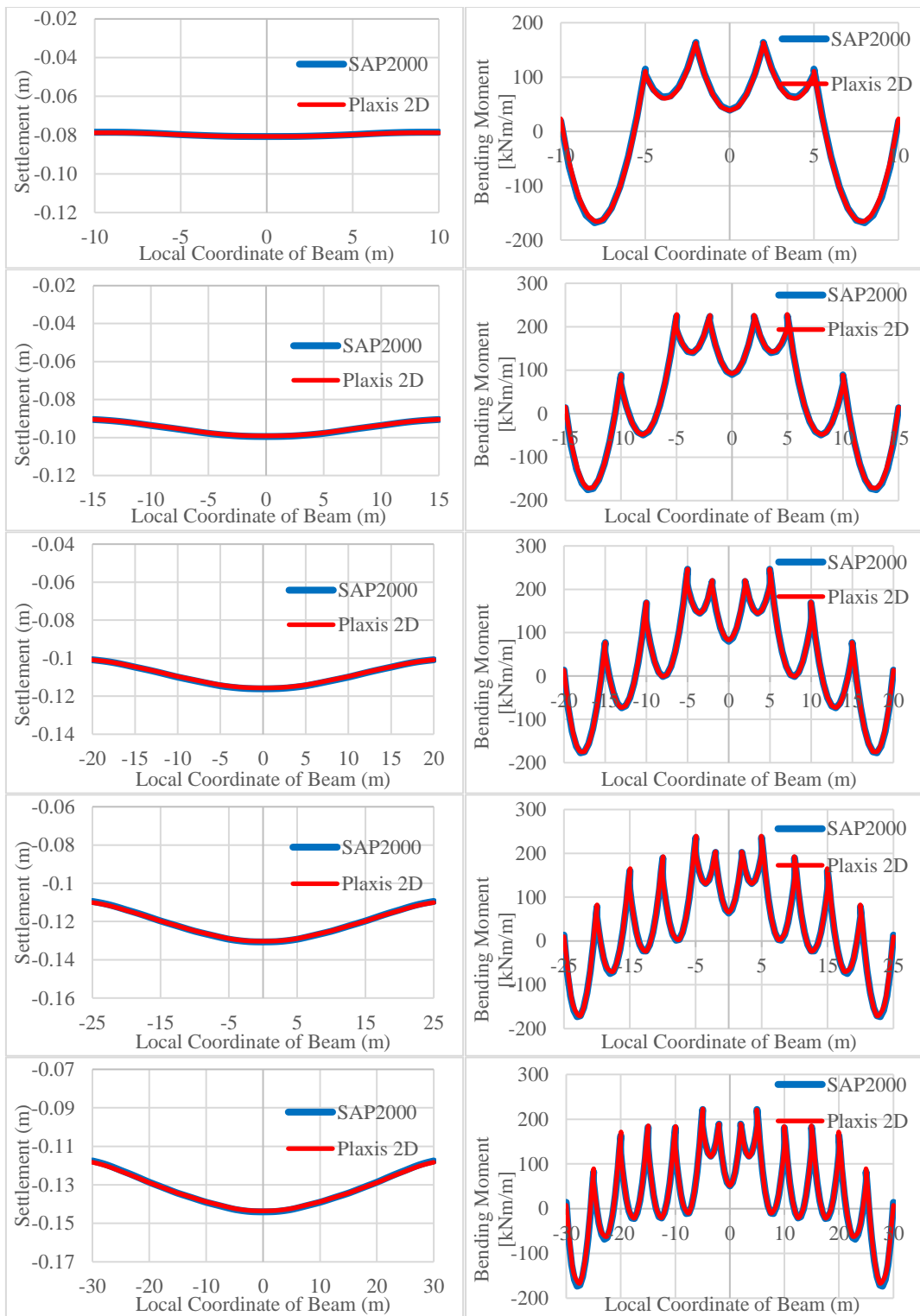


Figure 3.15 Settlement and bending moment results of the foundations for the 'Increasing Foundation (Structure) Width' case

The spring constant variation profile along the width of the raft for the first model (20-meter width) exhibits a typical U shape, with softer middle section springs and significantly stiffer edges. The spring constant at its maximum value was approximately 1.7 times higher than at the midpoint. Figure 3.16 displays the results for the first model and the other four expanding foundation (structure) models. As the superstructure expanded, the middle part of the U shape elongated, and even in the results of the last two models, the concave-up part that forms the center of the U shape started to bend slightly downwards. The increase in constants was more gradual towards the edges. In the third model (40-meter width), the ratio between the maximum spring constant and the midpoint was around 1.8, while for the last two models, it was approximately 1.9.

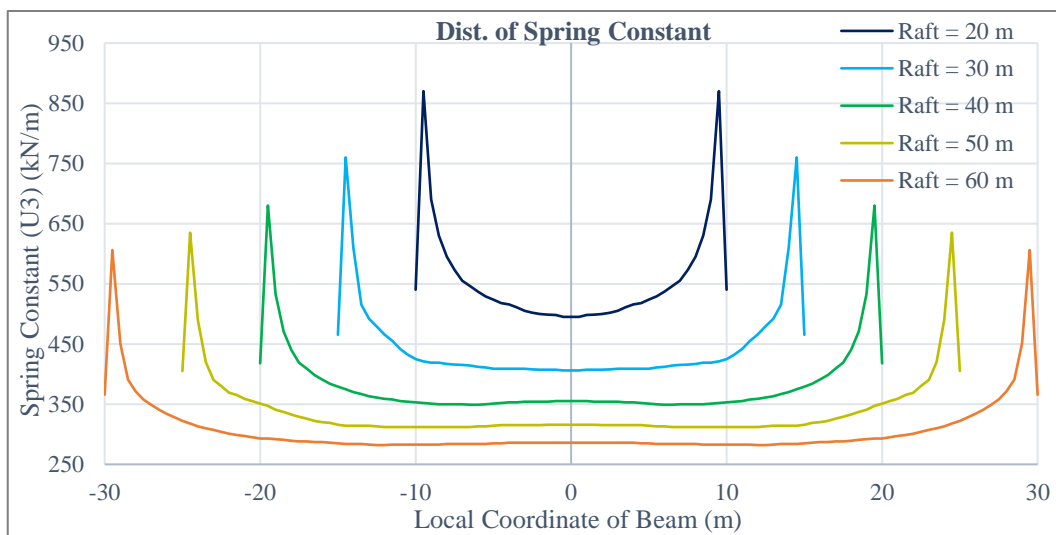


Figure 3.16 Representation of spring constant distributions for the 'Increasing Structure Width' case on a single graph

3.5 Effects of Soil Stiffness

In this part of the study, modeling analyses were carried out by changing the soil parameters while other variables remained constant. The first analysis in this section involved a 10-story building with a foundation thickness of 1 meter and a width of 40 meters, placed on a sand layer with soil properties of $E_{50}^{Ref} = 20000 \text{ kN/m}^2$ and $\phi = 31^\circ$ (Figure 3.17). Incremental changes of 5000 kN/m^2 and 1° were applied to the triaxial loading stiffness (E_{50}^{Ref}) and the angle of shearing resistance (ϕ) from the base scenario.

Only in the last analysis, instead of the 5000 kN / m^2 stiffness increment mentioned above, an increase of 10000 kN / m^2 was made for the triaxial loading stiffness (E_{50}^{Ref}), and the analysis was made with soil parameters of $E_{50}^{Ref} = 65000 \text{ kN / m}^2$ and $\phi = 38^\circ$. In this section, a total of 9 analyses were conducted. The results obtained by the iteration process are collected in Figure 3.18.

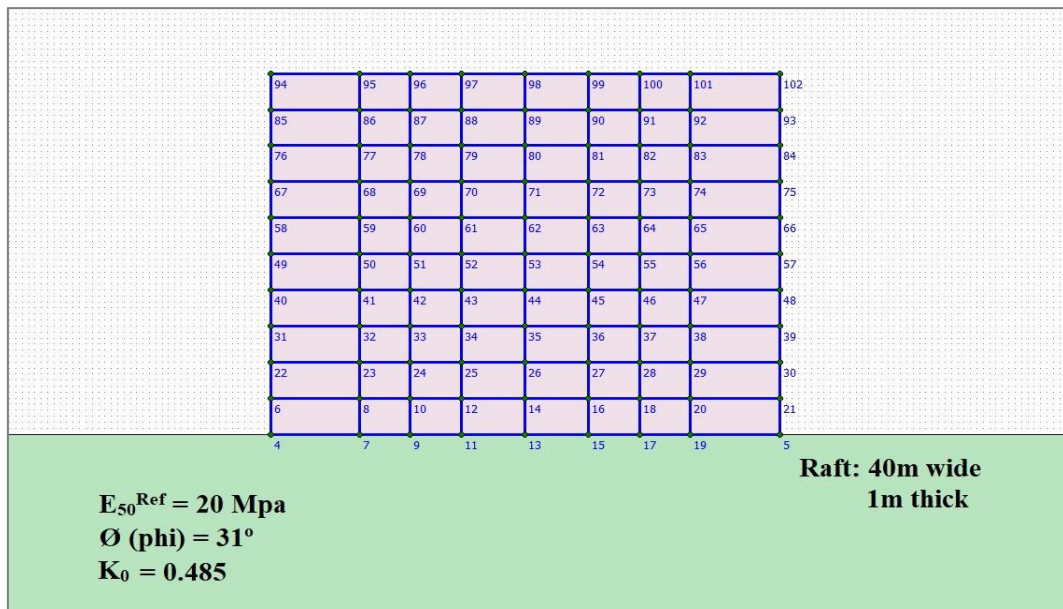


Figure 3.17 General appearance of the first PLAXIS 2D model used for the 'Increasing Soil Stiffness' case

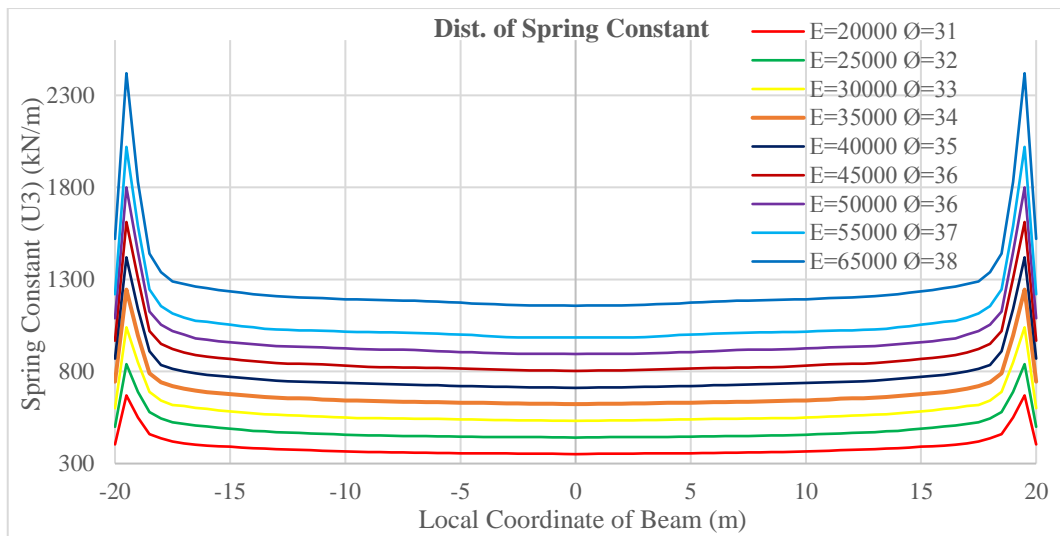


Figure 3.18 Representation of spring constant distributions for the 'Increasing Soil Stiffness' case on a single graph

Upon initial observation, it is apparent that the linear increase in soil parameters leads to an upward trend in the spring constant distributions. The increase in soil stiffness particularly causes a more pronounced rise in spring constants at the edges. The ratio between the maximum spring coefficient value and the midpoint value is approximately 1.9 for the loose sand models, 2.0 for the medium sand models, and 2.1 for the dense sand models.

On a 40-meter foundation, these sudden increases in spring constants begin around 2-3 meters before reaching the foundation edges. When the results are superimposed on a graph (Figure 3.19), it can be observed that as soil stiffness increases, the middle part of the spring constant distribution exhibits a more pronounced concave upward shape toward the edges. It is important to note that the interpretation of the results on the superimposed graph should not be taken in a strictly proportional or quantitative manner, as the vertical positioning of the results on the graph may distort the actual changes. Nevertheless, the superimposed graph provides an exaggerated visualization of the changes that occur with increasing soil stiffness.

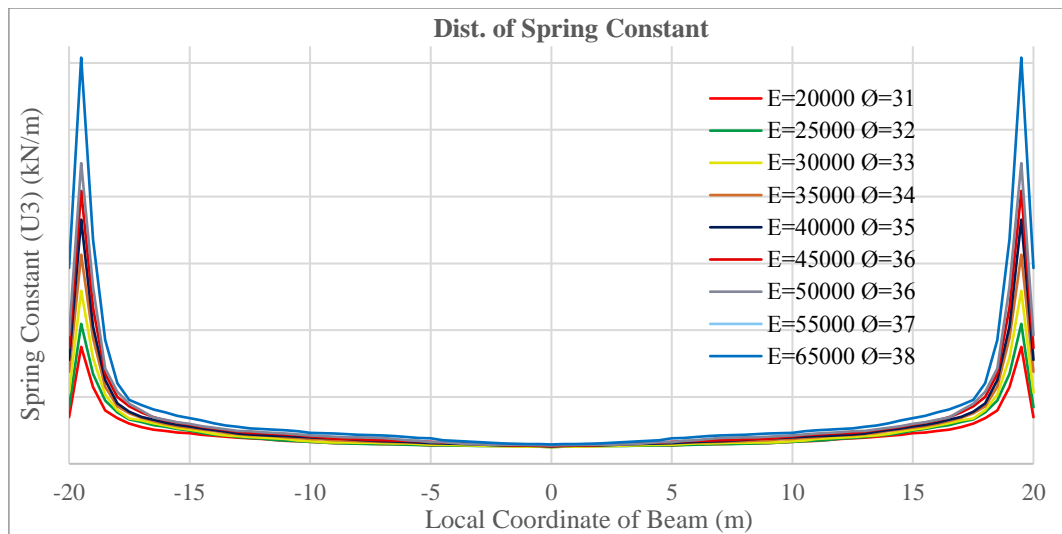


Figure 3.19 Superimposed view of spring constant distributions of the 'Increasing Soil Stiffness' case

3.6 Effects of Relative Stiffness of the Soil-Raft System

This section aims to investigate the influences of relative stiffness changes in the soil-raft system on the distribution of spring constants beneath the rafts. In this context, three interaction analyses were performed. On 20-meter-wide foundations, 0.5-meter-wide distributed loads were assigned to simulate column loads at four locations (Figure 3.20). By changing the foundation rigidity and soil stiffness at the same rate, the effects of the rigidity changes in the soil-raft system have been investigated.

The analyses began with a 1-meter-thick raft foundation, and subsequent analyses were carried out with foundation thicknesses of 1.3 meters and 1.5 meters while maintaining the same boundary and loading conditions. The increase in raft thickness led to approximately 2.2 times and 3.375 times increases in the foundation's flexural rigidity (EI) for the cases of 1 meter to 1.3 meters and 1 meter to 1.5 meters, respectively. These progressive increases in flexural rigidity (EI) were also reflected in the deformation parameters of the underlying soil, resulting in a linear variation in the stiffness of the soil-raft system.

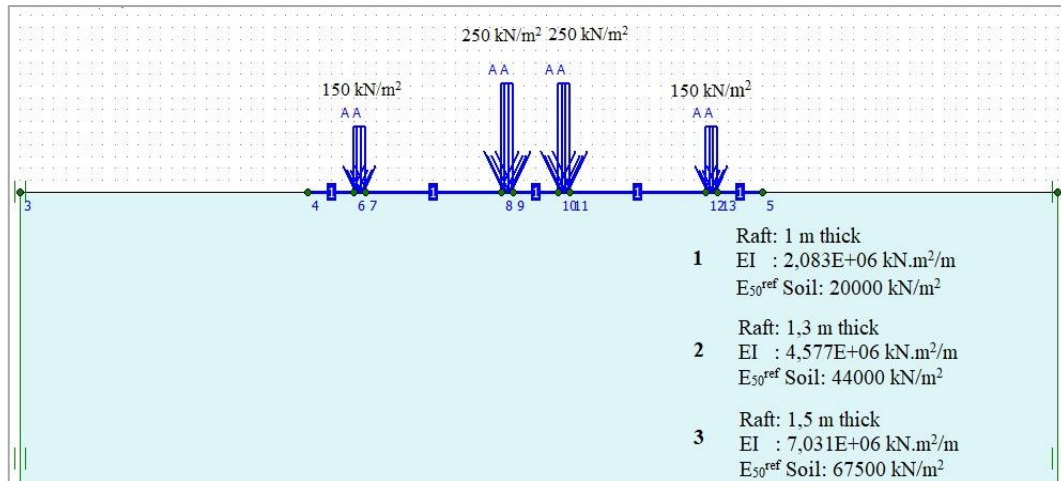


Figure 3.20 General view and properties of the models for the 'Relative Stiffness Changes in Soil-Raft System' case

As a result of changes in foundation thickness and soil parameters, different settlement values and spring constant distributions were obtained for all three cases. Figure 3.21 illustrates the settlement and bending moment results obtained from PLAXIS 2D, as well as the spring constant distributions used to obtain those results in SAP2000. It can be observed that increasing soil stiffness led to decreases in settlement values. However, the settlement shape and bending moment results showed no significant variations. In contrast to Section 3.1, where increasing the thickness of the raft foundation exhibited significant variations in settlement characteristics, maximum settlement values, and bending moment results, the current analysis reveals a different trend. In this case, the gradual increment in both the raft thickness and soil stiffness appears to balance out these differences. Despite the self-weight, acting as a distributed load due to the increase in foundation thickness, settlement and moment values in the foundation were mitigated. The increased soil stiffness resulted in higher spring constants and the general shape of the spring constant distributions remained in the U form. Sharp increases in spring constants were observed in the last 2.5-3.0 meters near the edges. Proportional evaluations of the maximum values and values at the midpoints yielded approximately 1.5 for all three distributions.

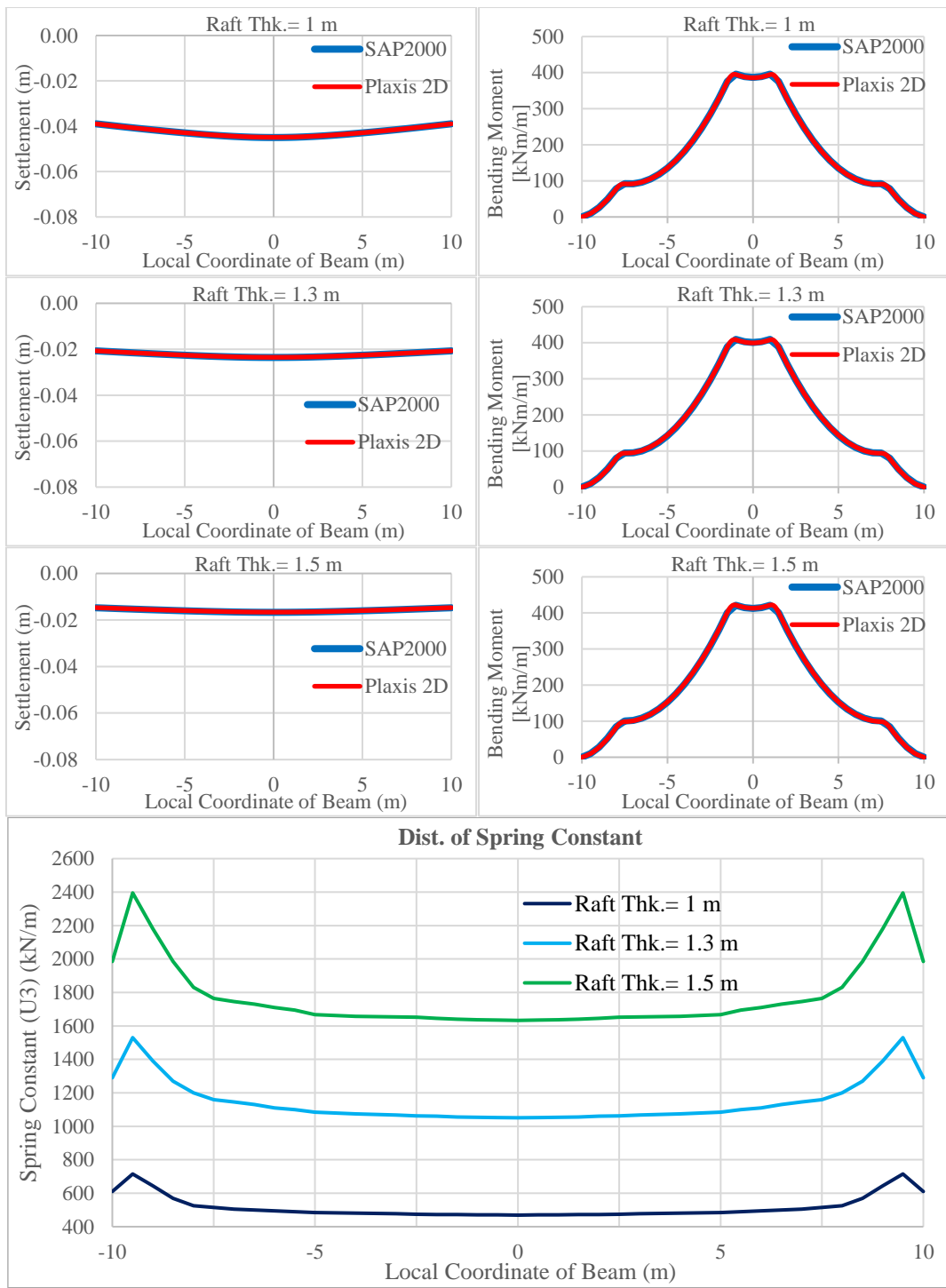


Figure 3.21 Settlement, bending moment, and the linked spring constant distribution results for the 'Stiffness Changes in Soil-Raft System' case

In order to figure out to what extent the gradual increment in the soil-raft system affects the increase of spring constants at the edges, a scale value at the rate of increment in the rigidity of the foundation was applied to the superimposed appearance of coefficient distributions (Figure 3.22). In more detail, the spring constants of the second case have been divided by 2.2 because of the approximately 2.2-fold increase in rigidity between the first and second cases, and the spring constants of the third case have been divided by 3.375 because of the approximately 3.375-fold increase in rigidity between the first and third cases. Upon examining the scaled superimposed appearance of the coefficient distributions, it can be observed that linear increases in the stiffness of the soil-raft system have an almost linear effect on the distribution of spring constants.

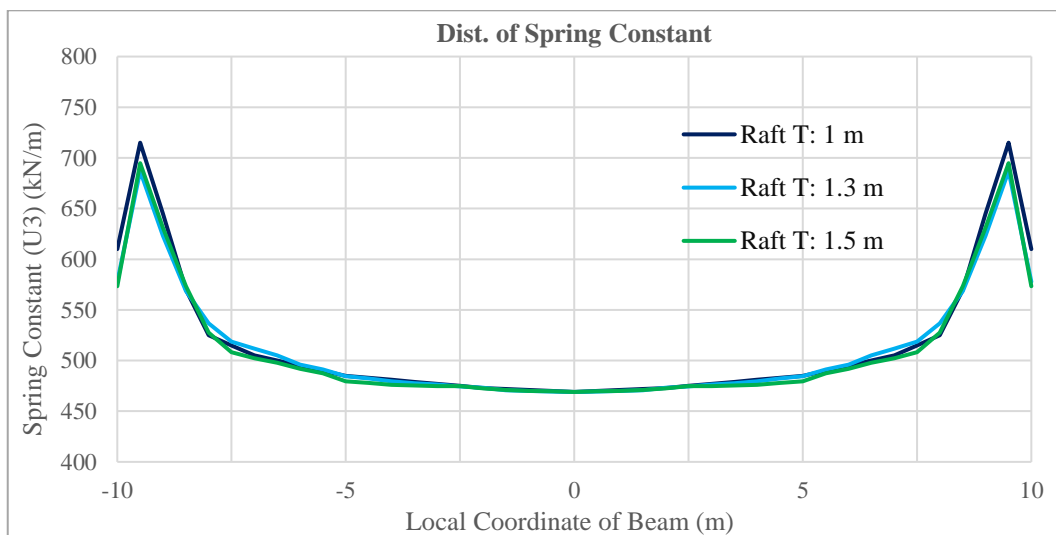


Figure 3.22 Scaled appearance of superimposed spring constant distributions of 'Relative Stiffness Changes in Soil-Raft System' case

3.7 Replacement of Superstructure with a Thicker Foundation

This part of the study tried to examine the changes that would occur in spring constant distributions in the case of expressing the rigidity of the superstructure system with a single thicker foundation. In this context, 2 cases were analyzed: a five-story four-span model and a four-story five-span model. First, linear static (non-staged) analyses were performed for both cases, and the spring constant distributions beneath the rafts and the forces acting on the frame elements were determined. Then, the flexural rigidity of the superstructure system was simply calculated, and the thickness of the new single raft foundation, with an equivalent flexural rigidity to the system, was determined. The weight difference between the two models was calculated, and the calculated difference has been applied to the column positions in the ratio of loads acting on the frame elements in the previous models.

Obtained new system was analyzed, and spring constant distributions were determined and compared. The general appearances of PLAXIS 2D models are shown in Figure 3.23, and the detailed calculations for the new single raft foundations are presented in Appendix B.

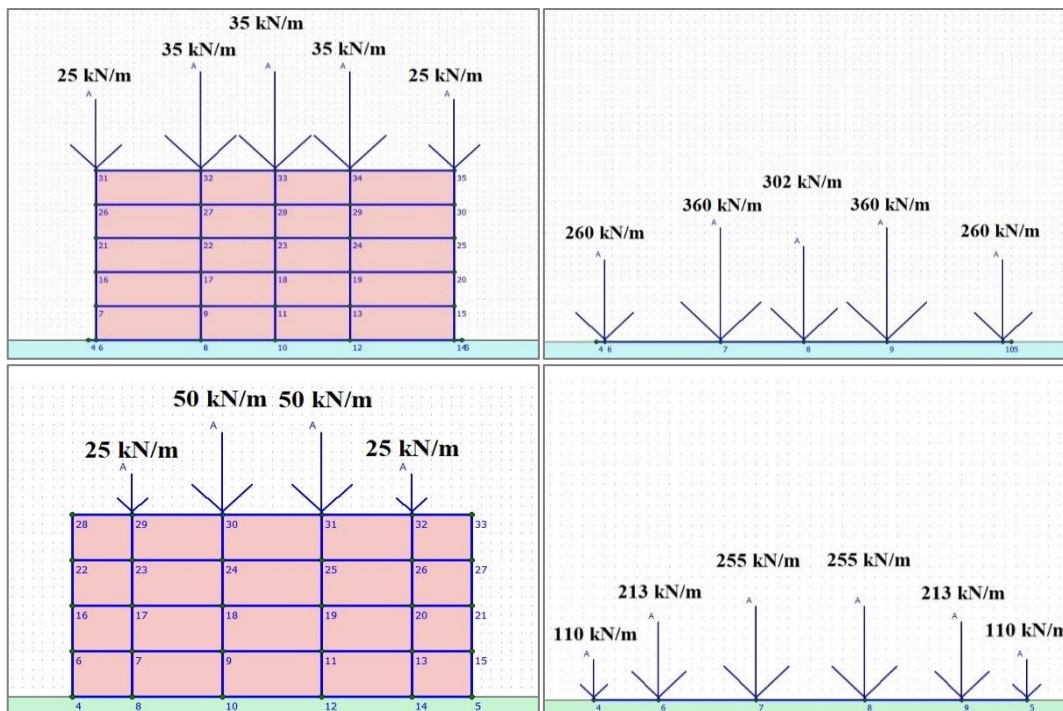


Figure 3.23 General appearance of the five-story four-span and four-story five-span superstructure models, as well as their replacement with thicker foundations

When the results are examined, it is seen that the spring constant distributions found by modeling the frame system are not very different from the results of the thickened raft model that replaces the frame system. In the condition of replacement of the structure and its' foundation with a single thicker foundation, the distribution results were almost the same in the middle parts of the foundations. Only slight decreases of about 5 percent are observed at the edges (Figure 3.24). Since there is no significant difference between the models in terms of total weight, the general averages of total spring resistances are too close to each other. In both cases, distributions are generally in a U form. While simulating the entire structure with a single thicker foundation neglects the interaction between the frame elements, it is worth noting that this simplification has only a slight impact on the spring constants at the edges of the foundation. This finding can be valuable in simplifying complex models without significantly compromising the accuracy of the spring constant distributions.

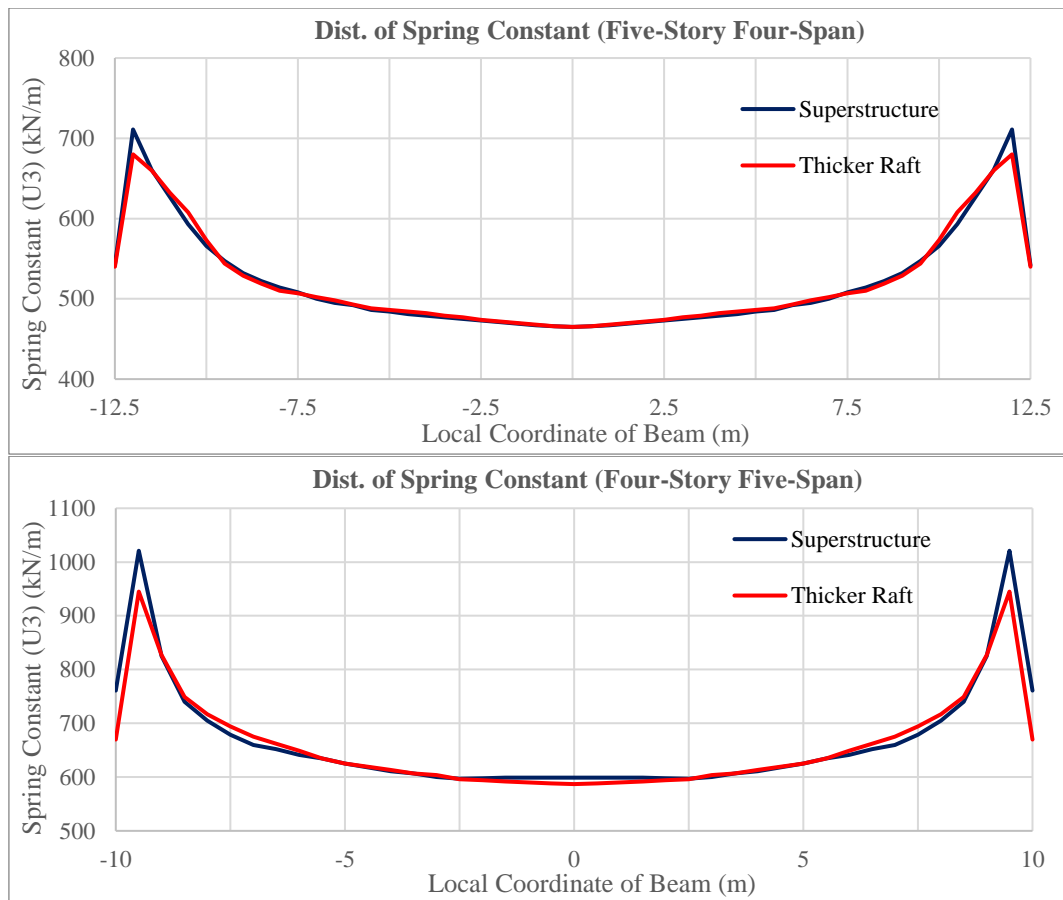


Figure 3.24 Distribution of spring constant values for the 'Superstructure Rigidity Reflected by a Single Thicker Foundation' case

3.8 The Case of Structure Width Less Than Foundation Width

Construction models with wider foundations than the superstructure, which are commonly employed in residential and office projects, are the focus of this part. Unlike previous modeling studies where the foundation and superstructure widths were equal, this section investigates cases where the raft widths are greater than the superstructure widths.

The modeling analyses started with a 30-meter-wide structure comprising 20 stories, placed on a 60-meter-wide foundation with a thickness of 1.20 meters (the foundation was wider than the structure by 15 meters on both sides). Subsequently,

in the following analyses, all model variables, such as soil properties, structure width, number of stories, and foundation thickness, remained constant except for the foundation width. The foundation width was 45 meters in the second analysis, 39 meters in the third analysis, 37 meters in the fourth, 34 meters in the fifth, and 30 meters in the sixth. As a seventh and final step, 4-story additional structural parts have been added to the raft edges that are wider than the superstructure at the right and left sides of the first model. Figure 3.25 provides a visual representation of this section's first, second, fourth, and seventh models.

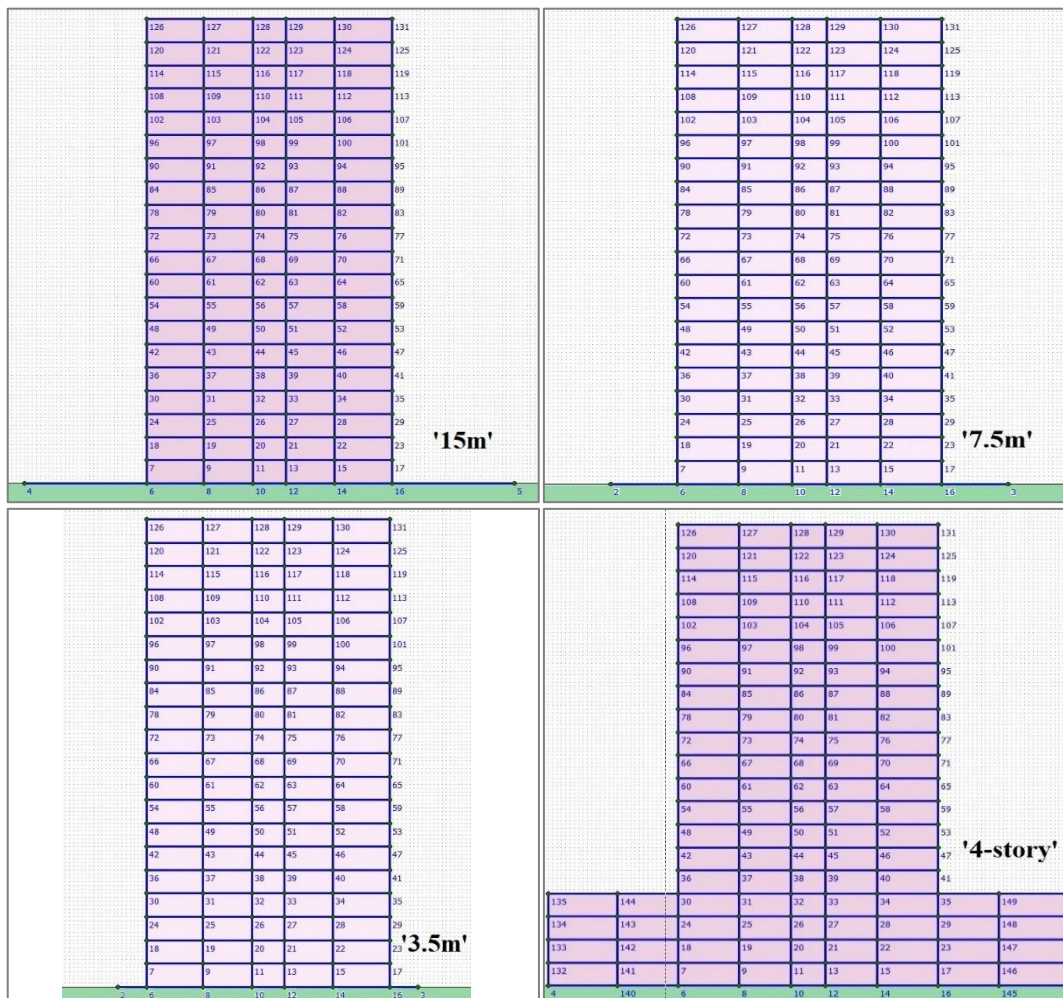


Figure 3.25 General view of the first, second, fourth, and seventh models for the 'Structure Width Less Than Foundation Width' case

In Figure 3.26, the foundation settlement and spring coefficient distributions, obtained from all the analyses of this case, are given. It can be seen that the amount of differential settlement formed in the foundations decreases as the widths of the foundations approach the widths of the buildings. The maximum total average settlement is seen on the '0m' model, which has the smallest raft width. As the raft width decreases, the settlement profile transforms from a U shape to a straight form. In the distribution of spring coefficients, the situation is the opposite. As can be recalled, the previous models, in the case of foundation width and building width being the same, resulted in the spring constant distribution being the usual U shape. However, here, as the settlement profile transforms from the U to a straight shape, the spring coefficients advance from the straight to the U shape. If the width of the foundation is much larger than the width of the building, it may even happen that the spring coefficients are less at the edges of the foundation and more at the middle of the foundation. Of course, the fact that the foundation width is 15 meters larger than the building width from the right and left sides express an exaggerated situation. Because it is not common for a 1.2-meter-thick foundation that is much larger than the width of the building without supporting any structure. However, this situation reveals that the spring constant distributions may not only be in the U shape.

When additional 4-story structural parts are added to the sides of the high-rise building, the spring constant distributions demonstrate an attempt to return to their classical distribution form. The analyses for this case show that the effects of loading conditions or positions are significant on the spring constant distributions. Actually, this reveals that the Pseudo-Coupled method, described in section 2.2.3, may lead to inaccurate results because it assumes that the spring constants are always higher at the foundation edges, regardless of the superstructure loading conditions. However, the findings from these analyses show that the foundation's loading conditions influence the spring constant distributions, and it is necessary to consider the specific loading conditions when determining the spring constant distributions rather than relying solely on a generalized approach.

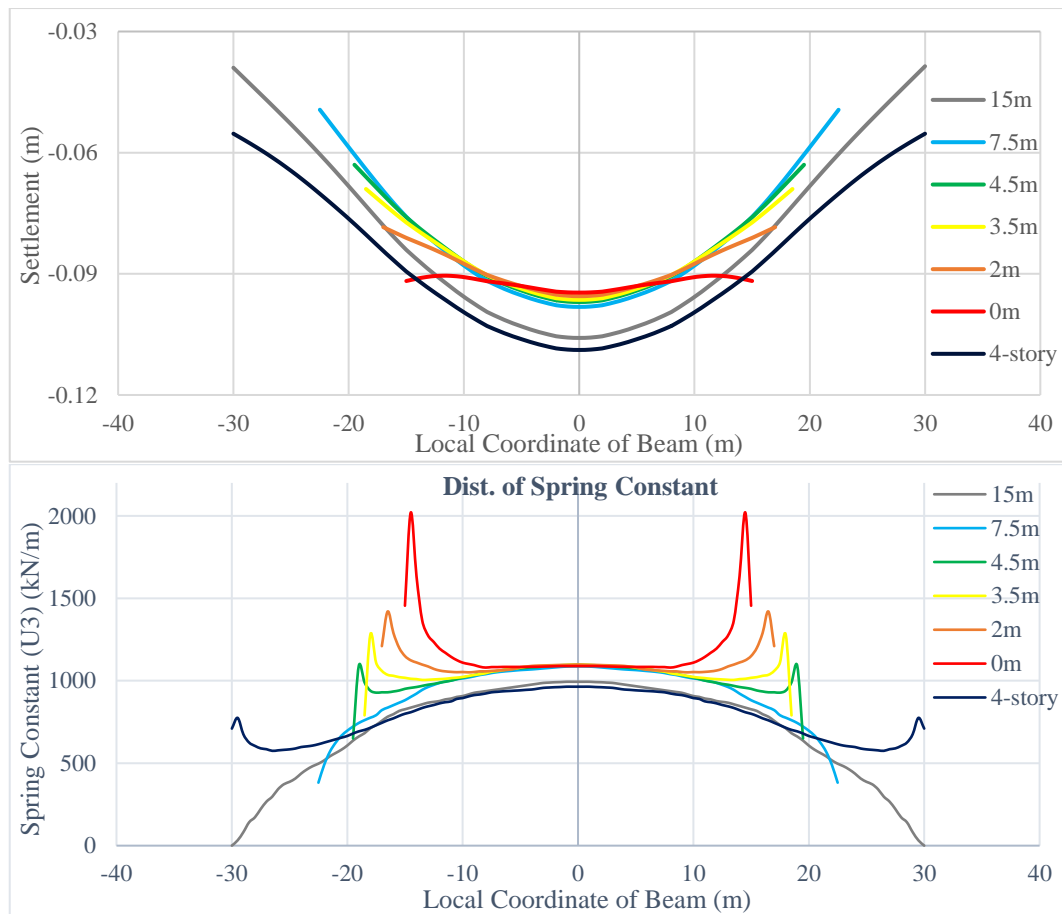


Figure 3.26 Superimposed appearance of settlement and spring constant distributions of the models for the 'Structure Width Less Than Foundation' case

3.9 Effects of Column (Loading) Positions

After examining the effects of superstructure loading positions on the spring coefficients, further investigations were conducted to analyze the impact of column positions. For this purpose, two cases involving 6-story structures were modeled with a raft thickness of 0.9 meters and a length of 21 meters. The soil parameters, including $E_{50}^{Ref} = 35000 \text{ kN/m}^2$ and $\phi = 33^\circ$, were identical for both models. The only difference between the two models was the distance between the two interior columns, which was 5 meters instead of 9 meters in the latter (Figure 3.27).

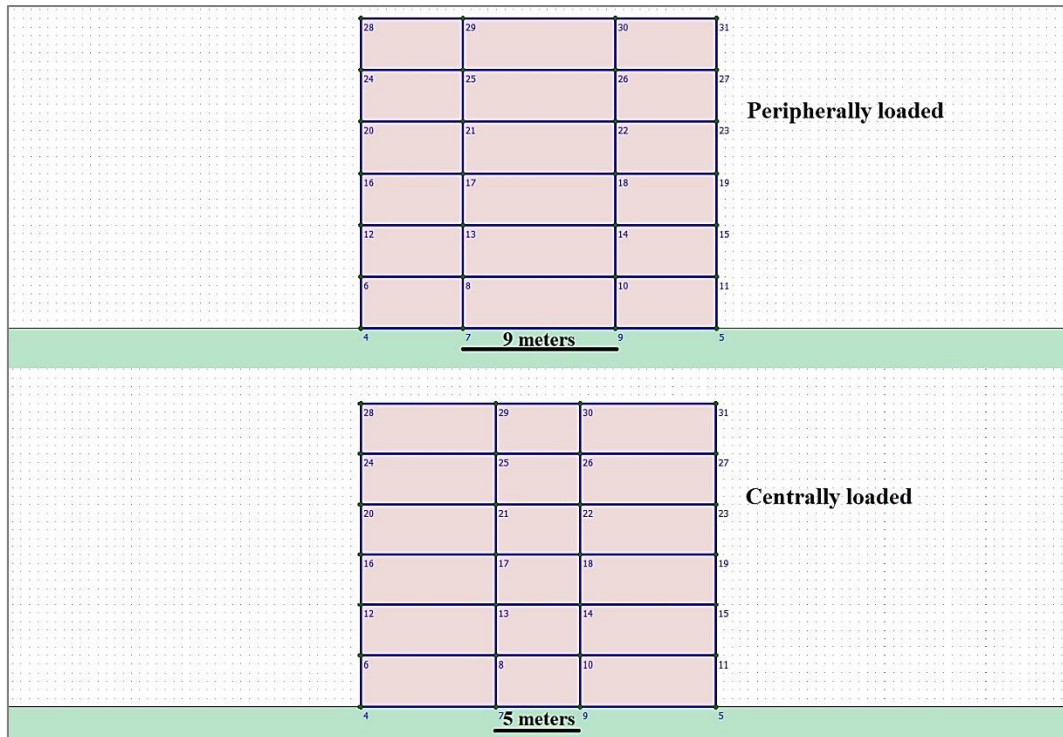


Figure 3.27 General appearance of the two PLAXIS 2D models used for the 'Column (Loading) Positions' case

When the settlement and bending moment results obtained from the two models are examined, it is observed that both foundations are settled equally in terms of the total average settlement. However, at the mid-section of the foundations, dissimilar settlement curves and, depending on the column positions, different maximum moment locations and values are observed (Figure 3.28). Figure 3.28 also provides a clear visualization of how this difference in column spans influences the distribution of spring constants.

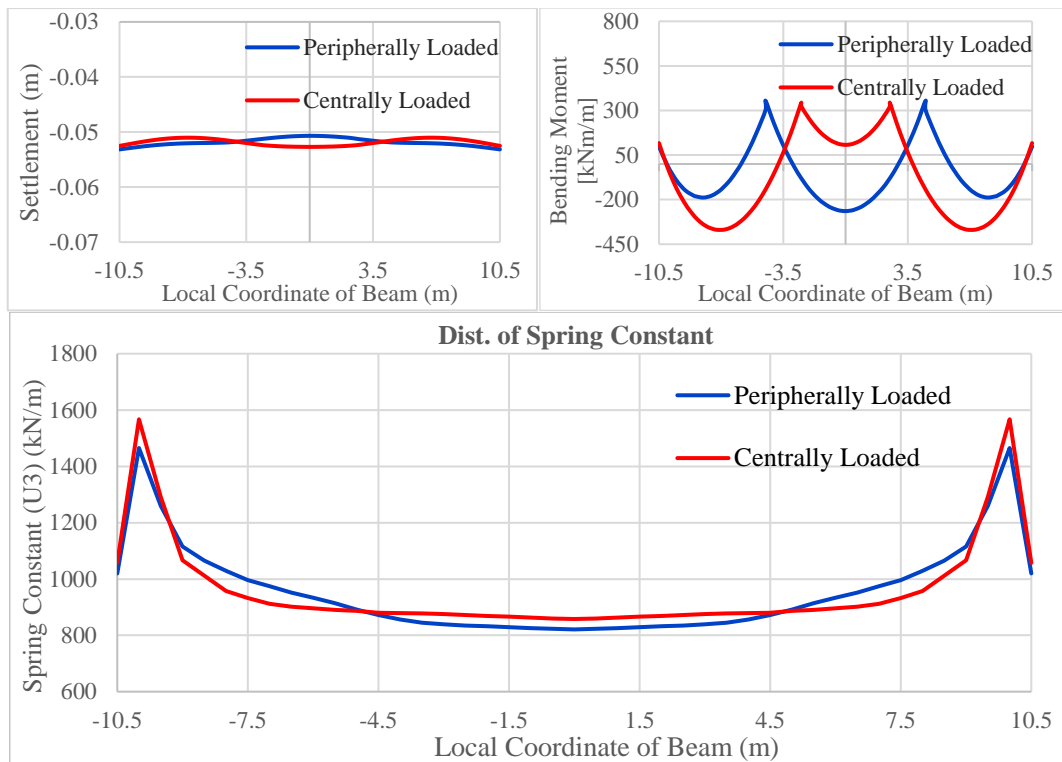


Figure 3.28 Settlement, bending moment diagrams, and variation of spring constant distributions according to column positions

In the centrally loaded case, the spring constants at the foundation edges were stiffer, despite the edge-to-center ratio being approximately 1.80 for both cases. The spring constants in the mid-part exhibited a more pronounced upward curvature when the column loads were located away from the foundation's center (peripherally loaded case) compared to when they were positioned closer to the center (centrally loaded case). This observation also explains the results observed in cases where the structure is narrower than the foundation width. In such situations, an inverted U-shape pattern emerges due to the structural loads predominantly being concentrated near the foundation's center. As the structural loads shift towards the edges, an upward curvature in the spring constant profile is initiated from the center. It is worth noting that the loading position is a critical factor in estimating and formulating spring coefficient distributions.

Based on these observations, the column positions of all 53 models were evaluated. Since all models were symmetrical with respect to the midpoint of the foundations, the resultant force positions of column loads acting on one-half of the foundation were calculated. The ratio of this resultant's distance from the foundation edge to the foundation width, referred to as the Load Concentration Ratio (LCR), was utilized to quantify the concentration of structural forces on the raft foundations (Figure 3.29). LCR can be calculated using the equation:

$$LCR = \frac{R_x}{W/2} \quad (3.1)$$

where R_x represents the resultant force's distance from the foundation edge, and W is the foundation width. This ratio indicates the concentration of resultant structural forces on the raft foundations. The LCR values calculated for all the models within the scope of this study are listed in Appendix C. When analyzing the distributions of spring coefficients, grouping the similarly distributed structural loads that concentrate on specific parts of the foundation and interpreting these groups is more accurate.

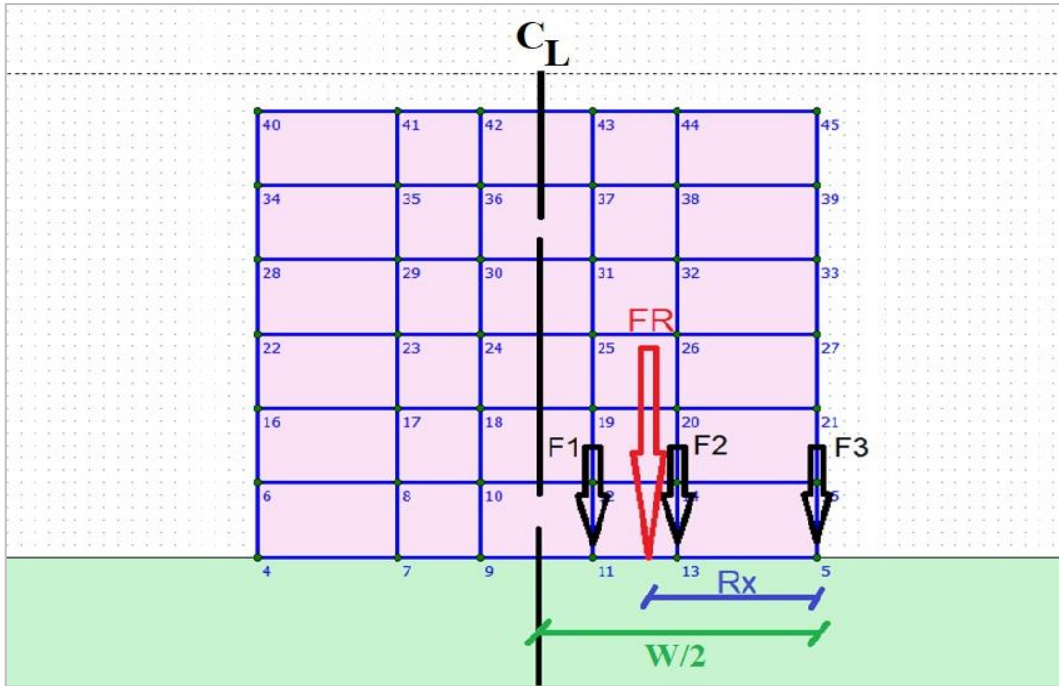


Figure 3.29 Sample view of the resultant force positions of the column loads acting on the foundation

CHAPTER 4

RELATIONSHIP BETWEEN SPRING CONSTANTS AND PROBLEM VARIABLES

As noted in the previous chapter, besides the minor effects of the number of stories, other variables, such as soil stiffness, foundation thickness, and loading positions, strongly influence the subgrade modulus distribution. These effects are case-specific and vary depending on the conditions. Understanding and predicting these spring constant distributions are crucial and form one of the main objectives of this study.

4.1 Correlating the Subgrade Modulus Distribution to Problem Parameters

Drawing from this knowledge and experience, a study has been initiated to establish a simple relationship and predict spring coefficient distributions by considering relevant variables. The emphasis on a 'simple relationship' stems from the intention to promote the practical use of assessments and results in routine engineering practice. While the existing literature may present complex findings and methods, they are often not utilized in routine projects and commercial software.

Generally, an increase in soil and structure stiffness leads to higher spring constants at the edges of the foundation. Moreover, when the superstructure loads are concentrated towards the center of the foundation, the spring constant distributions transform from a concave-up form to a concave-down shape in the middle of the foundation. In general, the distribution of spring constants follows a second-degree parabolic shape in the middle of the foundation, with abrupt variations at the edges. Thus, by taking the symmetric foundation's midpoint as a reference and dividing the distribution on the right side of the foundation into two segments, the spring coefficient distribution can be represented by the following relationship:

$$k(x) = k_0 + ax^2, \text{ if } x \leq x_1 \quad (4.1a)$$

$$k(x) = k_0 + ax_1^2 + c(x - x_1), \text{ if } x > x_1 \quad (4.1b)$$

where k_0 represents the initial value at the centerline, x denotes the absolute distance of a point on the foundation from the foundation's center, x_1 is the reference distance that determines the transition point between the two equations, and a and c are coefficients that control the variation and magnitude of the spring coefficient in their respective regions (Figure 4.1).

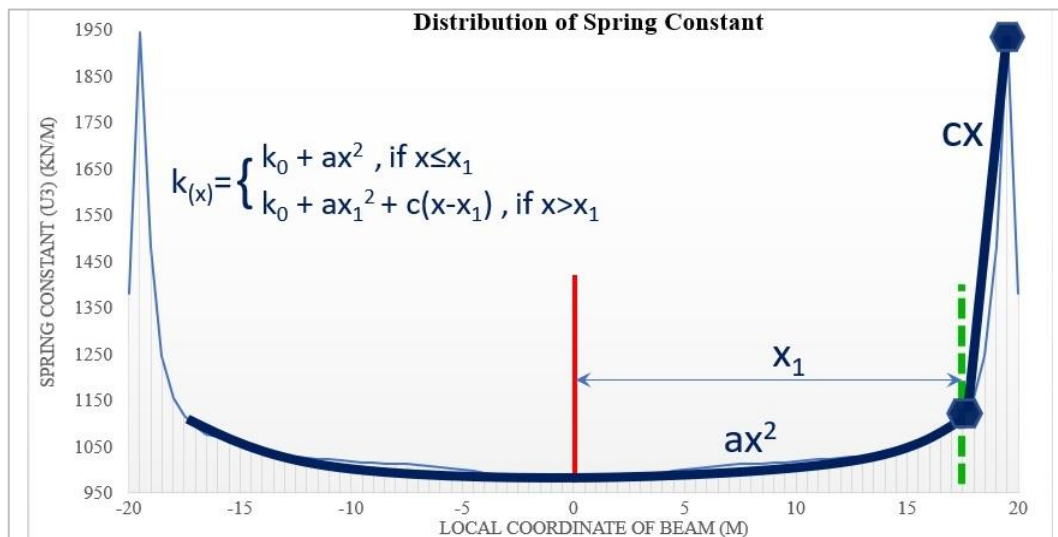


Figure 4.1 Functional representation of the distribution of spring constants

The three parameters, the coefficient 'a,' transition point 'x₁,' and coefficient 'c,' have been calculated for all 53 models studied thus far using an Excel solver and the least square method to derive the best-fit coefficient distributions. Scatter plots have also been prepared to seek correlations between these parameters and the 'relative rigidity' abscissa, which encompasses both soil stiffness and structural rigidity, the two main contributors to the distribution of spring coefficients. The purpose of these scatter plots is to identify any correlations through the use of best-fit lines. The complete set

of obtained results is graphically presented in Appendix D, including snapshots of the analyses. In these graphs, the blue line represents the spring coefficient distributions obtained through iterations, while the brown line depicts the best-fit distributions obtained from MS Excel. Additionally, the display in Appendix D includes the spring constant distributions obtained from the proposed relations, which will be discussed in detail below. These distributions are represented by black lines.

Based on the results, this relationship form effectively represents the distribution of spring constants. The highest deviations occur near the edges of the foundation, where sudden changes in spring constants are observed. However, the relationship form provides a good fit outside of those areas. While it is possible to achieve better results with higher-order relationships, it is important to emphasize that the primary objective of the study is to enhance current common practices by maintaining simplicity and convenience.

MS Excel Solver calculated the best-fit distribution for these 53 analyses and computed the terms that form the proposed Equation 4.1. Therefore, the results for the ' k_0 ', ' a ', ' x_i ', and ' c ' are present for each analysis. By understanding how these coefficients behave in response to variations in certain factors, such as changes in soil stiffness, foundation thickness, or building loading conditions, the expected values of the spring constants beneath the foundation can be determined based on some preliminary project information. This can provide valuable insights for design and analysis purposes, allowing for more accurate modeling and assessment of soil-structure interaction.

In this context, three scatter plots were created to visualize the correlations for the coefficient ' a ,' the transition point ' x_1 ,' and the ' k_{edge}/k_{x1} ' ratio under different conditions. As mentioned in Chapter 3, the system's rigidity is one of the most significant factors that influence the distribution of spring constants beneath the foundation. Therefore, in the scatter plots for the coefficient ' a ' and the ' k_{edge}/k_{x1} ' ratio, the x-axes are labeled as 'relative rigidity (RR),' which combines both soil

stiffness and structural rigidity. The choice to create a scatter plot for the ' k_{edge}/k_{x1} ' ratio instead of ' c ' is due to the observed limitations in establishing a well-defined relationship between ' c ' and the RR. However, the ' k_{edge}/k_{x1} ' ratio exhibited a stronger correlation with RR, making it a more suitable parameter for assessing the spring constant distribution. The position of ' k_{edge} ' is specifically chosen to be located at the node just before the foundation edge. In the models, where the spring node spacing is consistently set as 0.5 m, this corresponds to a distance of 0.5 m from the foundation edge. This choice also allows for the effective elimination of potential boundary effects associated with the direct interaction between the foundation edge and the surrounding soil.

The usual form of a rigidity measure contains the variables that are related to the stiffness of the mat in the numerator and the same for the soil in the denominator. Equation (4.2), which is both in the German standard (DIN 4018) and Egyptian code (ECP 196-1995), presents a relative rigidity ratio based on a strip having a unit width by comparing soil modulus with data such as foundation width, foundation thickness, and modulus of foundation material.

$$k_{st} = \frac{E_b}{E_s} \left(\frac{d}{W} \right)^3 \quad (4.2)$$

where E_b is the young modulus of foundation material, E_s is the young modulus of soil, d is the foundation thickness, and W is the foundation width. $k_{st} > 2$ indicates a very rigid foundation, $k_{st} < 0.005$ indicates a flexible foundation, and $0.005 < k_{st} < 2$ indicates a semi-rigid foundation according to Egyptian code.

Instead of solely assessing the rigidity between the soil and the raft foundation, relative rigidity (RR), which considers the combined rigidity of the entire superstructure, including the slabs on each floor, is employed. The flexural rigidity of the slabs is calculated based on the number of stories and is subsequently

incorporated into the existing flexural rigidity (EI) of the raft foundation. This results in the development of a thicker raft foundation with an equivalent flexural rigidity. The flexural rigidity of the new thicker raft foundation is then compared with the rigidity of the underlying soil, enabling the determination of the relative rigidity (RR). By accounting for the contribution of the slabs, this comprehensive approach offers a more accurate representation of the overall system rigidity, enhancing the analysis and design considerations for soil-structure interaction. It is essential to acknowledge that the neglect of column effects in the analyses is a simplification made for the study, as the inclusion of column effects is highly case-specific and would require additional investigation tailored to specific project conditions.

In order to accurately present the relationships between the spring coefficient distribution and the relative rigidity, it is also crucial to consider the loading positions of the superstructure. In presenting the associations between the coefficients and the proposed rigidity factor, the loading positions of the superstructure mentioned in Section 3.9 were also considered. To ensure accuracy, extreme cases where the resultant load from half of the superstructure is located in the middle of the foundation or very close to the foundation edges were excluded. The remaining 46 model results were used to create scatter plots, where the data were categorized based on LCR into three distinct groups representing different resultant positions of the superstructure forces. This categorization provides an understanding of how the varying loading positions influence the spring coefficient distribution.

According to Figure 4.2, the curvature parameter 'a' exhibits a range of values from -2 to +4. It ascends with increasing relative rigidity, indicating greater upward concavity in the middle portion of the distribution.

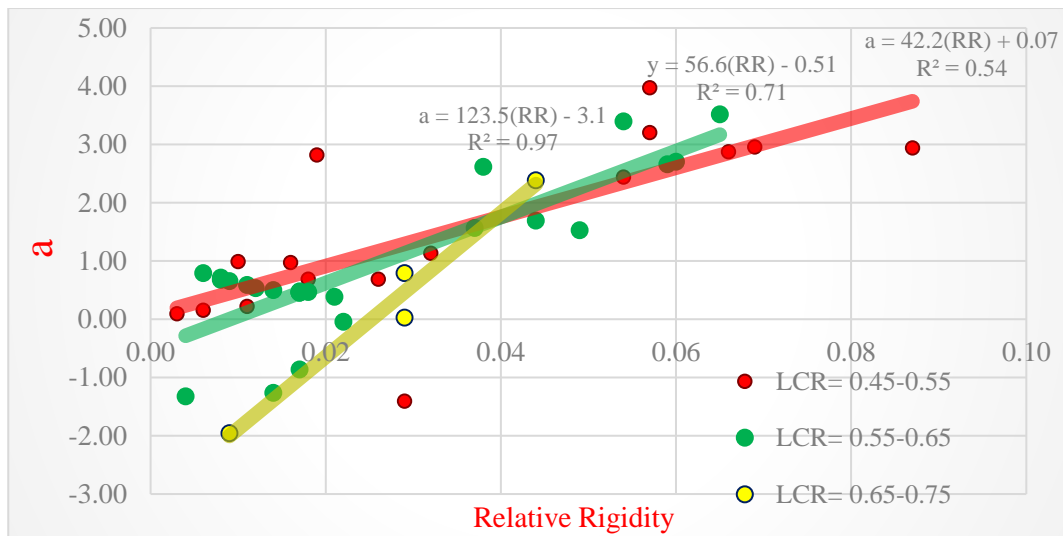


Figure 4.2 Scatter plot of calculated and grouped coefficient 'a' values versus relative rigidity

The investigation resulted in the derivation of distinct equations for different LCR groups, further substantiating the relationship between 'a' and the relative rigidity factor. The equations for each group are as follows:

For $0.45 \leq \text{LCR} < 0.55$;

$$a = 42.2(RR) + 0.07 \quad (4.3a)$$

For $0.55 \leq \text{LCR} < 0.65$;

$$a = 56.6(RR) - 0.51 \quad (4.3b)$$

For $0.65 \leq \text{LCR} < 0.75$;

$$a = 123.5(RR) - 3.10 \quad (4.3c)$$

Moreover, when the 'x₁' values, which represent the threshold point where the quadratic function changes its form, are plotted against the foundation widths, a clear linear relationship is observed (Figure 4.3). Specifically, the sudden increase in spring coefficients begins at a point located approximately 85-95 percent of the half-

width of the foundation away from the middle. The linear correlation between 'x₁' and the half foundation widths is represented by the Equation:

$$x_1 = 0.96 \left(\frac{W}{2} \right) - 0.80 \quad (4.4)$$

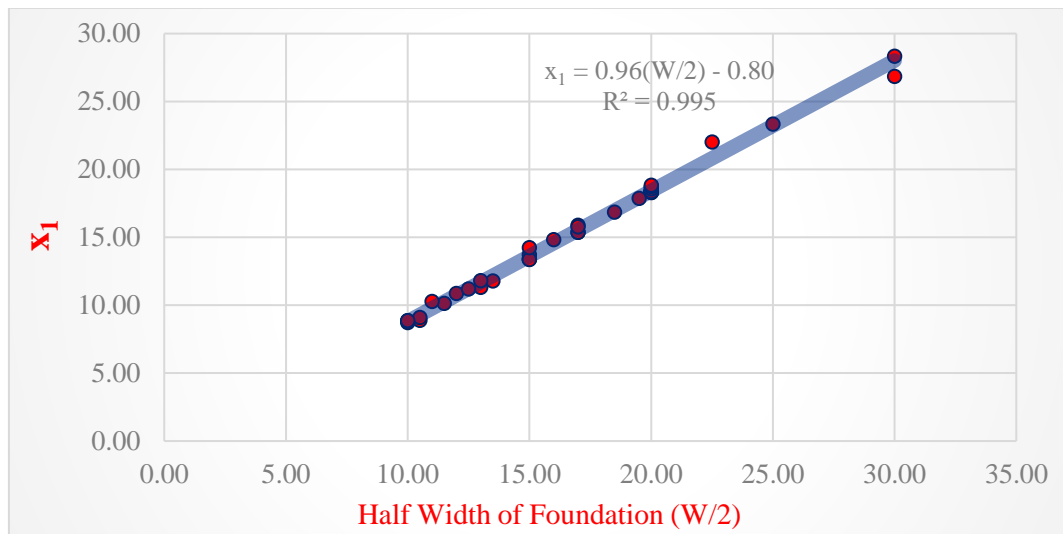


Figure 4.3 Scatter plot of quadratic function length versus foundation width

The parameter 'c' represents the slope of the linear portion of the function, which corresponds to the region with significant variations. In line with this, the ratios of 'k_{edge}/k_{x1}' that correlate with RR are aggregated on a plot. By grouping LCR, similar to the approach taken in the 'a' and relative rigidity plot, linear best-fit lines can be determined (Figure 4.4). The scatter plot reveals that the 'k_{edge}/k_{x1}' ratio mostly ranges from 1.3 to 1.9 for models with low relative rigidity, and it becomes limited between 1.4 and 1.6 at higher relative rigidity values. The equations corresponding to each group in the scatter plot are as follows:

For $0.45 \leq \text{LCR} < 0.55$;

$$\frac{k_{edge}}{k_{x_1}} = -3.04(RR) + 1.80 \quad (4.5a)$$

For $0.55 \leq \text{LCR} < 0.65$;

$$\frac{k_{edge}}{k_{x_1}} = -2.76(RR) + 1.69 \quad (4.5b)$$

For $0.65 \leq \text{LCR} < 0.75$;

$$\frac{k_{edge}}{k_{x_1}} = 14.22(RR) + 0.89 \quad (4.5c)$$

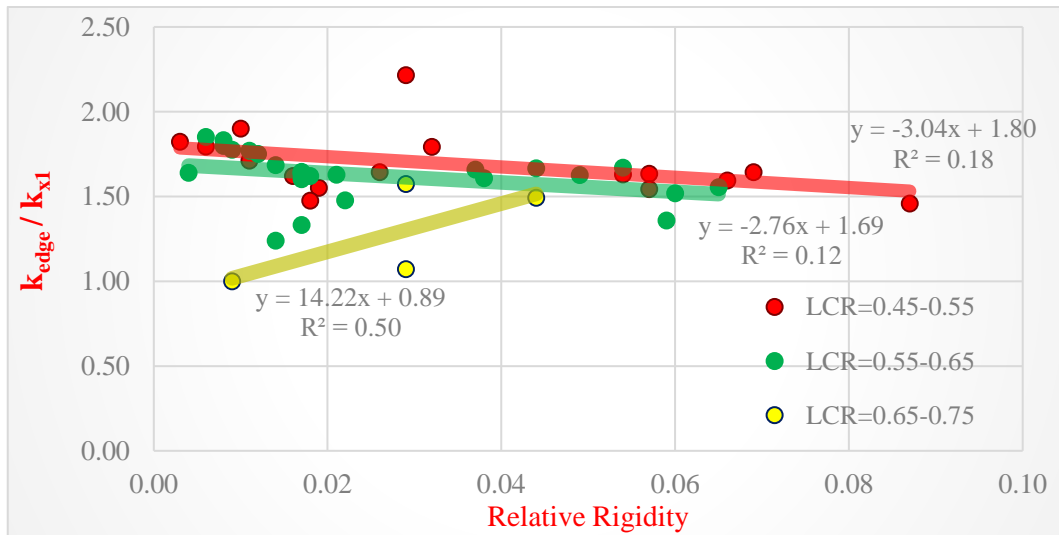


Figure 4.4 Scatter plot of the ratio of spring coefficient values at the points; end of quadratic function and edge of the foundation versus relative rigidity

The transformation from the ' k_{edge}/k_{x_1} ' ratio to the parameter 'c' can be achieved through Equation (4.6), which can be expressed as follows:

$$c = \frac{k_{edge} - k(x_1)}{x_{edge} - x_1} \quad (4.6)$$

where $k(x_l)$ represents the spring constant at the transition point, and k_{edge} represents the spring constant at the edge of the foundation at the node just before the edge of the foundation.

4.2 Proposed Methodology

The proposed approach begins with the assessment of the stiffness attributes of the superstructure. This involves the calculation of the stiffness for each individual floor, which is then multiplied by the total number of floors in the building. Simultaneously, the stiffness attributed to the mat foundation is added to this cumulative value. Consequently, the flexural rigidity specific to the superstructure is ascertained. Notably, these computations are executed separately for both orthogonal directions, x and y. To elaborate, the flexural rigidity is determined by considering the length of the foundation or slab in the corresponding x or y direction.

Subsequently, the resultant flexural rigidity is compared to the soil stiffness, as specified in Equation 4.2, leading to the derivation of relative rigidity values for both the x and y directions. This is followed by detecting the loading force positions of the superstructure. Based on the column locations, the region on the foundation where the superstructure load is concentrated is determined again for both directions as mentioned in Section 3.9.

The identification of relative rigidity and Load Concentration Ratio (LCR) values enables the application of the equation series expounded in Equations 4.3, 4.4, and 4.5. Specifically, the starting k_0 value is entered such that the average of the resultant spring constant distribution aligns with the subgrade modulus value presented by the geotechnical consultant. Subsequently, the computed values are incorporated into the partial functions presented as Equations 4.1a and 4.1b. This incorporation facilitates the determination of spring coefficients for the x and y directions at every point on the foundation.

In the context of three-dimensional analysis, the spring constants for each individual node are determined by averaging the values previously obtained for the x and y directions. These resultant values are divided by 4 for the foundation corners, accounting for the tributary area condition, and by 2 for the foundation edges.

4.3 Validation and Comparative Analysis of Proposed Approach

In order to test the effectiveness of the scatter plots and the corresponding relationships, two 2-dimensional validation analyses were conducted. In the first analysis, the coefficient 'a' and the ' k_{edge}/k_{x1} ' ratio were selected to be relatively far from the linear regressions defined for their group. This selection allows for evaluations to be made regarding the results that would be obtained for a poor scenario.

For the first case, analysis number 49 was selected. This analysis model has a relative rigidity ratio of 0.029 and a load concentration ratio of 0.51. For this analysis, the calculated coefficient 'a,' the ' x_1 ' value, and the ' k_{edge}/k_{x1} ' ratio by MS Excel Solver were -1.40, 13.4, and 2.21, respectively. These values can be observed in Figures 4.2, 4.3, and 4.4. The results obtained from calculating these values using scatter plots and relationships are as follows: 1.30, 13.6, and 1.72, respectively. These values can be seen in Appendix C. The settlement and bending moment results from proposed relations based on these values were compared with those found through the iteration process, the constant spring coefficient approach, and the pseudo-coupled method. The results of iterations that match the continuum serve as the benchmark of reality. Figure 4.5 illustrates the spring constant distributions obtained from the FE continuum through the iteration process, the spring coefficients obtained using relationships, the constant spring coefficients, and the pseudo-coupled approach springs. It also includes the settlement and bending moment results from the analyses conducted using the four different approaches mentioned above.

The proposed relation yields settlement results that closely resemble the response of the system. The constant spring coefficient approach also provides similar results, while the results from the pseudo-coupled method differ from these two approaches. Regarding bending moment results, the relationship-based approach yields outcomes close to those obtained through spring constants matching the FE continuum. The difference in the maximum moment values at the center of the foundation is similar to the difference obtained with the constant spring approach. However, in other locations along the foundation, the moment values obtained with the relationship-based approach are very close to the spring constants obtained through the iteration to match the continuum results.

On the other hand, the bending moment results obtained from the pseudo-coupled approach show notable discrepancies compared to the continuum values, similar to the findings observed in the settlement results. This difference actually highlights the potential drawbacks of the pseudo-coupled approach. The ratio between the edge and innermost zones is approximately 2 in the proposed and pseudo-coupled methods. However, in the pseudo-coupled method, the point at which this 2-fold increase starts is different. While in the proposed approach, it occurs at around 90 percent of the foundation half-length, in the pseudo-coupled method, it starts earlier at around 75 percent. Additionally, in the pseudo-coupled method, the ratio between the intermediate and center zones is 1.5. However, if the spring coefficients in the intermediate part exhibit a concave-downward pattern, indicating a negative coefficient 'a' in our terms, the pseudo-coupled method may yield inaccurate results, as observed.

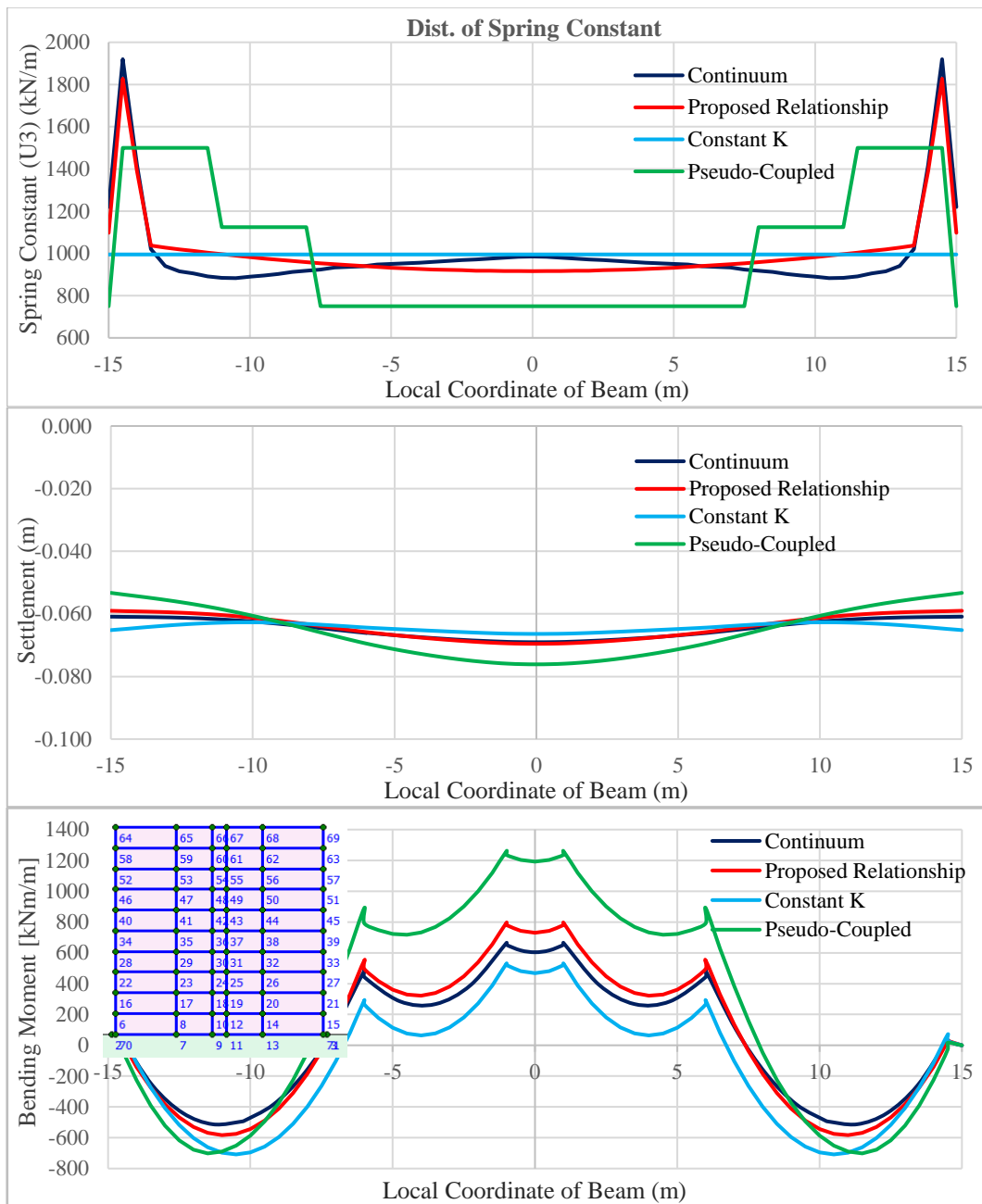


Figure 4.5 Spring constant distribution of different approaches and the corresponding settlement and bending moment results (Analysis No: 49)

For the second two-dimensional trial analysis, analysis number 40 was selected, which had a relative rigidity ratio of 0.019 and an LCR of 0.46. The calculated coefficient 'a,' 'x_i' value, and 'k_{edge}/k_{x1}' ratio using MS Excel Solver were 2.82, 13.7, and 1.55, respectively. The results from scatter plots and relationships were 0.89, 13.6, and 1.74, respectively.

Figure 4.6 illustrates the spring coefficient distributions obtained through the FE continuum-based iteration process, proposed relationships, constant spring coefficient, and the pseudo-coupled approach springs. It also presents the settlement and bending moment results obtained from SAP2000 analyses.

The proposed relationships yield settlement results that closely resemble PLAXIS 2D results and exhibit accurate behavior. Regarding bending moment, the proposed approach outperforms both the constant spring and pseudo-coupled methods, providing more accurate and consistent results at almost every point along the foundation. These two trial analyses demonstrate that relationship-based spring constant distributions yield more accurate results than commonly used approaches.

The utilization of scatter plots and proposed equations presents a practical approach for civil engineers, particularly those involved in structural design. By gaining a comprehensive understanding of the system's characteristics, including foundation dimensions, column locations, and soil properties, engineers can effectively anticipate the subsoil reaction beneath a beam. This methodology allows engineers to accurately predict subsoil reactions, facilitating more efficient foundation design without modeling both soil and structure in a single complex finite element analysis.

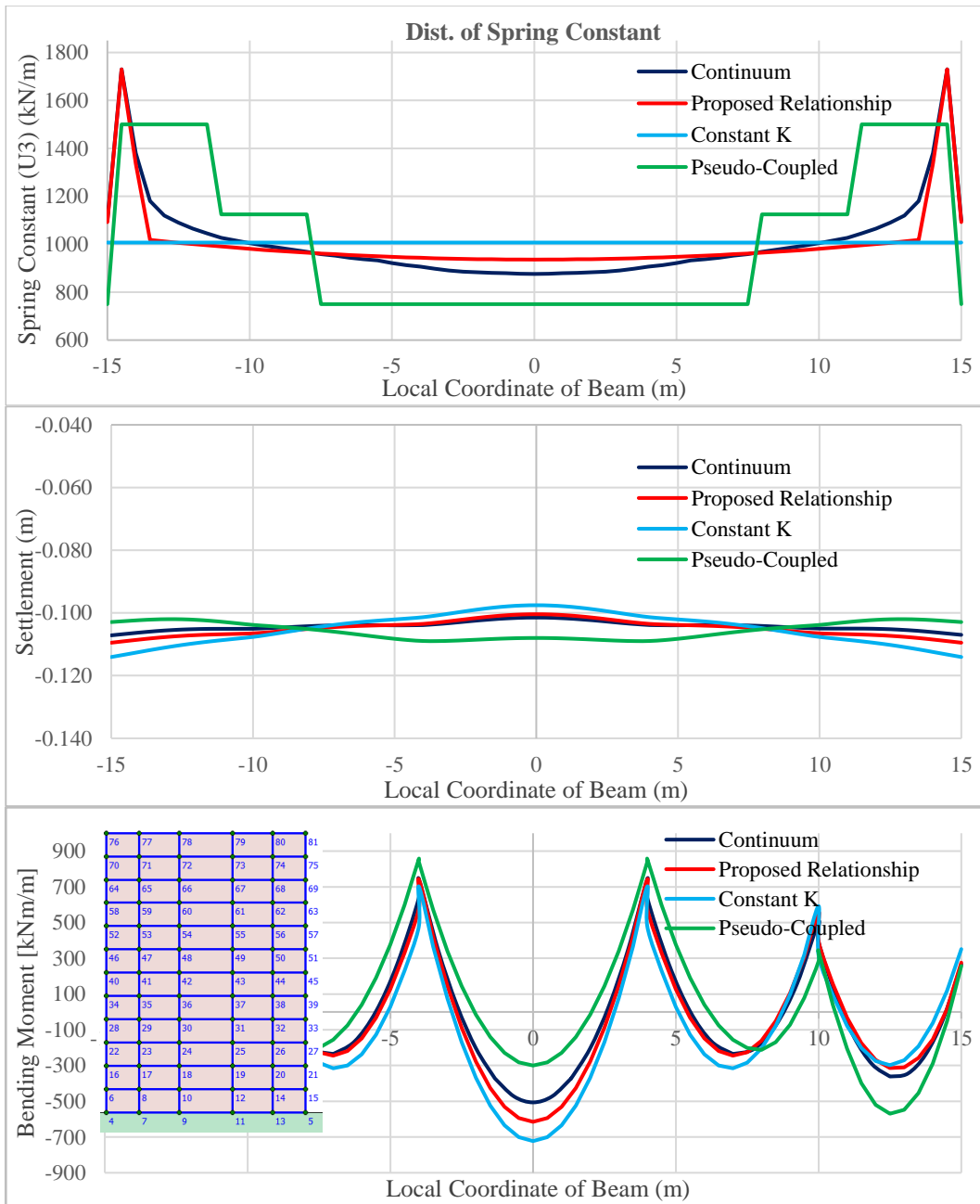


Figure 4.6 Spring constant distribution of different approaches and the corresponding settlement and bending moment results (Analysis No: 40)

CHAPTER 5

EXPLORING 3-D TRIALS: EXAMPLE ANALYSES

Based on the studies conducted in 2D analyses, which have revealed the direct dependence of spring constant distribution on system stiffness and loading conditions, it was essential to assess the applicability of these findings in a 3D context. In order to achieve this, two trials of 3D analysis were conducted using both PLAXIS 3D and SAP2000 software. These trials aimed to investigate whether the insights obtained from the 2D analyses could be successfully extended to the 3D analysis domain and provide valuable insights for understanding the behavior of spring coefficients in three dimensions.

While creating three-dimensional models, two-dimensional analyses conducted within the scope of the study were utilized, incorporating known dimensions and results. The 3D problems were divided into two 2D models, each representing a cross-section in orthogonal directions. These models shared the same soil parameters, equivalent foundation thicknesses, and other properties, except for the foundation widths. The general view of the initial 3D analysis is presented in Figure 5.1. It is a combination of 2D models with model numbers 14 and 52. The foundation has a thickness of 1 meter, with a long side of 40 meters and a short side of 26 meters. The properties of the corresponding two-dimensional models can be found in Appendix C. As a result, a foundation for a structure covering an area of 1040 m² and supported by 4293 nodes, with a mesh spacing of 0.5 m x 0.5 m, is obtained.

The iteration process employed in the 2D analyses to calculate the distribution of spring constants cannot be directly extended to 3D analyses due to the impracticality of iteratively determining a foundation support system consisting of thousands of spring nodes. Therefore, the findings obtained from the 2D analyses are being evaluated and tested in the 3D models.

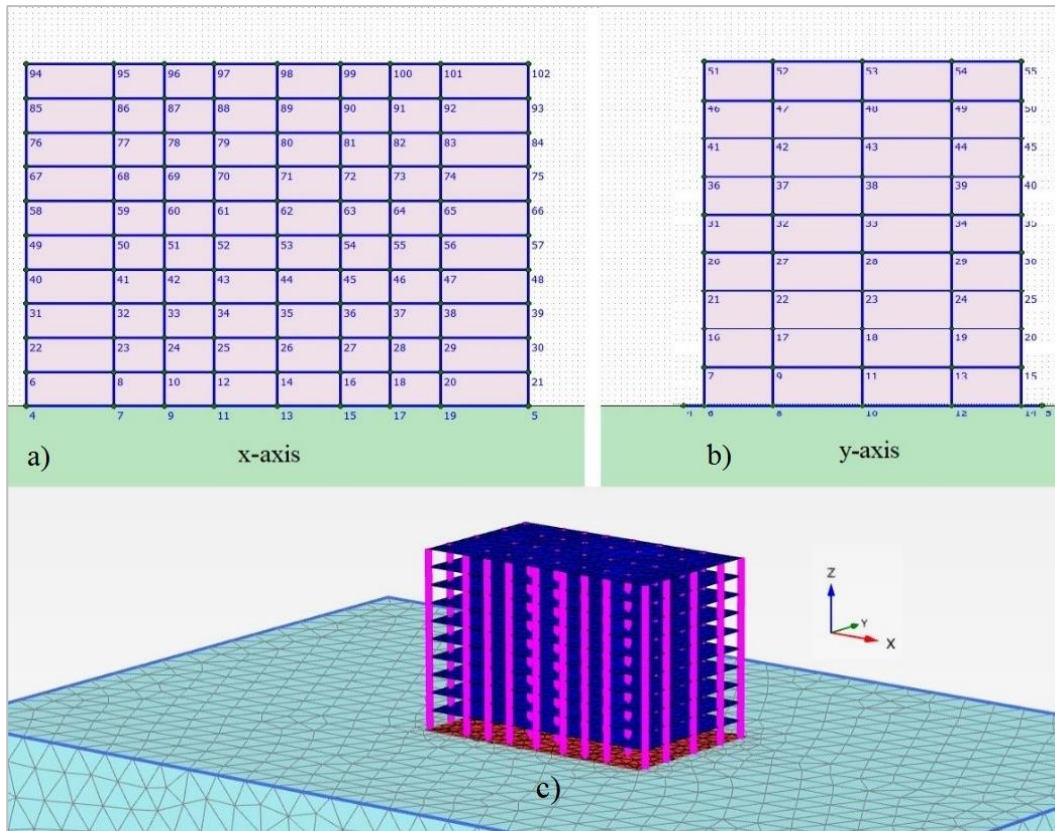


Figure 5.1 General view of the first trial 3D analysis

While determining the spring support system for the 3D analysis, scatter plots and proposed relations derived from the 2D analyses were utilized. In this process, the relationships obtained from the 2D analyses were input into an Excel spreadsheet. The Excel spreadsheet has a dedicated data entry page where various parameters related to the raft, such as the widths in both directions, thickness, slab thicknesses, number of stories, soil and concrete stiffness values, and LCR values in both directions, are entered. The expected spring constant distribution under the 3D foundation for each node with known coordinates could be obtained by inputting essential data related to the soil and superstructure on the input page. These spring joint assignments, presented in a list format, can easily be inserted into the SAP2000 program through a simple copy-paste operation. Several screenshots of the Excel file, which is being provided along with this thesis study, are included in Appendix E for reference.

The spring constants in the x and y directions, which share the same local coordinates, are averaged while determining the spring support beneath a foundation node. These average values are divided by two at the foundation edges and four at the foundation corners. Thus, a distribution map was generated (Figure 5.2) to depict the spring system beneath the foundation, considering the tributary area of each node.

The results obtained from both software were plotted on a graph with similar contour shading levels, allowing for an easy comparison through the same color-coding of contours. Additionally, the settlement and element force results obtained from SAP2000 and PLAXIS 3D could be easily transferred to Excel, enabling visual and numerical comparisons for verification purposes. This seamless integration of data between Excel and the analysis software greatly facilitated the process of visual and quantitative analysis, enhancing overall convenience and efficiency.

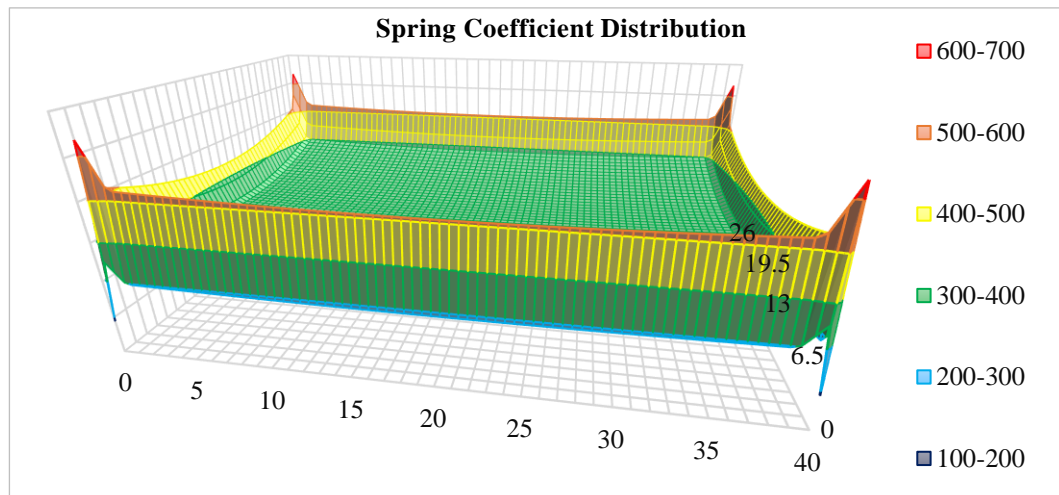


Figure 5.2 Spring coefficient distribution calculated for the first trial 3D analysis

The comparison includes the results obtained from SAP2000 using the proposed approach within the scope of this study, as well as the results obtained from the conventional constant spring coefficient distribution approach. The purpose of this comparison was to assess the effectiveness of the proposed approach in contrast to the conventional constant spring coefficient approach.

Figure 5.3 illustrates the overall findings, highlighting the limitations of the conventional constant spring coefficient approach in accurately predicting settlement response. Under this approach, the individual uncoupled springs settle independently under a relatively evenly distributed structural load, resulting in a settlement profile that significantly underestimates the actual curvature of the foundation. In contrast, the proposed approach yields settlement characteristics and values that closely align with those obtained from PLAXIS 3D. The settlement response predicted by the proposed approach demonstrates similar trends and magnitudes, indicating a significant improvement over the conventional method.

In the bending moment results of the x-direction (long side), the proposed approach demonstrates improved accuracy in capturing moments, particularly in the middle of the foundation, as well as accurately identifying the high moment values formed at the column points (Figure 5.4). The maximum moment value at column positions is 623 kN-m/m in PLAXIS 3D, 492 kN-m/m in the proposed approach solution, and 438 kN-m/m in the constant spring approach. This represents an enhancement of approximately 12.3 percent achieved by the proposed approach.

For the bending moment results of the y-direction (short side), the proposed approach is better than the constant spring coefficient approach because it captures the settlement response as accurately as possible (Figure 5.5). The average moments formed in the raft in the y-direction are observed to be 163 kN-m/m in PLAXIS 3D, 152 kN-m/m in the proposed approach solution, and 71 kN-m/m in the constant spring approach. This indicates a significant improvement achieved by the proposed approach, with an approximately 114.1% increase in average moments compared to the constant spring approach.

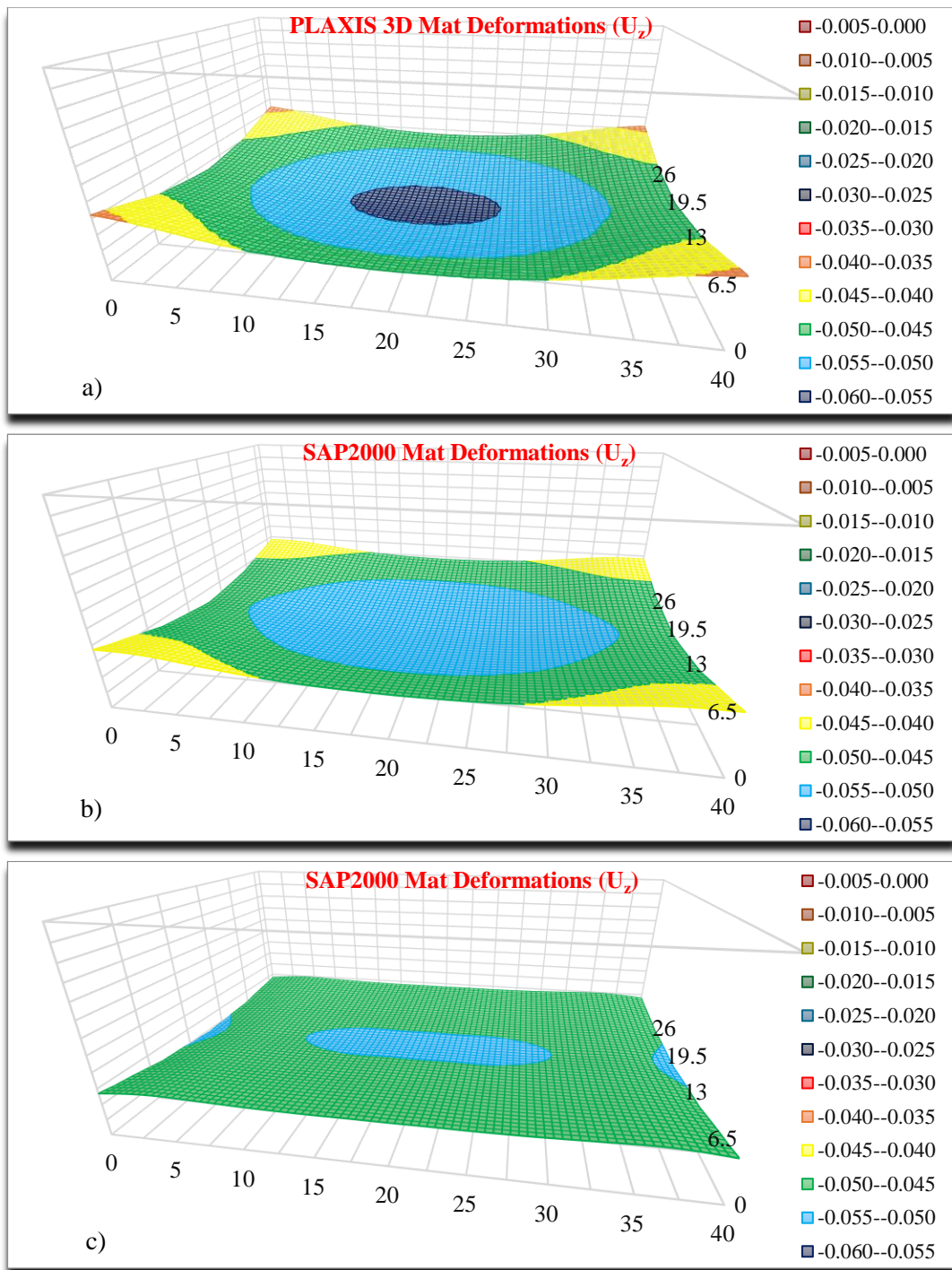


Figure 5.3 Settlement results of the first trial 3D analysis; (a) PLAXIS 3D, (b) Proposed approach, (c) Constant spring approach

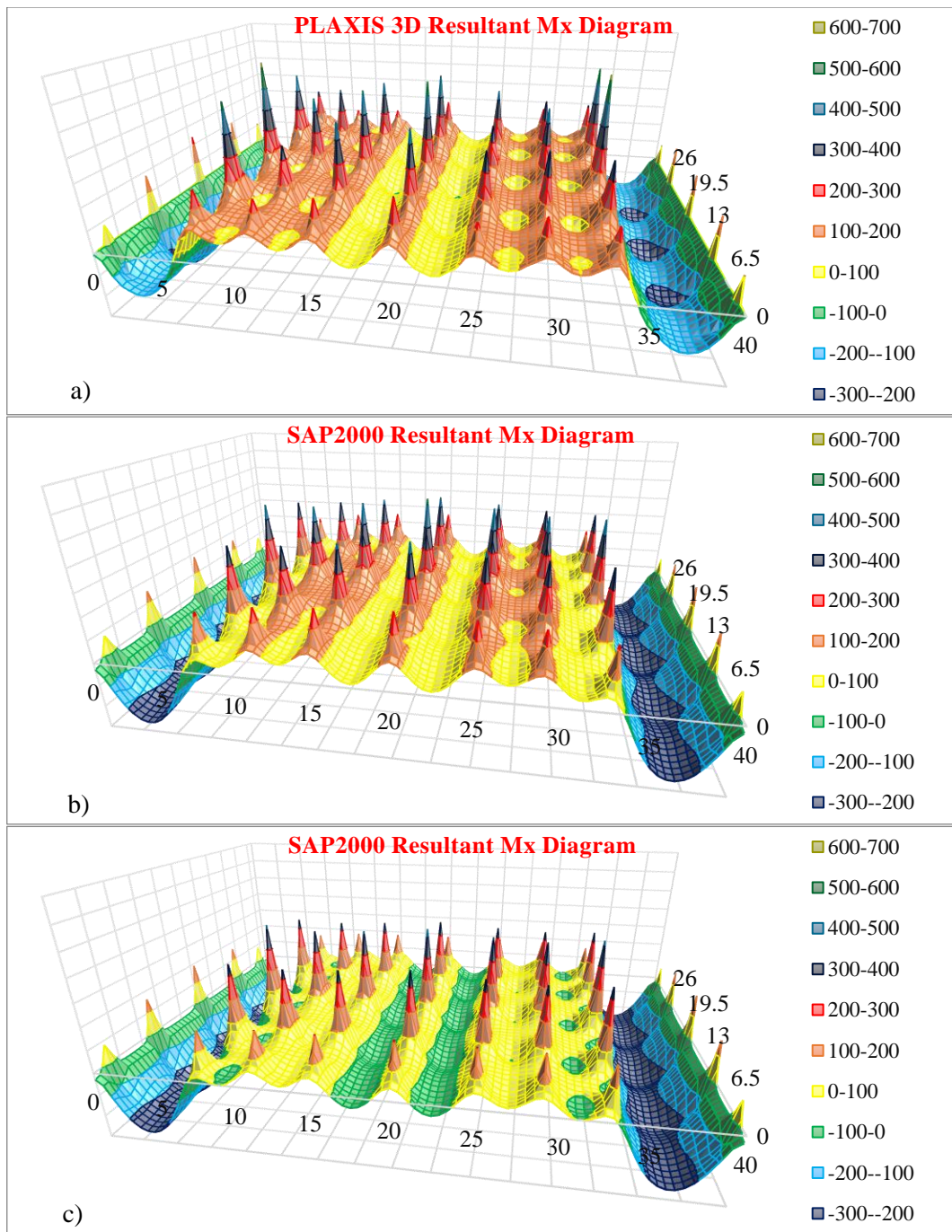


Figure 5.4 First 3-D analysis bending moment results; comparison in x-direction:
 (a) PLAXIS 3D, (b) Proposed approach, (c) Constant spring approach

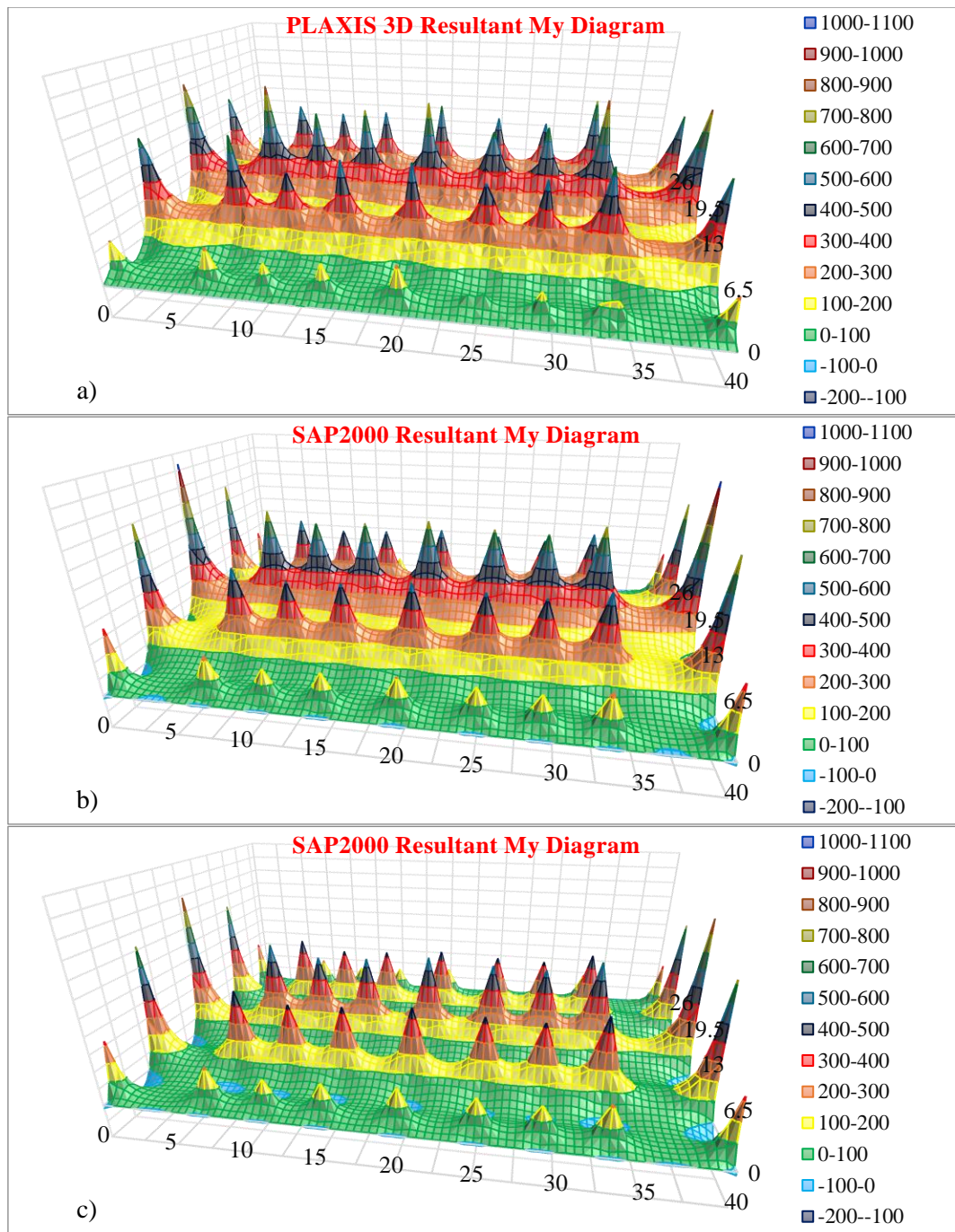


Figure 5.5 First 3-D analysis bending moment results; comparison in y-direction:
 (a) PLAXIS 3D, (b) Proposed approach, (c) Constant spring approach

It is important to note that an inaccurate settlement response can directly impact the forces developed in the foundation, leading to improper distribution. While the proposed approach showcases improved performance in capturing the settlement characteristics, it is worth mentioning that deviations from the maximum moment value obtained from PLAXIS 3D can occur, particularly for columns located at the edges where boundary effects come into play. These discrepancies indicate that the moment values may deviate to some extent under such specific conditions. In the y-direction, for example, the maximum moment value in PLAXIS 3D is 856 kN-m/m, while in the proposed approach, it is 1039 kN-m/m, and in the constant spring approach, it is 890 kN-m/m. It is important to note that these deviations are due to point load application at column locations and, therefore, unrealistic, as the actual moment to be used in structural design would be at the edge/face of the column, not the center. Hence the sharp peaks are not good indicators in evaluating the proposed approach's overall performance.

Table 5.1 provides a comprehensive comparison of the settlement and moment results obtained from the first trial 3D analysis. The table showcases the values obtained using three approaches: PLAXIS 3D, the proposed approach based on Equation (4.1), and the constant spring approach. The average and maximum settlement values, as well as the average and maximum moments in the x-direction and y-direction, are provided for each approach.

Table 5.1 Comparison of settlement and moment results of the first trial 3D analysis

| | PLAXIS 3D | Proposed Approach | Constant Spring |
|--|-----------|-------------------|-----------------|
| Average Settlement (m) | -0.0494 | -0.0506 | -0.0485 |
| Maximum Settlement (m) | -0.0561 | -0.0554 | -0.0509 |
| Minimum Settlement (m) | -0.0387 | -0.0440 | -0.0455 |
| Average Moment (kN-m/m) in x-direction | 42.75 | -3.60 | -31.97 |
| Maximum Moment (kN-m/m) in x-direction | 623.50 | 492.30 | 437.58 |
| Average Moment (kN-m/m) in y-direction | 163.40 | 151.65 | 70.80 |
| Maximum Moment (kN-m/m) in y-direction | 855.63 | 1038.76 | 889.69 |

For the second trial of 3D analysis, two 2D models were selected: model 53 and model 32. These models were combined to represent a foundation with dimensions of 30 meters (long side) and 24 meters (short side), with a uniform thickness of 0.9 meters. The foundation covers an area of 720 m² and is supported by 2989 nodes, with a mesh spacing of 0.5 meters in both the x and y directions. The general view of the second 3D analysis is presented below in Figure 5.6, while Figure 5.7 illustrates the three-dimensional spring coefficient distribution obtained using the proposed scatter plots and equations, taking into account the tributary area phenomenon for a comprehensive analysis.

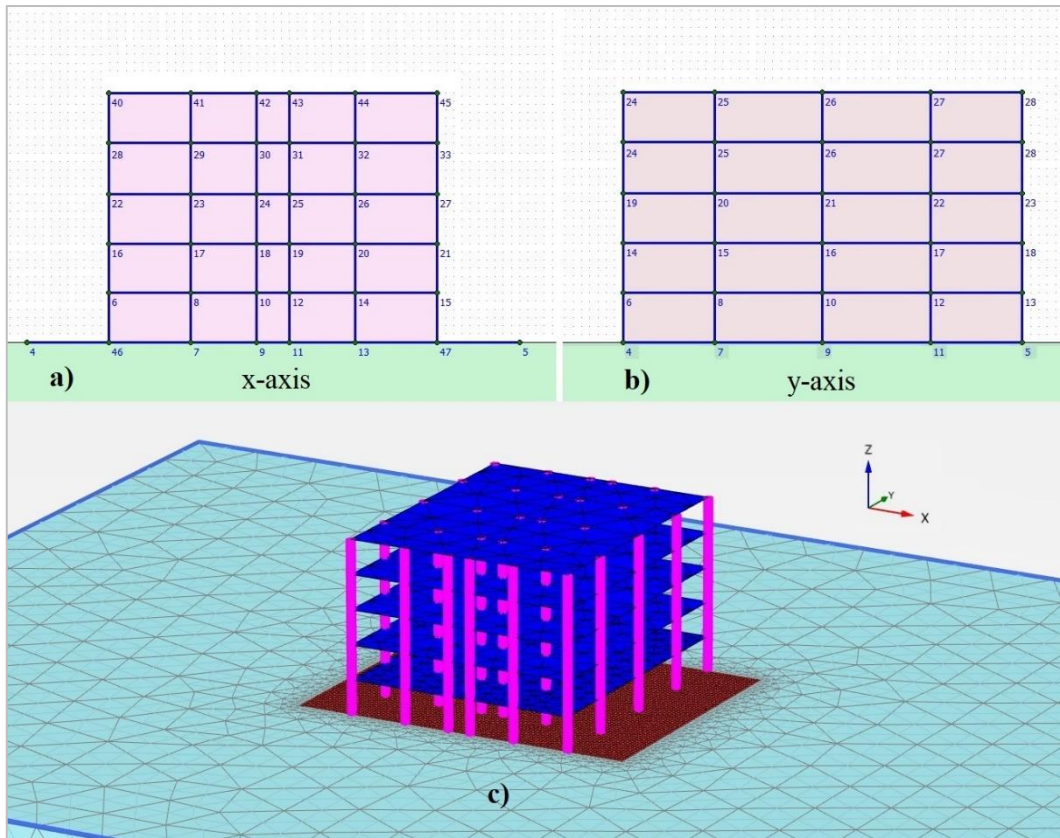


Figure 5.6 General view of the second trial 3D analysis

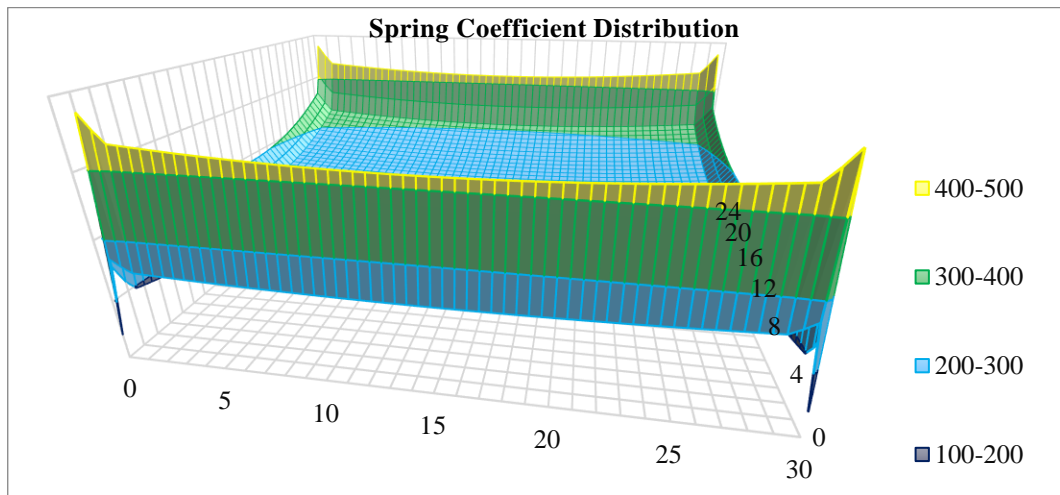


Figure 5.7 Spring coefficient distribution calculated for the second trial 3D analysis

Figure 5.8 visually presents the settlement results, displaying the settlement profiles obtained from each approach. At first glance, the contour lines for the proposed approach and the constant spring approach closely resemble the settlement response observed in PLAXIS 3D. However, upon closer examination, it becomes apparent that the proposed approach provides a more accurate representation of the settlement curvature, particularly in the y-direction.

The results illustrated in Figure 5.9 reveal the improved accuracy of the proposed approach in capturing moments, particularly in the middle of the foundation, and accurately identifying the highest moment values formed at the column points. The proposed approach yields a maximum moment value of 430 kN-m/m at column positions, which closely approximates the corresponding value of 457 kN-m/m obtained from PLAXIS 3D. This signifies the effectiveness of the proposed approach in accurately predicting the moment distribution and achieving a high level of agreement with the reference PLAXIS 3D results. On the other hand, the constant spring approach yields a maximum moment value of 401 kN-m/m.

It can be observed that both the proposed approach and the constant spring approach closely approximate the average moment values in the x-direction obtained from PLAXIS 3D. The proposed approach exhibits an average moment of 167 kN-m/m, which is in close proximity to the reference value of 153 kN-m/m obtained from PLAXIS 3D. Similarly, the constant spring approach shows a comparable average moment value of 159 kN-m/m.

Analyzing the y-direction moments, Figure 5.10 provides a comprehensive visualization of the results. It is apparent that the proposed approach excels in capturing the moment behavior in this direction when compared to the constant spring approach. The maximum moment value obtained from the proposed approach is 324 kN-m/m, which closely approximates the corresponding value from PLAXIS 3D (333 kN-m/m). In contrast, the constant spring approach exhibits a maximum moment value of 210 kN-m/m.

Additionally, when considering the average moments in the y-direction, the proposed approach yields an average moment value of 46 kN-m/m, which is again in close agreement with the PLAXIS 3D result (47 kN-m/m). The constant spring approach, however, yields an average moment value of -11 kN-m/m, demonstrating a significant deviation from the accurate results obtained in PLAXIS 3D. This success of the proposed approach in accurately capturing the moment behavior in the y-direction can be attributed to its ability to better represent the settlement curvature response in that direction.

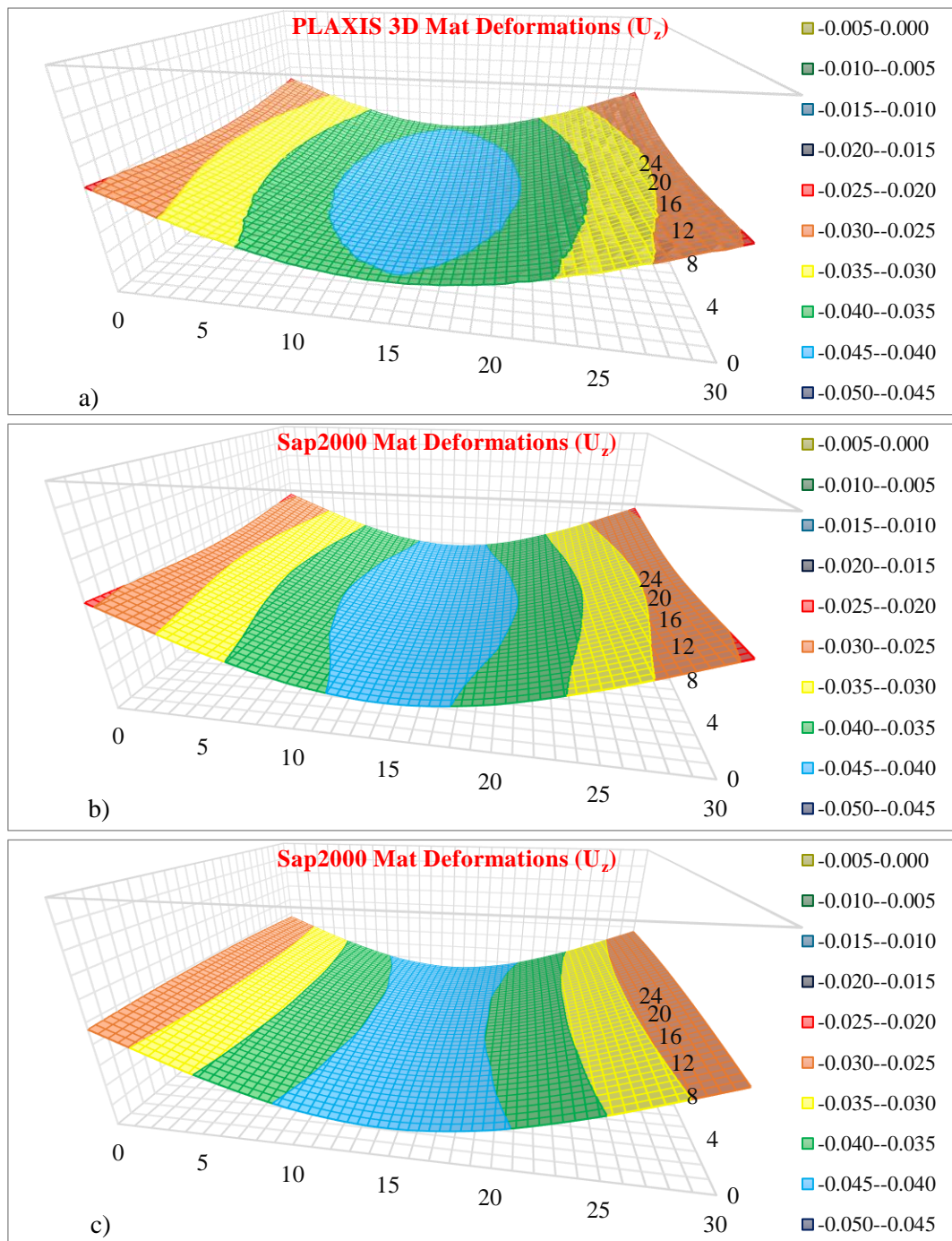


Figure 5.8 Settlement results of the second trial 3D analysis; (a) PLAXIS 3D, (b) Proposed approach, (c) Constant spring approach

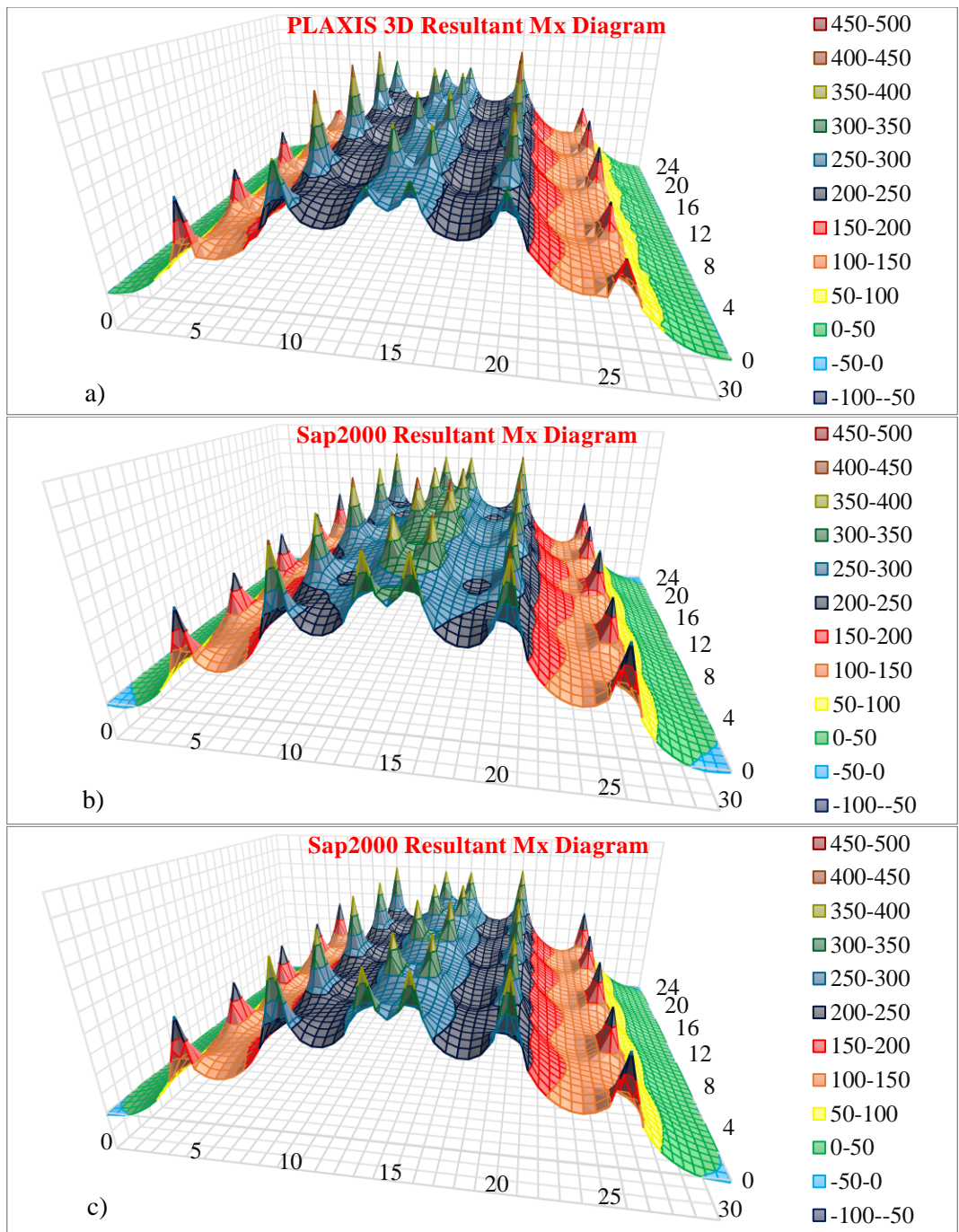


Figure 5.9 Second 3-D analysis bending moment results; comparison in x-direction: (a) PLAXIS 3D, (b) Proposed approach, (c) Constant spring approach

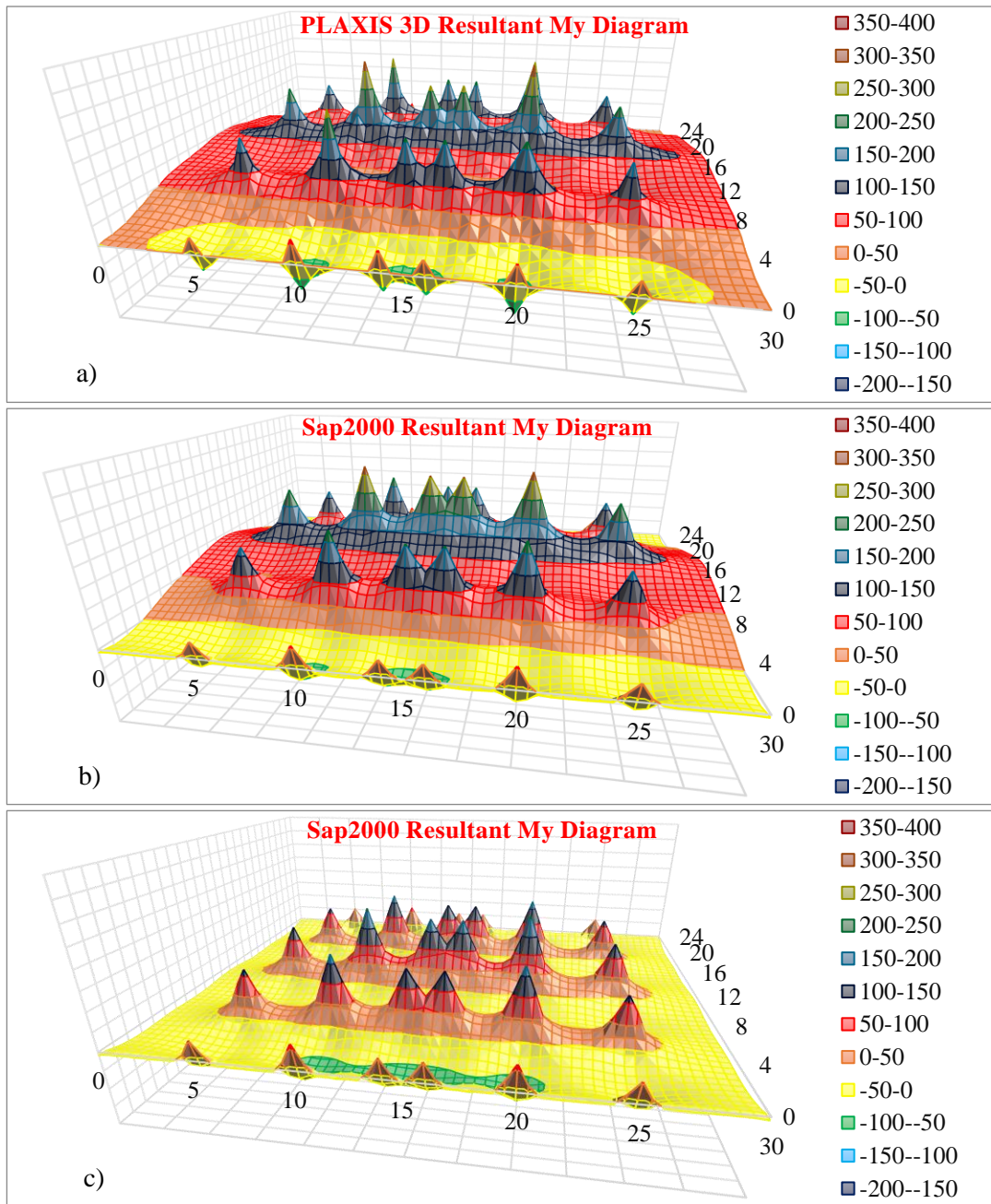


Figure 5.10 Second 3-D analysis bending moment results; comparison in y-direction: (a) PLAXIS 3D, (b) Proposed approach, (c) Constant spring approach

Table 5.2 presents a comprehensive compilation of the settlement and moment analysis results in both the x-direction and y-direction. Presenting the numerical values in a tabular format facilitates a clear and concise representation of the performance of each approach. Notably, the proposed approach demonstrates competitive results, closely aligning with the reference values from PLAXIS 3D and outperforming the constant spring approach in certain aspects. This highlights the effectiveness of the proposed approach in accurately predicting settlement and moment behavior under varying loading conditions.

Table 5.2 Comparison of settlement and moment results of the second trial 3D analysis

| | PLAXIS 3D | Proposed Approach | Constant Spring |
|--|-----------|-------------------|-----------------|
| Average Settlement (m) | -0.0360 | -0.0359 | -0.0358 |
| Maximum Settlement (m) | -0.0432 | -0.0433 | -0.0431 |
| Minimum Settlement (m) | -0.0243 | -0.0242 | -0.0256 |
| Average Moment (kN-m/m) in x-direction | 152.93 | 167.27 | 159.42 |
| Maximum Moment (kN-m/m) in x-direction | 457.49 | 430.17 | 400.83 |
| Average Moment (kN-m/m) in y-direction | 47.32 | 46.42 | -11.19 |
| Maximum Moment (kN-m/m) in y-direction | 332.70 | 324.38 | 209.61 |

CHAPTER 6

CONCLUSION

The application of subgrade modulus values to structural design, while often relatively simplified in the design literature, is actually a complex process that is vulnerable to misuse and misunderstanding. The structural design of the foundations is generally made with rough methods that do not consider the characteristics of the soil under the foundation and neglect the soil-mat-superstructure interaction.

6.1 Summary of Work

This study aims to investigate the behavior of shallow raft foundations under static loading by considering the interaction between the soil and the foundation. PLAXIS 2D/3D and SAP2000 software, widely used in geotechnical and structural analysis, are employed to analyze various cases and derive accurate distributions of the subgrade modulus.

The methodology involves iterative processes applied to springs in SAP2000 to determine subgrade modulus distributions aligned with the bending moment and settlement results obtained from PLAXIS 2D. A set of relations are proposed to account for the parameters that significantly influence the subgrade modulus distributions. These relations considered factors such as foundation thickness, structure width, soil stiffness, number of stories, and column positions, ensuring a comprehensive analysis of the foundation system. Also, in order to extend the findings from two-dimensional assessments to three-dimensional scenarios, two separate 3D parametric studies were conducted.

Overall, this research fills a gap in the existing literature by addressing the shortcomings of the Winkler method and providing a more accurate representation

of soil-foundation interaction. The practical implications of the findings empower structural engineers to make informed decisions when designing shallow raft foundations.

6.2 Conclusions

The research findings highlight the significant influence of various factors on the distribution of spring constants in raft foundations. It is evident that multiple variables, including soil properties, foundation geometry, loading conditions, and soil-structure interaction, can impact the accurate determination of spring constant distribution. Considering these variables is crucial to obtain more reliable and realistic results. Based on the analyses conducted in this study, the following key conclusions can be drawn:

- (1) Differential settlements and bending moments in a raft foundation cannot be accurately predicted by using a single value of spring constant under the entire foundation.
- (2) The settlement profile of the raft and resulting bending moments are directly influenced by the spring coefficients defined under the raft.
- (3) The constant spring approach or the pseudo-coupled method, which consistently doubles the spring constants at the edge nodes, may lead to significant errors in raft foundation design moments on a case-by-case basis.
- (4) Soil stiffness, structural rigidity, and loading distribution are the most important variables affecting the spring coefficient distribution beneath a foundation.
- (5) The thickness of the mat and the clear span between columns have a more critical impact on the raft's response than the number of superstructure floors.
- (6) Assigning variable values of subgrade reaction modulus in different parts of a foundation, based on the proposed methodology, including Equation (4.1) and scatter

plots, is a convenient method for considering static soil-structure interaction without relying on a full finite element model of the soil continuum.

The resultant procedure of this study encompasses the assessment of superstructure stiffness attributes, the calculation of flexural rigidity for both directions, the determination of relative rigidity, the detection of loading force positions, the application of equation series, and the integration of computed values into partial functions to ascertain spring coefficients at every foundation point. The resultant values for the x and y directions are further averaged for three-dimensional analysis. Lastly, the initial k_0 value is fine-tuned to align the average resultant spring constant distribution with the subgrade modulus value provided by the geotechnical consultant.

It is important to note that the soil-foundation-structure relationship cannot be adequately explained using a single linear method or equation. The interplay of various variables within the system, including soil parameters, superstructure dimensions, and loading conditions, contributes to significant variations in the results. Consequently, it is recognized that the findings of this study alone cannot provide a definitive solution for assigning constant spring coefficients in raft foundations. However, it is evident that better results can be achieved compared to the widely employed methods in current practice. Attaining an exact solution necessitates using sophisticated software capable of modeling both the soil and building elements within the same system. Nevertheless, this study contributes to the current understanding of static soil-structure interaction in raft foundations and is expected to enhance communication and collaboration between geotechnical and structural engineers.

6.3 Recommendations for Future Researches

Based on the findings and limitations of this study, several areas for future research can be identified further to enhance our understanding of soil-structure interaction in foundation design. Firstly, it is recommended to incorporate the effects of structural elements such as columns and shear walls into the analysis. While the current study focused primarily on the behavior of raft foundations, considering the influence of vertical and lateral structural components can provide a more comprehensive understanding of the system's response to loads.

Additionally, the use of three-dimensional foundation models can be explored to capture the complexities of real-world scenarios. In this study, the spring coefficients in three-dimensional foundations were determined by averaging the values obtained from two-dimensional analyses. Conducting dedicated three-dimensional analyses can provide more accurate and detailed insights into the distribution of spring constants, particularly in terms of side effects and corner effects. These effects, which were not extensively addressed in this study, can impact the behavior of the foundation system and should be considered in future research.

While this study is concentrated on dry sands, it is essential to acknowledge that further investigations may be conducted to explore the behavior of foundations in other types of soil, especially those influenced by water levels and varying moisture conditions. These soil types introduce a complex range of unknowns, making the analysis and design of foundation systems more challenging. The interaction between soil and water can lead to dynamic changes in soil properties, introducing uncertainties that require careful consideration in engineering practices. As such, future researches may encompass a broader spectrum of soil types to develop a comprehensive understanding of soil-structure interaction across various scenarios.

Furthermore, investigating the behavior of asymmetrical buildings or foundations is another valuable area for future research. While all of the cases considered in this study assumed symmetrical arrangements, it is important to acknowledge that real-

world variability encountered in practical applications may deviate from this assumption. Exploring the response of asymmetrical structures can provide valuable insights into the influence of geometric irregularities on the foundation's performance and help develop design guidelines for such situations.

In conclusion, this study has shed light on various aspects of soil-structure interaction in foundation design. However, further research is needed to address the recommendations mentioned above. By incorporating the effects of structural elements, utilizing three-dimensional foundation models, considering side and corner effects, encompassing a broader range of soil types, and studying asymmetrical buildings or foundations, future studies can advance our understanding of foundation behavior and contribute to more accurate and efficient design practices.

REFERENCES

- Adhikary, S., Singh, Y., & Paul, D. K. (2014). Modelling of Soil-Foundation-Structure system. Department of Earthquake Engineering, IIT Roorkee
- Alshorafa, M.A. (2008). Modifications of conventional rigid and flexible methods for mat foundation design. Master's Thesis, Islamic University of Gaza, Palestine.
- American Concrete Institute (ACI). (1993). Suggested analysis and design procedures for combined footings and mats. ACI 336.2R-88 (Reapproved 1993).
- Amornfa, K., Phienwej, N., & Kitpayuck, P. (2012). Current practice on foundation design of high-rise buildings in Bangkok. *Lowland Technology International*, 14(2), 70-83.
- Aristoneras, G., & Gómez, J. (2014). Design issues for structural engineers. *Structure Magazine*, 9-11. Retrieved from <https://www.studocu.com/in/document/gujarat-university/mechanical-engineering/c-struc-design-gomez-dec141/8952968>
- Aron, C., & Jonas, E. (2012). Structural element approaches for soil-structure interaction. *Structural Engineering and Building Performance Design*, Chalmers University of Technology.
- Bowles, J. E. (1997). *Foundation analysis and design* (5th edition). McGraw-Hill.
- Breeveld, B. J. S. (2013). Modelling the interaction between structure and soil for shallow foundations. Thesis. Delft University of Technology. Retrieved from <https://repository.tudelft.nl/islandora/object/uuid:f86d6980-d298-4e42-9fa2-3d6c4c261ad1?collection=education>
- Chang, D., Chih-Wei, L., Yu-Jhang, T., & Shih-Hao, C. (2022). Settlements and subgrade reactions of surface raft foundations subjected to vertically uniform load. *Applied Sciences*, 12(11), 5484. <https://doi.org/10.3390/app12115484>
- Coduto, D. (2001). *Foundation design: principles and practices* (2nd edition). Prentice Hall.
- Coduto, D. P., Kitch, W. A., & Yeung, M. R. (2016). *Foundation design: Principles and practices*. Pearson.
- Dutta, S. C., & Roy, R. (2002). A critical review on idealization and modeling for interaction among soil-foundation-structure system. *Computers and Structures*, 80(19-20), 1579-1594.
- Elsamee, W. N. (2013). An experimental study on the effect of foundation depth, size and shape on subgrade reaction of cohesionless soil. *Engineering* 2013. 5(10), 785-795.
Available at: <http://dx.doi.org/10.4236/eng.2013.510095>
- Fang, H. (1990). *Foundation engineering handbook* (2nd edition).

- French, J., Mack, D., Shafer, R., & Moore, K. (2006). Clarifying the application of subgrade modulus in structural analysis and design. Conference Proceedings, EERI 100th Anniversary Earthquake Conference, San Francisco.
- Gazetas, G. (1991). Formulas and charts for impedances of surface and embedded foundations, *Journal of Geotechnical Engineering*, ASCE, 117, 1363-1381.
- Girgin, S. C., Mısır S., Özden G., & Kahraman S. (2008). Yapı-Zemin etkileşiminin yapısal tasarımdaki rolü. Dokuz Eylül University Faculty of Engineering. *Journal of Science and Engineering*, 27-37
- Gragnano, C.G., Fagnoli, V., Boldini, D. & Amorosi, A. 2014. Comparison of structural elements response in PLAXIS 3D and SAP2000. *PLAXIS Bulletin*, Issue 35/Spring 2014: 6–11.
- Gouw, Tjje-Liong. (2001). Notes on the application of spring constant and soil structure interaction problem. *The Advancement & Trend in Soil Structural Engineering in The Third Millennium*. Jakarta, Indonesia.
- Gupta, S. C. (1997). *Raft Foundations: Design and analysis with a practical approach*. New Age International.
- Hemsley, J.A. (2000). *Design applications of raft foundations*. Thomas Telford Ltd., London.
- Horvath, J. S. (1993). Subgrade modeling for soil-structure interaction analysis of horizontal foundation elements. Research Report No. CE/GE-93-I. Manhattan College, New York.
- Horvath, J. S. (1995). Subgrade modeling for mat foundations: A review and critique of analytical methods. Report No. SP 152-5, Detroit.
- Horvath, J. S. (2002). Soil-structure interaction research project: Basic SSI concepts and applications overview. Report No. CGT-2002-2. Manhattan College, New York.
- Kahraman, S., Mısır, S., & Ozden, G., (2007). Sabit ve değişken yatak katsayısı yaklaşımlarının yapı davranışına etkisi. Sixth National Conference on Earthquake Engineering, Istanbul, 217-228.
- Larkela A., Mengelt M., & Stapelfeldt T. (2013). Determination of distribution of modulus of subgrade reaction. Proceedings of the 18th International Conference on Soil Mechanics and Geotechnical Engineering, Paris, 1313-1315.
- Liao, S. S. C. (1991). Estimating the coefficient of subgrade reaction for tunnel design. Internal research report. Parsons Brinkerhoff, Inc.
- Loukidis, D., & Tamiolakis, G.-P. (2017). Spatial distribution of Winkler spring stiffness for rectangular mat foundation analysis. *Engineering Structures*, 137, 443–459.
- Marto, A., Latifi, N., Janbaz, M., Kholghifard, M., Khari, M., Alimohammadi, P., & Banadaki, A. D. (2012). Foundation size effect on modulus of subgrade reaction on sandy soils. *Electronic Journal of Geotechnical Engineering*, 17, 2523-2530.

- Móczár, B., Polgár, Z., & Mahler, A. (2016). A comparative study of soil-structure interaction in the case of frame structures with raft foundation. Department of Engineering Geology and Geotechnics, Budapest University of Technology and Economics.
- Obrzud, F. R. (2018). On the use of the Hardening Soil Small Strain model in geotechnical practice. Elmepress International, Lausanne.
- Obrzud, F. R., & Truty, A. (2020). The Hardening Soil Model – A Practical Guidebook (PC 100701 Report, Revised 02.01.2020). Z Soil.
- Özer, Ö., & Yüksel, B. (2021). Comparison of the effect of foundation analysis methods on structural analysis results of tall buildings. *International Advanced Researches and Engineering Journal*, 15(1), 106-112.
- Poulos, H. G. (2000). *Foundation settlement analysis - Practice versus Research*. College Station Hilton.
- Patil, S. S., Kalyanshetti, M. G., & Dyawarkonda, S. S. (2016). Parametric study of RC frames with raft foundation considering soil structure interaction using spring. *International Journal of Scientific Development and Research*, 1(4), 63-67.
- Reference Manual PLAXIS 3D. (2013). PLAXIS bv.
- Scott R. F. (1981). *Foundation analysis*. Englewood Cliffs, NJ. Prentice Hall (1981)
- Sommer, H. (1965). A method for the calculation of settlements, contact pressures and bending moments in a foundation including the influence of the flexural rigidity of the superstructure. In *Proceedings of the 6th International Conference on Soil Mechanics and Foundation Engineering*, Montréal, Que. Vol. 2, 194–201.
- Stavridis, L. T. (2000). Simplified analysis of layered soil-structure interaction. *Journal of Structure Engineering*. ASCE, 126(2), 224-230.
- Stewart, J., Crouse, C., Hutchinson, T., Lizundia, B., Naeim, F., & Ostadan, F. (2012). *Soil-structure interaction for building structures*, Grant/Contract Reports, National Institute of Standards and Technology, Gaithersburg. Available at: https://tsapps.nist.gov/publication/get_pdf.cfm?pub_id=915495
- Sun, X., & Wu, L. (2011). Analysis on influence of superstructure stiffness of tall building-foundation-subsoil interaction. *Applied Mechanics and Materials*, 71-78.
- Tabsh, S.W., & El-Emam, M. (2021). Influence of foundation rigidity on the structural response of mat foundation. *Advances in Civil Engineering*. Retrieved from <https://doi.org/10.1155/2021/5586787>
- Terzaghi, K. (1955). Evaluation of coefficients of subgrade reaction. *Géotechnique*, 5(4), 297-326. <http://dx.doi.org/10.1680/geot.1955.5.4.297>.
- Tjie Liong, G. (2001). Notes on the application of spring constant and soil structure interaction problem. *Indo Construction*, 2(8), 29-33.

Tribedi, A. (2013). Correlation between soil bearing capacity and modulus of subgrade reaction. Structure Magazine. Retrieved from <http://www.structuremag.org/?p=1239> [Accessed 23 Oct. 2019].

Walker, W. W., & Holland, J. A. (2016). Modulus of subgrade reaction-which one should be used? SSI Structural Services, Inc.

Retrieved from

<https://www.ssiteam.com/uploads/collections/ModulusofSubgradeReaction.pdf>

Winkler, E. (1867). Die lehre von der elastizität und festigkeit [The theory of elasticity and strength] Dominicus, Prague.

APPENDICES

A. Material Properties of the Structural Concrete Elements (rafts, columns, beams) for PLAXIS 2D and SAP2000

| Parameter | Name | Concrete Elements | Unit |
|-----------------|-------|-------------------|-------------------|
| Material Type | - | Elastic | - |
| Isotropic | - | Yes | - |
| Young's modulus | E | 25×10^6 | kN/m ² |
| Poisson's ratio | ν | 0.15 | - |

B. Single Thicker Foundation Calculations for Superstructure Replacement

Calculations for single thicker foundation to replace the five-story four-span superstructure, is presented below;

Raft Thickness: 1.2 meters, Raft Width: 25 meters

Slab Thickness: 0.3 meters, Number of Floors: 5

Column Width: 0.3 meters, Column Height: 2.5 meters

Total Weight of the five-story structure = $1.2 * 25 * 25 \text{ kN/m}^3 + 0.3 * 5 * 25 * 25 \text{ kN/m}^3 + 0.3 * 25 * 2.5 * 25 \text{ kN/m}^3 + (25 + 35 + 35 + 35 + 25) \cong \mathbf{2311 \text{ kN/m}}$

$EI \text{ Raft} = 25 \text{ MPa} * 1/12 * 1 * 1.2^3 = 3.6 * 10^6 \text{ kN.m}^2$

$EI \text{ Slab} = 25 \text{ Mpa} * 1/12 * 1 * 0.3^3 = 56250 \text{ kN.m}^2$

For 5 Slabs = $56250 * 5 = 281250 \text{ kN.m}^2$

$EI \text{ Total} = 3.6 * 10^6 \text{ kN.m}^2 + 281250 \text{ kN.m}^2 = 3.881 * 10^6 \text{ kN.m}^2$

Raft Thick. of Thicker Found. = $(3.881 * 10^6 \text{ kN.m}^2 / 25 \text{ Mpa} * 12 / 1)^{1/3} = \mathbf{1.23 \text{ m}}$

Weight of the thicker foundation = $1.23 * 25 * 25 \text{ kN/m}^3 = \mathbf{769 \text{ kN/m}}$

Total, $2311 \text{ kN/m} - 769 \text{ kN/m} = \mathbf{1542 \text{ kN/m}}$ load should be applied at column positions on thicker foundation.

Calculations for single thicker foundation to replace the four-story five-span superstructure, is presented below;

Raft Thickness: 0.6 meters, Raft Width: 20 meters

Slab Thickness: 0.3 meters, Number of Floors: 4

Column Width: 0.3 meters, Column Height: 2.5 meters

Total Weight of the five-story structure = $0.6 * 20 * 25 \text{ kN/m}^3 + 0.3 * 4 * 20 * 25 \text{ kN/m}^3 + 0.3 * 24 * 2.5 * 25 \text{ kN/m}^3 + (25 + 50 + 50 + 25) \cong \mathbf{1500 \text{ kN/m}}$

$EI \text{ Raft} = 25 \text{ MPa} * 1/12 * 1 * 0.6^3 = 4.5 * 10^5 \text{ kN.m}^2$

$EI \text{ Slab} = 25 \text{ Mpa} * 1/12 * 1 * 0.3^3 = 56250 \text{ kN.m}^2$

For 4 Slabs = $56250 * 5 = 225000 \text{ kN.m}^2$

$EI \text{ Total} = 4.5 * 10^5 \text{ kN.m}^2 + 225000 \text{ kN.m}^2 = 6.75 * 10^5 \text{ kN.m}^2$

Raft Thick. of Thicker Found. = $(4.5 * 10^5 \text{ kN.m}^2 / 25 \text{ Mpa} * 12 / 1)^{1/3} \cong \mathbf{0.69 \text{ m}}$

Weight of the thicker foundation = $0.69 * 20 * 25 \text{ kN/m}^3 = \mathbf{344 \text{ kN/m}}$

Total, $1500 \text{ kN/m} - 344 \text{ kN/m} = \mathbf{1556 \text{ kN/m}}$ load should be applied at column positions on thicker foundation.

C. Summary of Analyses

Table C.1 Analyses Specifications

| Analysis No | Raft Length (m) | Raft Thick. (m) | Soil E_{50}^{ref} (MPa) | E Concrete | Slab Thickness (m) | Number of Floors | Equivalent Raft Thickness (m) | Relative Rigidity (RR) | Load Concentration Ratio (LCR) | Computed 'a' values | Computed 'xi' values | Computed 'k _{edge} /k(x _i)' ratio |
|-------------|-----------------|-----------------|---------------------------|------------|--------------------|------------------|-------------------------------|------------------------|--------------------------------|---------------------|----------------------|--|
| 1 | 20 | 0.80 | 20 | 25000 | 0.2 | 6 | 0.82 | 0.087 | 0.48 | 3.76 | 8.8 | 1.55 |
| 2 | 30 | 0.80 | 20 | 25000 | 0.2 | 6 | 0.82 | 0.026 | 0.49 | 1.16 | 13.6 | 1.73 |
| 3 | 40 | 0.80 | 20 | 25000 | 0.2 | 6 | 0.82 | 0.011 | 0.50 | 0.53 | 18.4 | 1.77 |
| 4 | 50 | 0.80 | 20 | 25000 | 0.2 | 6 | 0.82 | 0.006 | 0.50 | 0.30 | 23.2 | 1.78 |
| 5 | 60 | 0.80 | 20 | 25000 | 0.2 | 6 | 0.82 | 0.003 | 0.50 | 0.21 | 28 | 1.79 |
| 6 | 40 | 1.00 | 25 | 25000 | 0.2 | 8 | 1.02 | 0.017 | 0.56 | 0.43 | 18.4 | 1.64 |
| 7 | 40 | 1.00 | 25 | 25000 | 0.2 | 10 | 1.03 | 0.017 | 0.56 | 0.45 | 18.4 | 1.64 |
| 8 | 40 | 1.00 | 25 | 25000 | 0.2 | 12 | 1.03 | 0.017 | 0.56 | 0.46 | 18.4 | 1.64 |
| 9 | 40 | 1.00 | 25 | 25000 | 0.2 | 14 | 1.04 | 0.017 | 0.56 | 0.47 | 18.4 | 1.64 |
| 10 | 40 | 1.00 | 25 | 25000 | 0.2 | 16 | 1.04 | 0.018 | 0.56 | 0.49 | 18.4 | 1.64 |

Table C.1 (cont'd)

| Analysis No | Raft Length (m) | Raft Thick. (m) | Soil E_{50}^{ref} (MPa) | E Concrete | Slab Thickness (m) | Number of Floors | Equivalent Raft Thickness (m) | Relative Rigidity (RR) | Load Concentration Ratio (LCR) | Computed 'a' values | Computed 'xi' values | Computed $'k_{edge}/k(x_i)'$ ratio |
|-------------|-----------------|-----------------|---------------------------|------------|--------------------|------------------|-------------------------------|------------------------|--------------------------------|---------------------|----------------------|------------------------------------|
| 11 | 40 | 1.00 | 20 | 25000 | 0.2 | 10 | 1.03 | 0.021 | 0.56 | 0.68 | 18.4 | 1.63 |
| 12 | 40 | 1.00 | 25 | 25000 | 0.2 | 10 | 1.03 | 0.017 | 0.56 | 0.45 | 18.4 | 1.64 |
| 13 | 40 | 1.00 | 30 | 25000 | 0.2 | 10 | 1.03 | 0.014 | 0.56 | 0.29 | 18.4 | 1.65 |
| 14 | 40 | 1.00 | 35 | 25000 | 0.2 | 10 | 1.03 | 0.012 | 0.56 | 0.17 | 18.4 | 1.66 |
| 15 | 40 | 1.00 | 40 | 25000 | 0.2 | 10 | 1.03 | 0.011 | 0.56 | 0.09 | 18.4 | 1.66 |
| 16 | 40 | 1.00 | 45 | 25000 | 0.2 | 10 | 1.03 | 0.009 | 0.56 | 0.02 | 18.4 | 1.66 |
| 17 | 40 | 1.00 | 50 | 25000 | 0.2 | 10 | 1.03 | 0.008 | 0.56 | -0.03 | 18.4 | 1.67 |
| 18 | 40 | 1.00 | 55 | 25000 | 0.2 | 10 | 1.03 | 0.008 | 0.56 | -0.08 | 18.4 | 1.67 |
| 19 | 40 | 1.00 | 65 | 25000 | 0.2 | 10 | 1.03 | 0.006 | 0.56 | -0.14 | 18.4 | 1.67 |
| 20 | 60 | 1.20 | 55 | 25000 | 0.2 | 20 | 1.24 | 0.004 | 0.75 | Eliminated | Eliminated | Eliminated |
| 21 | 45 | 1.20 | 55 | 25000 | 0.2 | 20 | 1.24 | 0.009 | 0.66 | -1.95 | 20.8 | 1.03 |
| 22 | 39 | 1.20 | 55 | 25000 | 0.2 | 20 | 1.24 | 0.014 | 0.61 | 0.31 | 17.92 | 1.65 |

Table C.1 (cont'd)

| Analysis No | Raft Length (m) | Raft Thick. (m) | Soil E_{50}^{ref} (MPa) | E Concrete | Slab Thickness (m) | Number of Floors | Equivalent Raft Thickness (m) | Relative Rigidity (RR) | Load Concentration Ratio (LCR) | Computed 'a' values | Computed 'xi' values | Computed ' $k_{edge}/k(x_i)$ ' ratio |
|-------------|-----------------|-----------------|---------------------------|------------|--------------------|------------------|-------------------------------|------------------------|--------------------------------|---------------------|----------------------|--------------------------------------|
| 23 | 37 | 1.20 | 55 | 25000 | 0.2 | 20 | 1.24 | 0.017 | 0.59 | 0.45 | 16.96 | 1.64 |
| 24 | 34 | 1.20 | 55 | 25000 | 0.2 | 20 | 1.24 | 0.022 | 0.55 | 0.73 | 15.52 | 1.63 |
| 25 | 30 | 1.20 | 55 | 25000 | 0.2 | 20 | 1.24 | 0.032 | 0.49 | 1.41 | 13.6 | 1.71 |
| 26 | 60 | 1.20 | 55 | 25000 | 0.2 | 20 | 1.24 | 0.004 | 0.62 | -0.28 | 28 | 1.68 |
| 27 | 34 | 1.50 | 60 | 25000 | 0.2 | 14 | 1.52 | 0.037 | 0.56 | 1.58 | 15.52 | 1.58 |
| 28 | 34 | 1.50 | 50 | 25000 | 0.2 | 7 | 1.51 | 0.044 | 0.56 | 1.96 | 15.52 | 1.57 |
| 29 | 32 | 1.30 | 35 | 25000 | 0.2 | 6 | 1.31 | 0.049 | 0.57 | 2.26 | 14.56 | 1.55 |
| 30 | 27 | 1.10 | 35 | 25000 | 0.3 | 5 | 1.14 | 0.053 | 0.44 | Eliminated | Eliminated | Eliminated |
| 31 | 26 | 1.00 | 30 | 25000 | 0.3 | 5 | 1.04 | 0.054 | 0.45 | 2.34 | 11.68 | 1.65 |
| 32 | 24 | 0.90 | 25 | 25000 | 0.3 | 4 | 0.94 | 0.060 | 0.61 | 2.91 | 10.72 | 1.52 |
| 33 | 23 | 1.00 | 40 | 25000 | 0.2 | 7 | 1.02 | 0.054 | 0.60 | 2.56 | 10.24 | 1.54 |
| 34 | 22 | 0.70 | 20 | 25000 | 0.3 | 6 | 0.80 | 0.059 | 0.61 | 2.84 | 9.76 | 1.52 |

Table C.1 (cont'd)

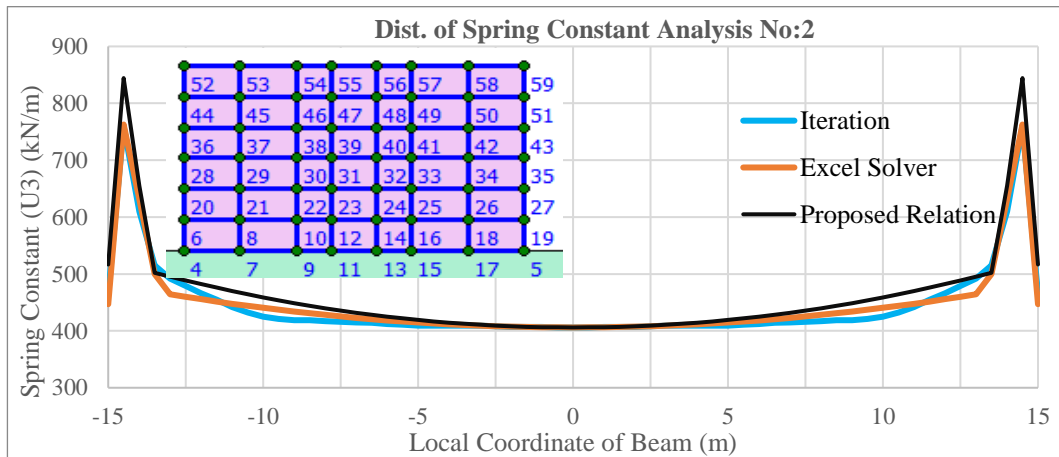
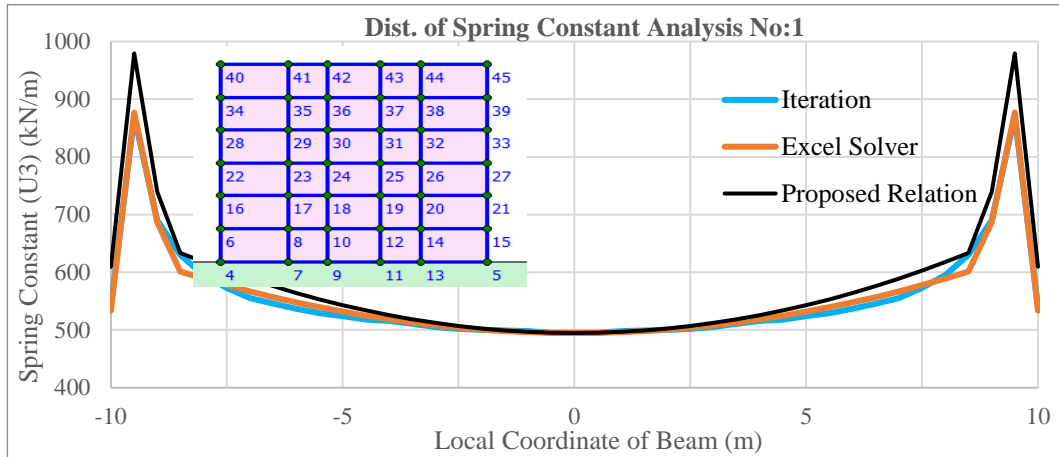
| Analysis No | Raft Length (m) | Raft Thick. (m) | Soil E_{50}^{ref} (MPa) | E Concrete | Slab Thickness (m) | Number of Floors | Equivalent Raft Thickness (m) | Relative Rigidity (RR) | Load Concentration Ratio (LCR) | Computed 'a' values | Computed 'xi' values | Computed ' $k_{edge}/k(x_i)$ ' ratio |
|-------------|-----------------|-----------------|---------------------------|------------|--------------------|------------------|-------------------------------|------------------------|--------------------------------|---------------------|----------------------|--------------------------------------|
| 35 | 20 | 0.80 | 40 | 25000 | 0.3 | 8 | 0.90 | 0.057 | 0.46 | 2.47 | 8.8 | 1.64 |
| 36 | 20 | 0.80 | 35 | 25000 | 0.3 | 8 | 0.90 | 0.065 | 0.58 | 3.17 | 8.8 | 1.5 |
| 37 | 21 | 0.80 | 30 | 25000 | 0.3 | 8 | 0.90 | 0.066 | 0.46 | 2.84 | 9.28 | 1.61 |
| 38 | 21 | 0.90 | 35 | 25000 | 0.3 | 6 | 0.96 | 0.069 | 0.41 | Eliminated | Eliminated | Eliminated |
| 39 | 21 | 0.90 | 35 | 25000 | 0.3 | 6 | 0.96 | 0.069 | 0.47 | 2.97 | 9.28 | 1.6 |
| 40 | 30 | 0.80 | 40 | 25000 | 0.3 | 12 | 0.94 | 0.019 | 0.46 | 0.89 | 13.6 | 1.74 |
| 41 | 20 | 0.70 | 40 | 25000 | 0.2 | 9 | 0.75 | 0.032 | 0.44 | Eliminated | Eliminated | Eliminated |
| 42 | 20 | 0.70 | 55 | 25000 | 0.2 | 6 | 0.73 | 0.022 | 0.44 | Eliminated | Eliminated | Eliminated |
| 43 | 25 | 1.00 | 45 | 25000 | 0.2 | 7 | 1.02 | 0.038 | 0.63 | 1.64 | 11.2 | 1.58 |
| 44 | 26 | 0.95 | 35 | 25000 | 0.3 | 5 | 1.00 | 0.040 | 0.44 | Eliminated | Eliminated | Eliminated |
| 45 | 20 | 0.70 | 50 | 25000 | 0.3 | 5 | 0.78 | 0.030 | 0.42 | Eliminated | Eliminated | Eliminated |
| 46 | 40 | 0.95 | 35 | 25000 | 0.2 | 6 | 0.97 | 0.010 | 0.48 | 0.49 | 18.4 | 1.77 |

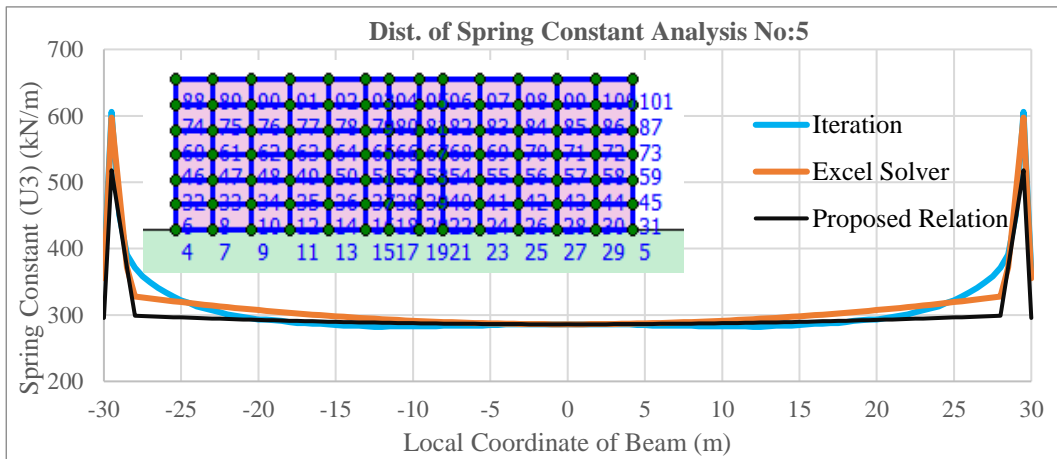
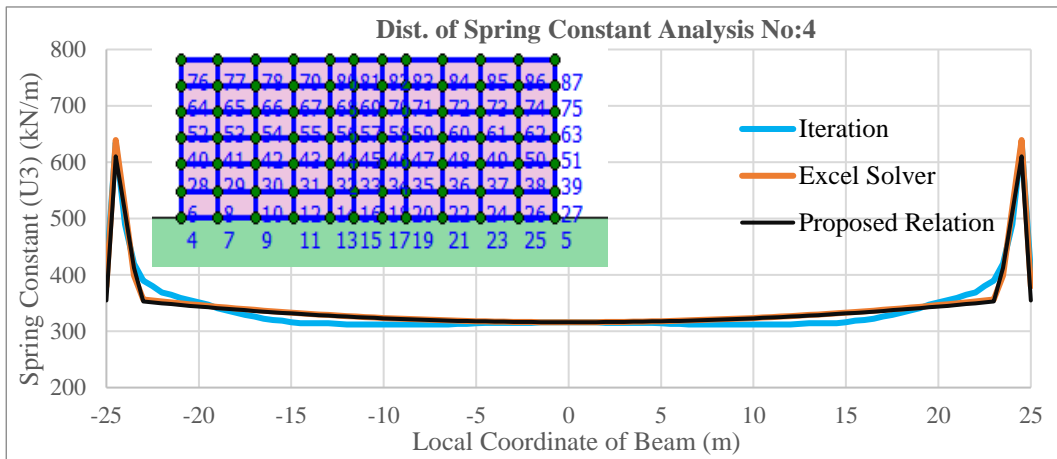
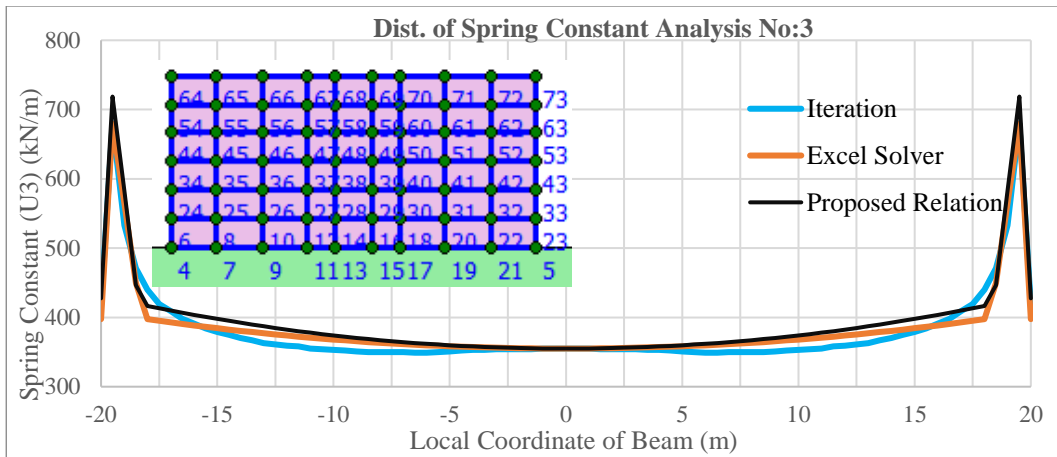
Table C.1 (cont'd)

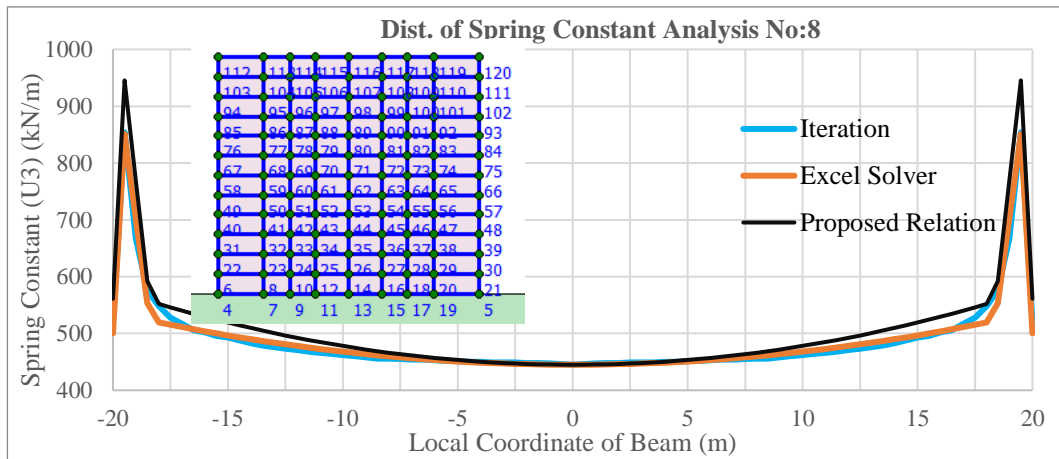
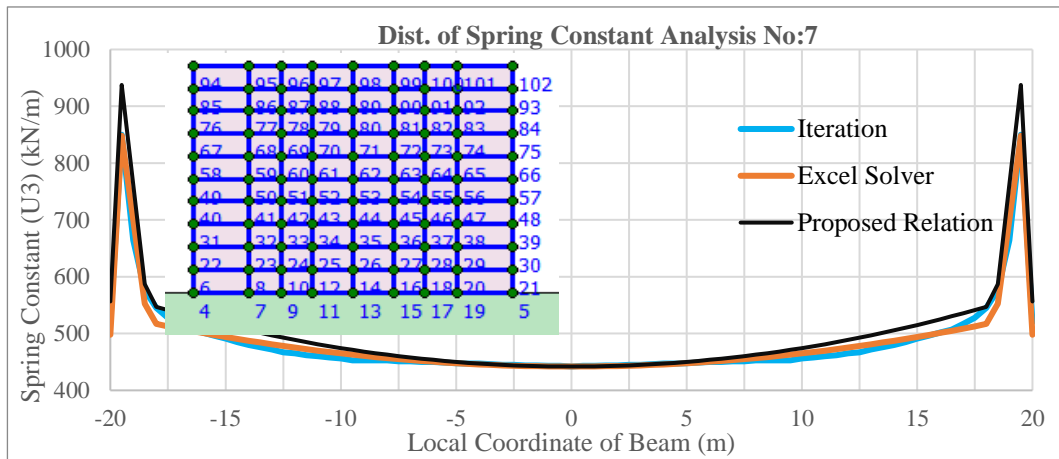
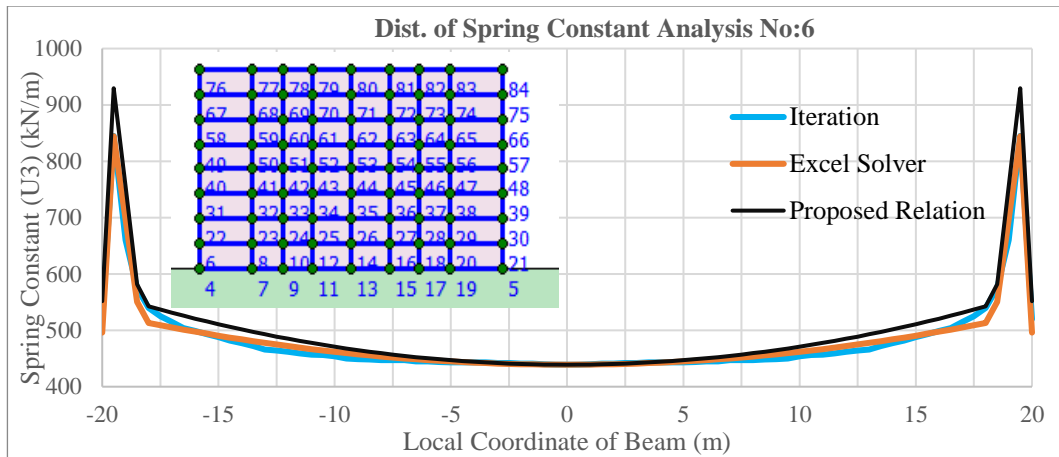
| Analysis No | Raft Length (m) | Raft Thick. (m) | Soil E_{50}^{ref} (MPa) | E Concrete | Slab Thickness (m) | Number of Floors | Equivalent Raft Thickness (m) | Relative Rigidity (RR) | Load Concentration Ratio (LCR) | Computed 'a' values | Computed 'xi' values | Computed $k_{edge}/k(x_i)$ ratio |
|-------------|-----------------|-----------------|---------------------------|------------|--------------------|------------------|-------------------------------|------------------------|--------------------------------|---------------------|----------------------|----------------------------------|
| 47 | 40 | 1.10 | 35 | 25000 | 0.2 | 12 | 1.13 | 0.016 | 0.48 | 0.74 | 18.4 | 1.75 |
| 48 | 20 | 0.80 | 40 | 25000 | 0.3 | 8 | 0.90 | 0.057 | 0.53 | 2.47 | 8.8 | 1.64 |
| 49 | 30 | 1.10 | 45 | 25000 | 0.2 | 11 | 1.12 | 0.029 | 0.51 | 1.30 | 13.6 | 1.72 |
| 50 | 34 | 1.10 | 50 | 25000 | 0.2 | 13 | 1.13 | 0.018 | 0.54 | 0.84 | 15.52 | 1.75 |
| 51 | 27 | 0.95 | 40 | 25000 | 0.2 | 7 | 0.97 | 0.029 | 0.66 | 0.46 | 12.16 | 1.33 |
| 52 | 26 | 1.00 | 35 | 25000 | 0.2 | 9 | 1.02 | 0.044 | 0.66 | 2.26 | 11.68 | 1.56 |
| 53 | 30 | 0.90 | 25 | 25000 | 0.2 | 6 | 0.92 | 0.029 | 0.66 | 0.44 | 13.6 | 1.33 |

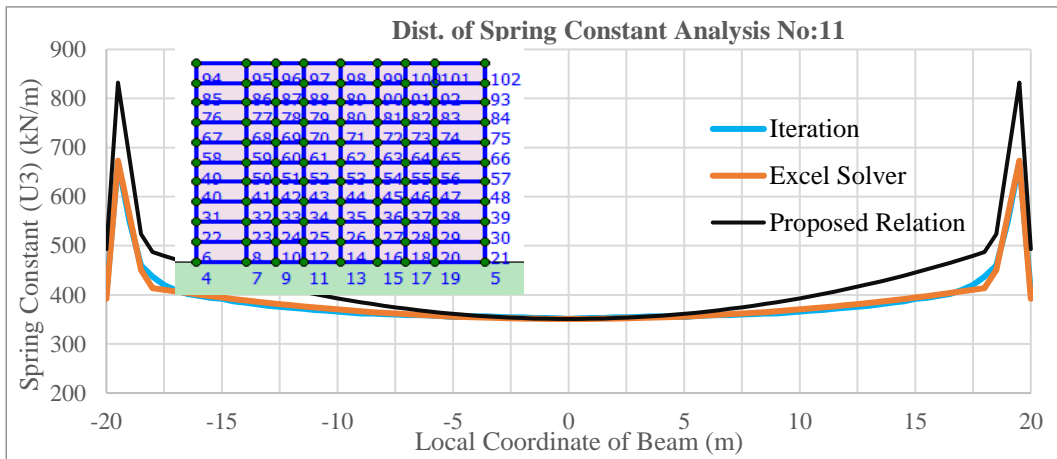
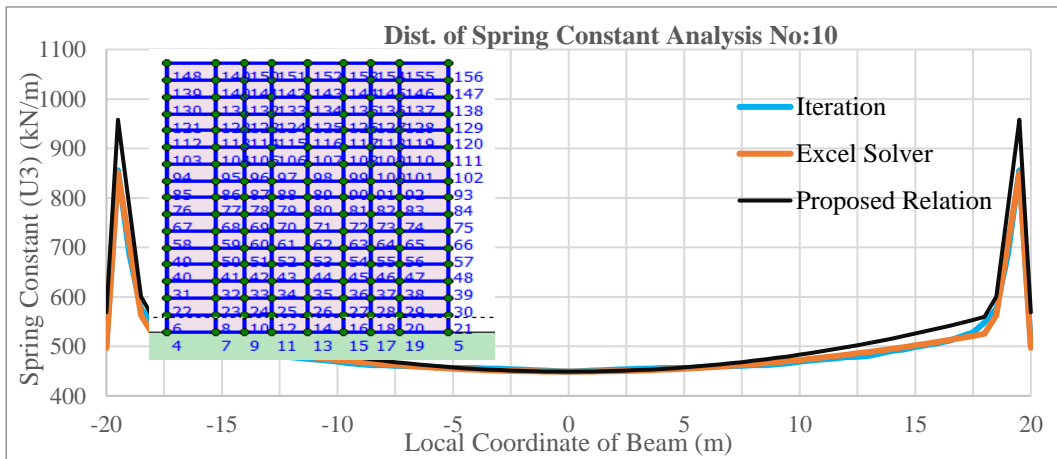
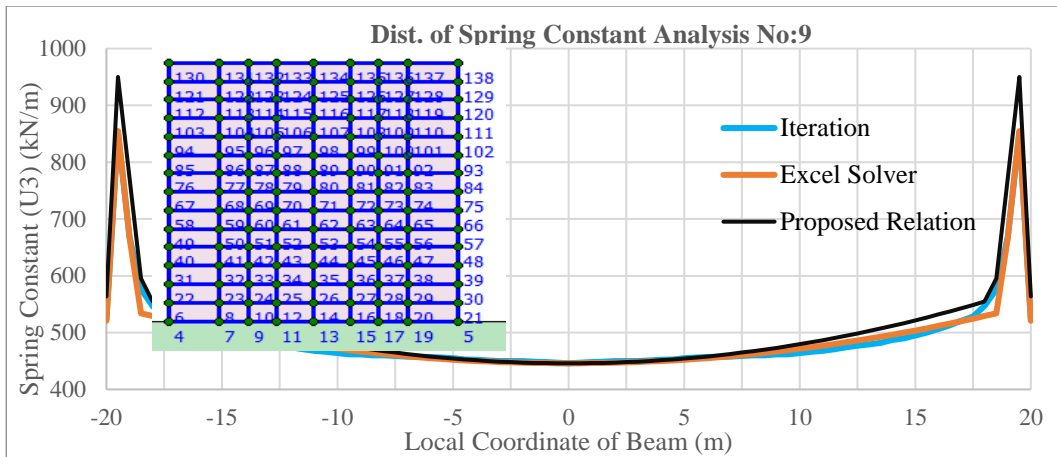
*Please refer to Section 4.1 for explanations of the extreme cases eliminated.

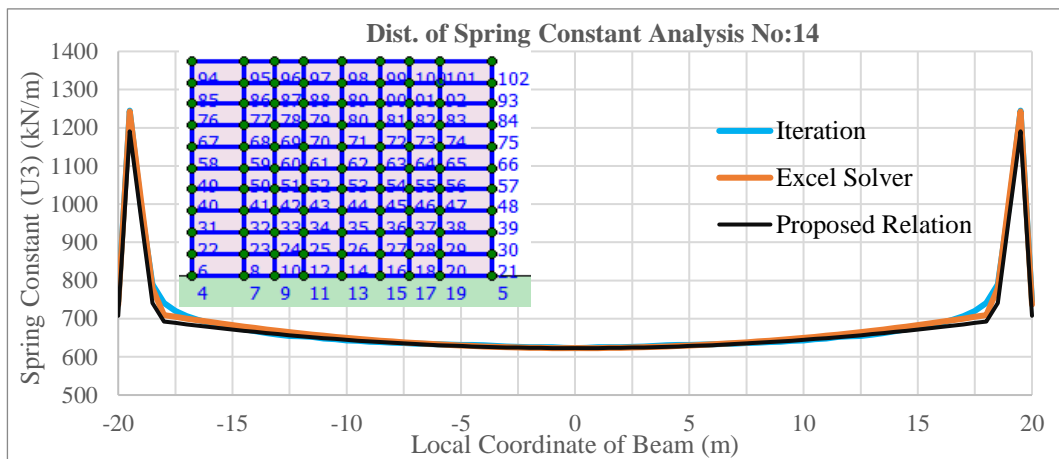
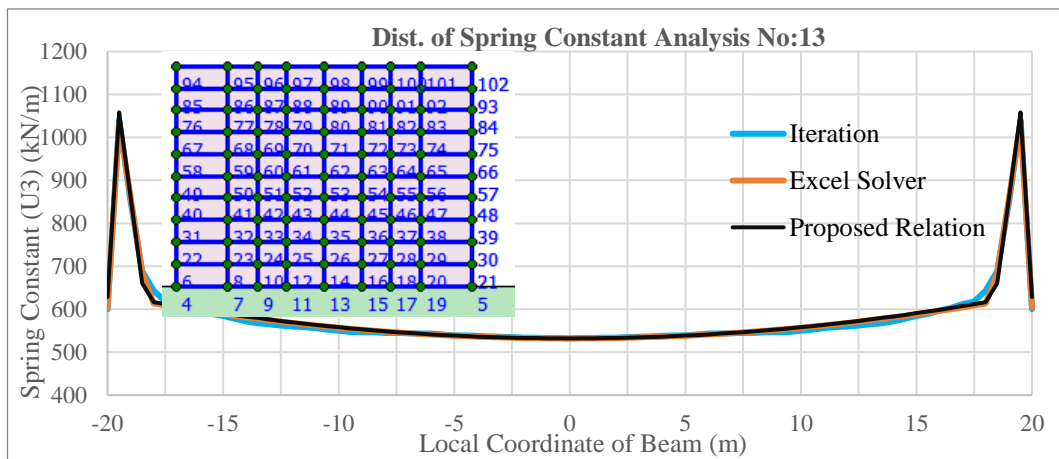
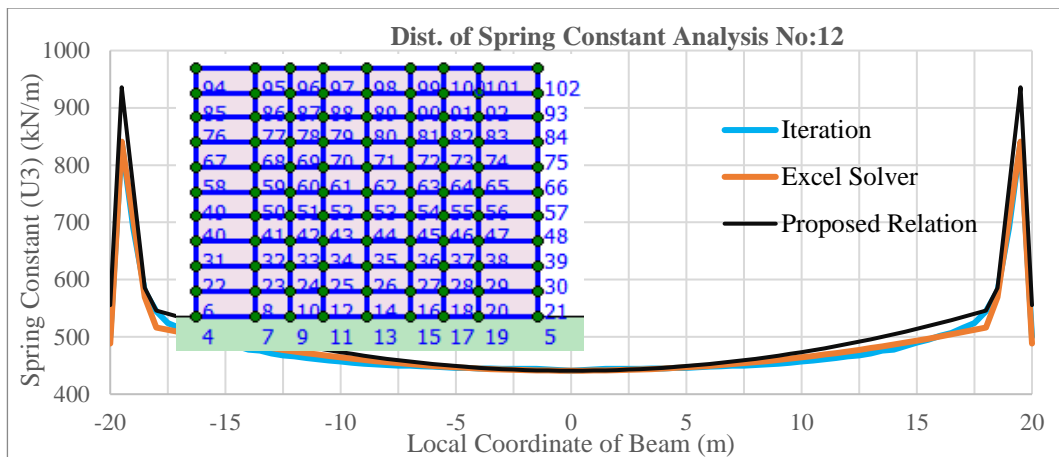
D. Spring Constant Distribution Results for 53 Analyses - Including Iteration (Continuum), Excel Solver Findings, and Proposed Relations

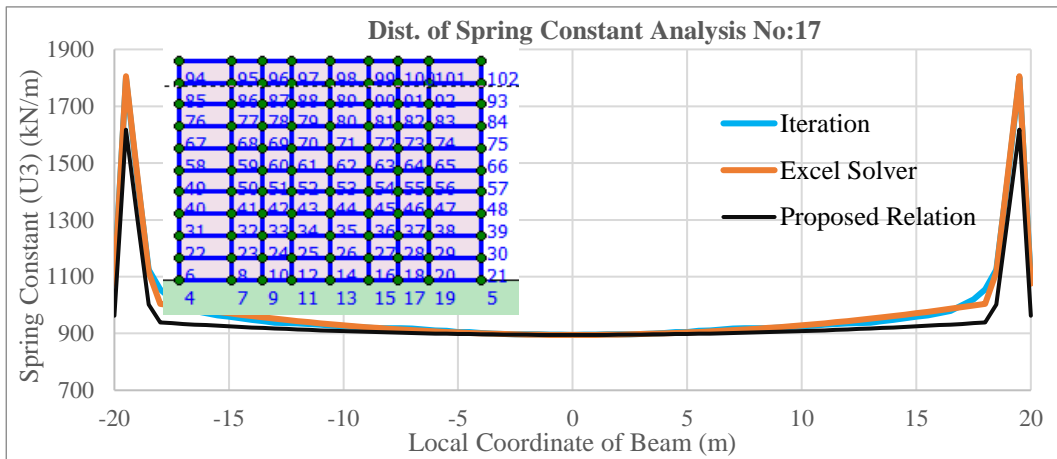
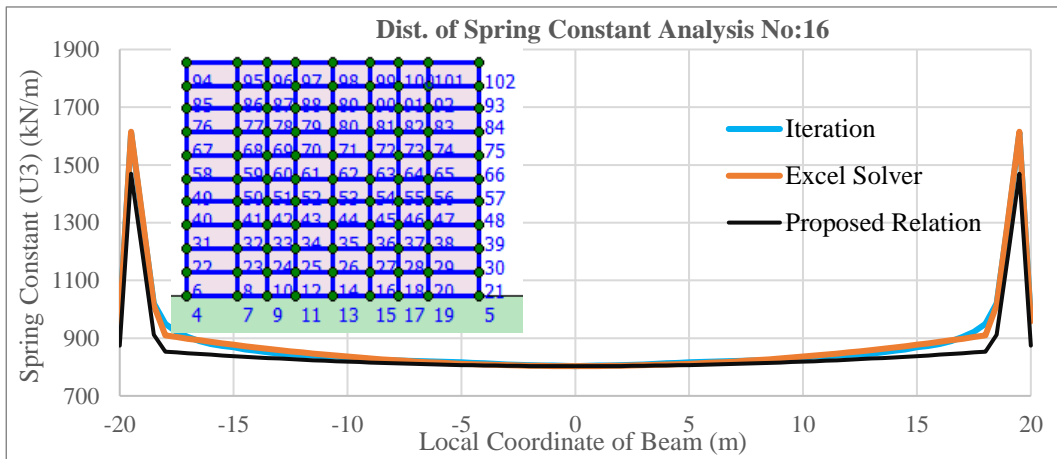
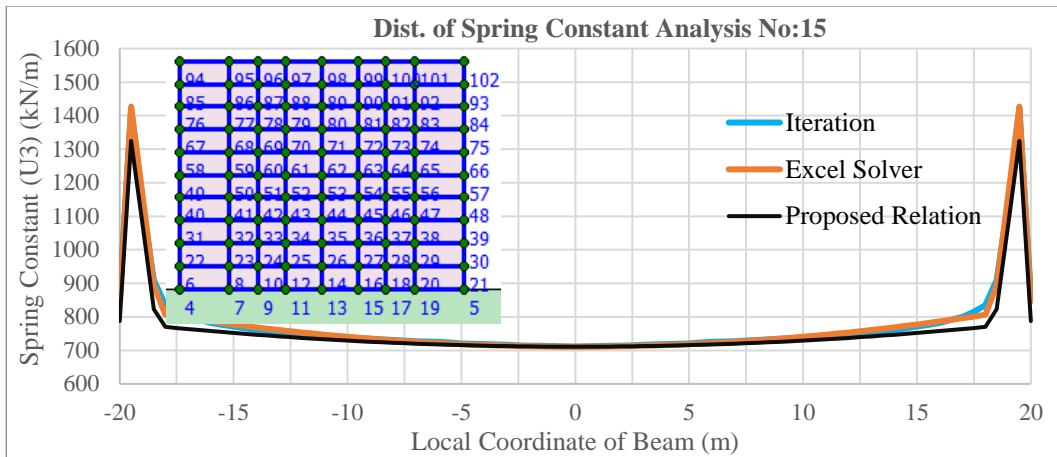


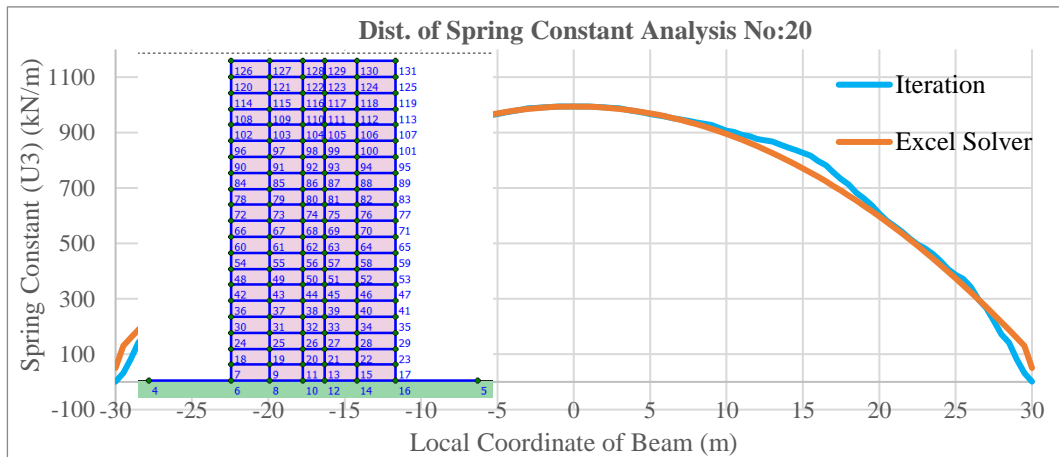
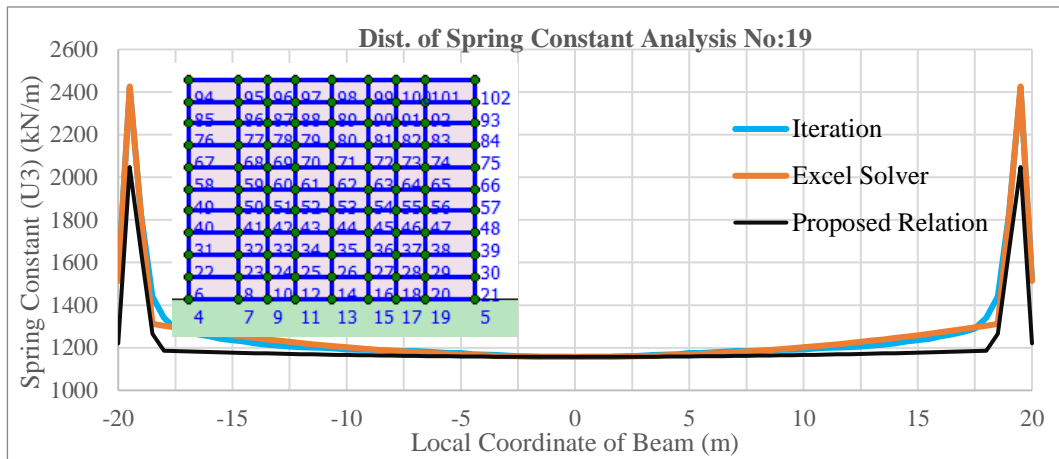
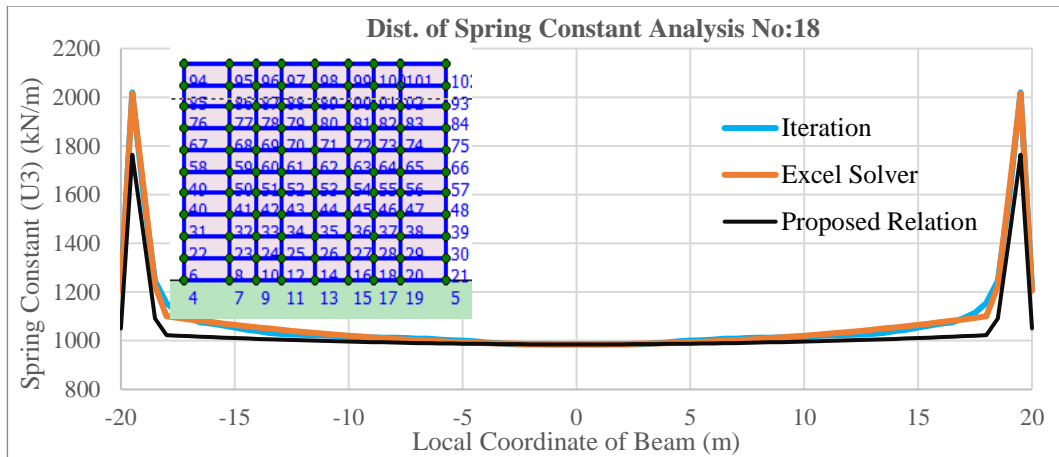


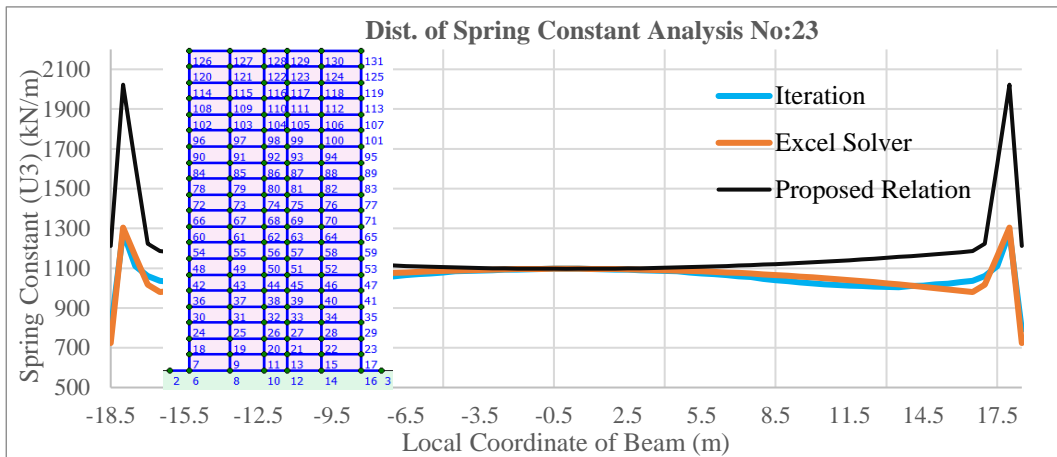
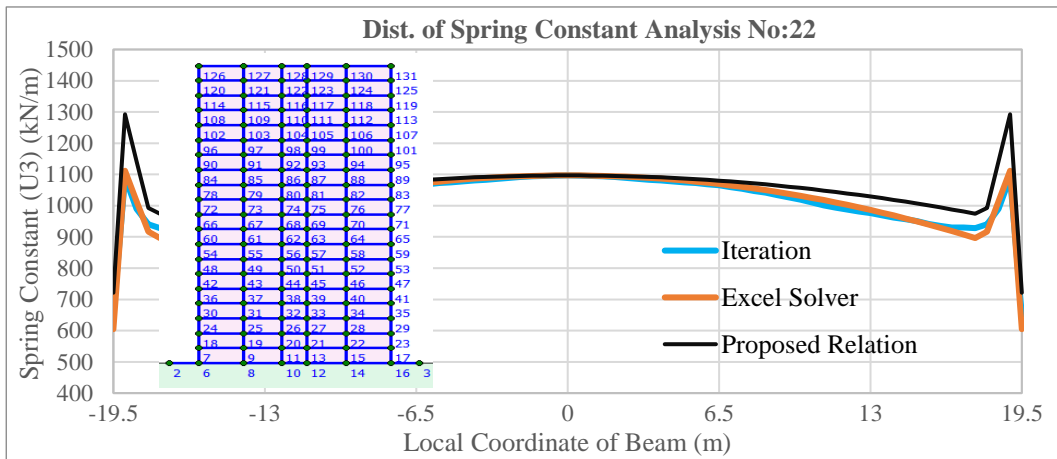
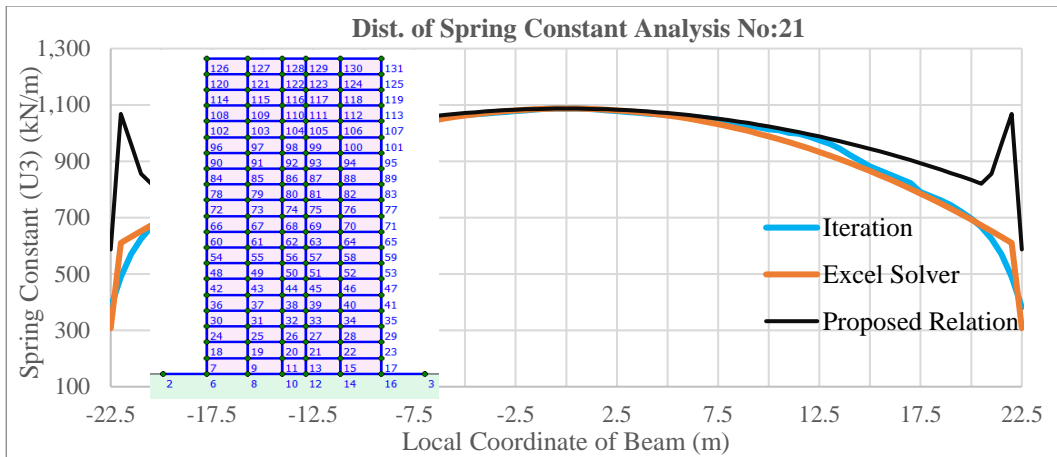


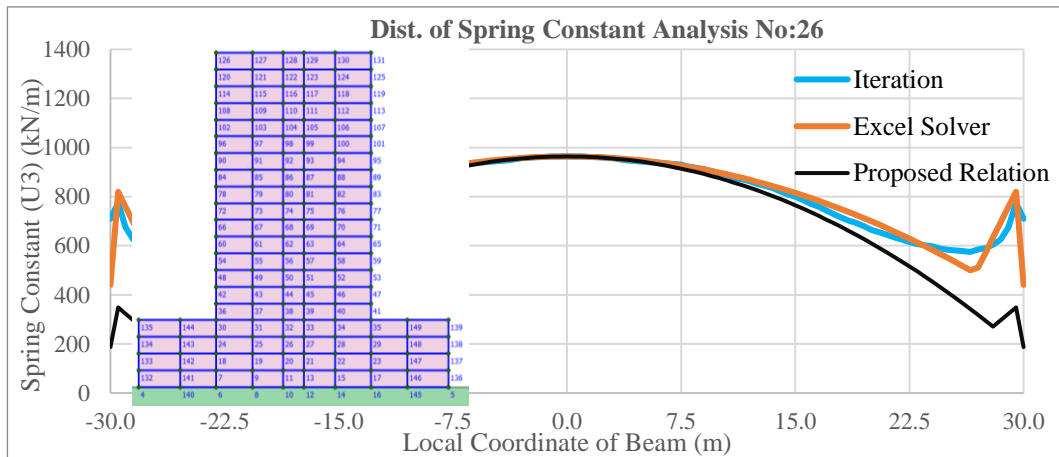
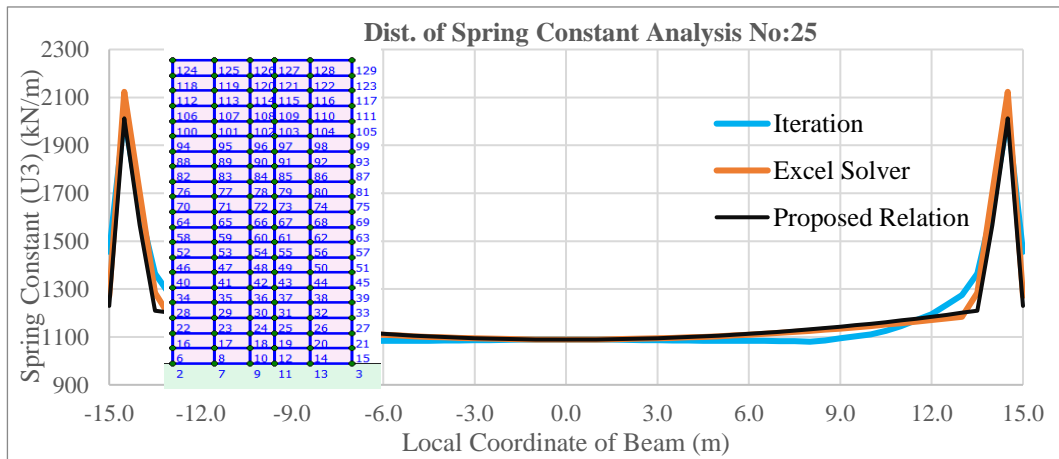
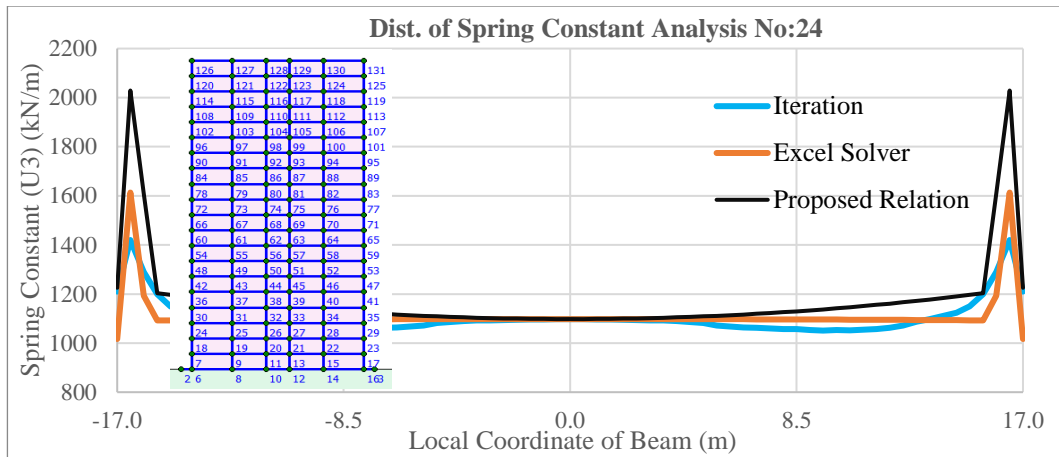


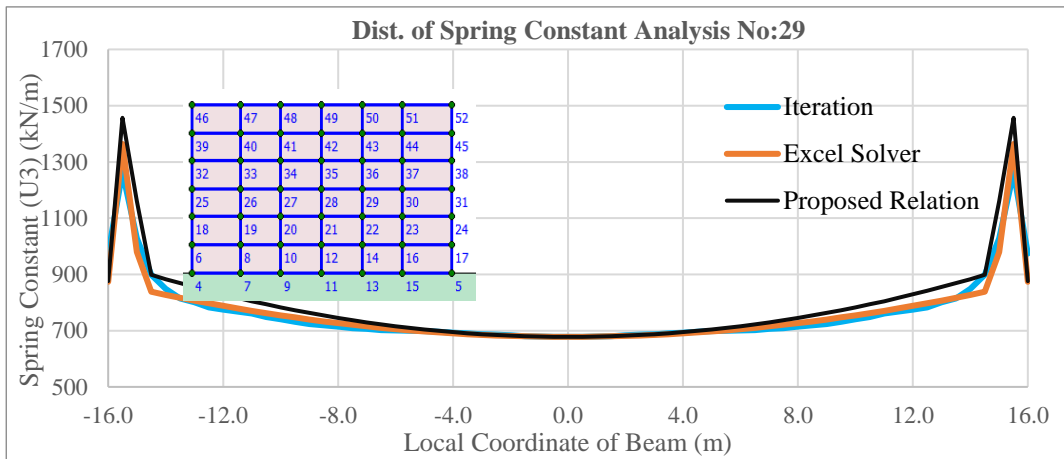
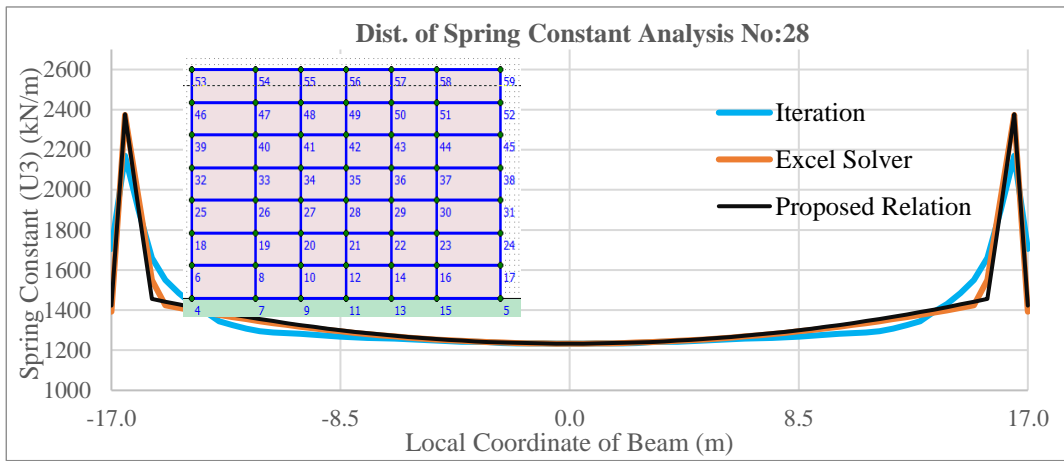
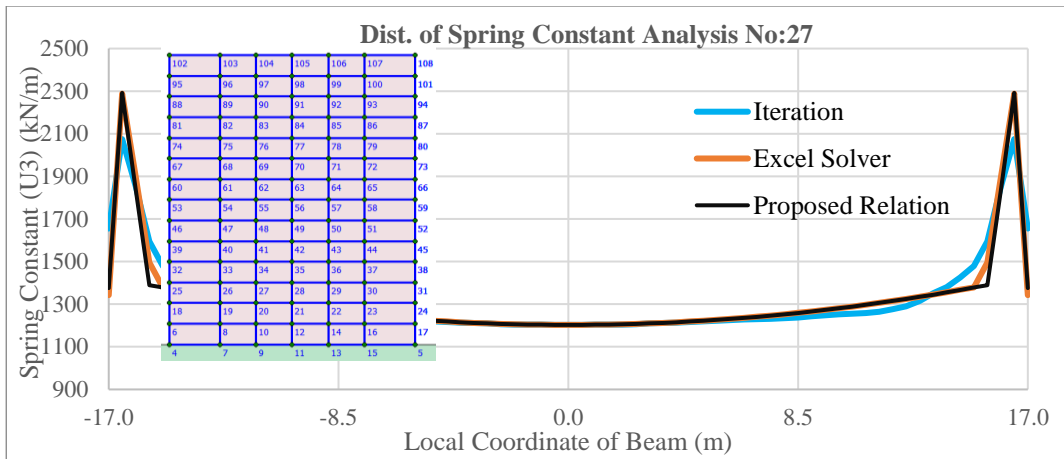


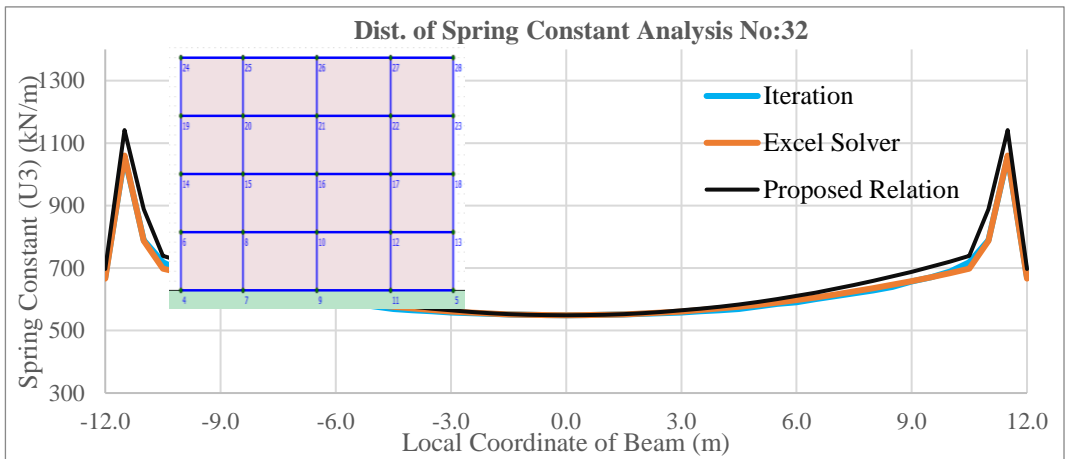
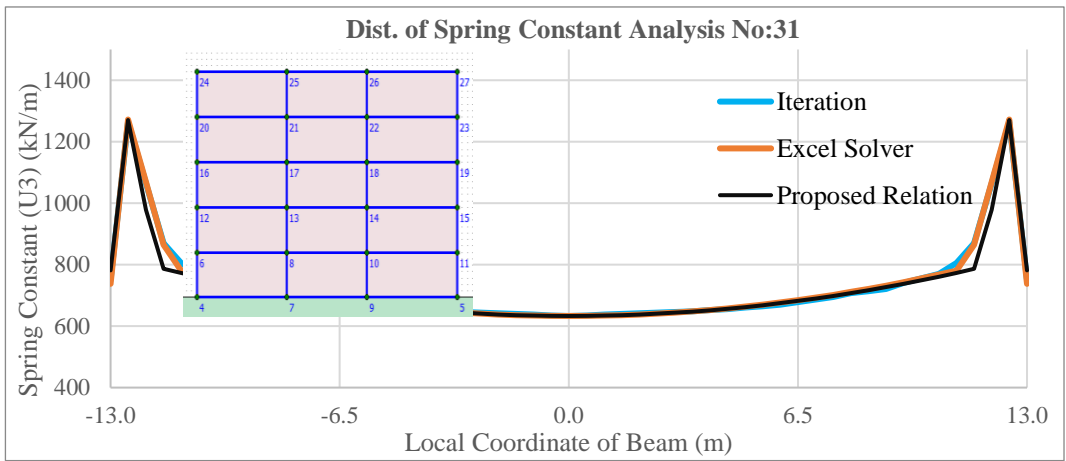
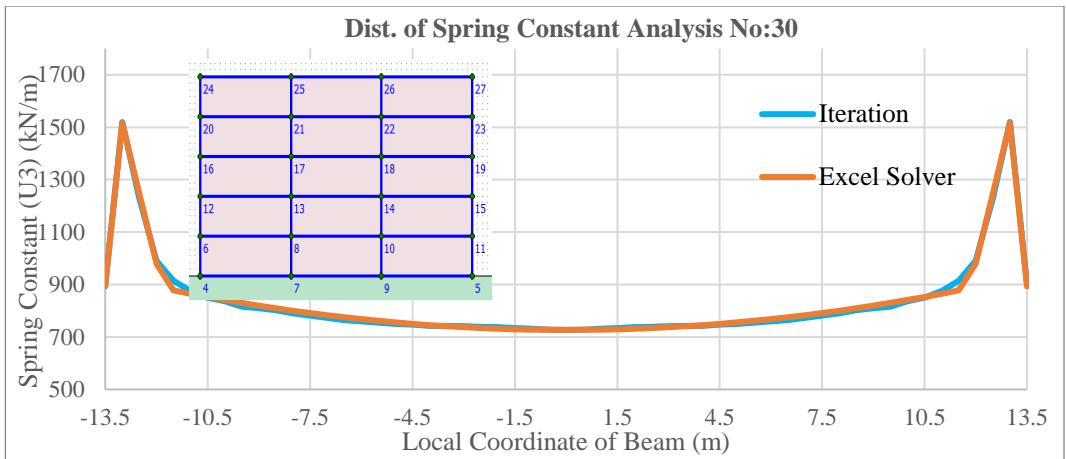


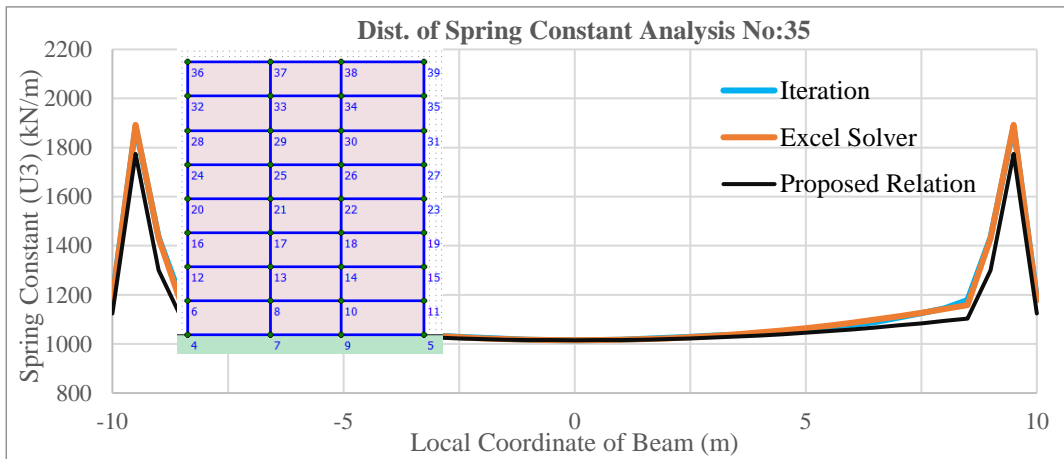
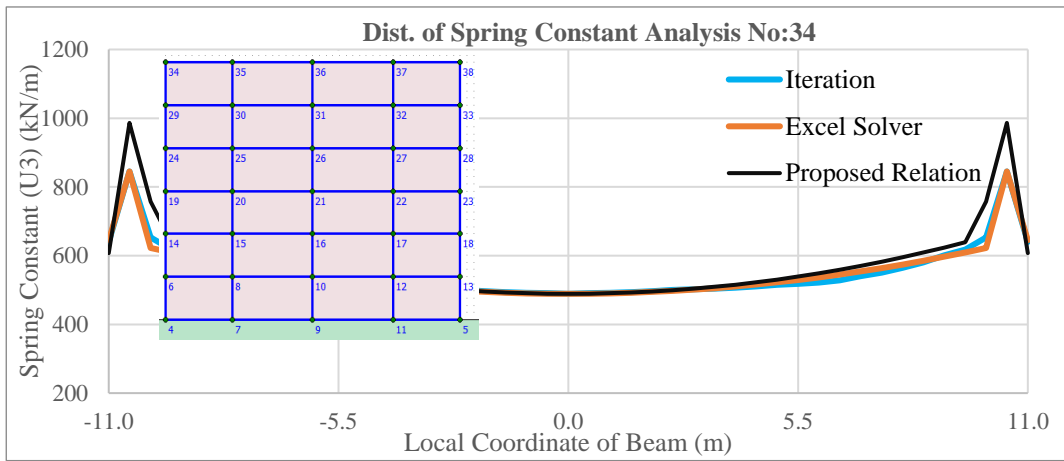
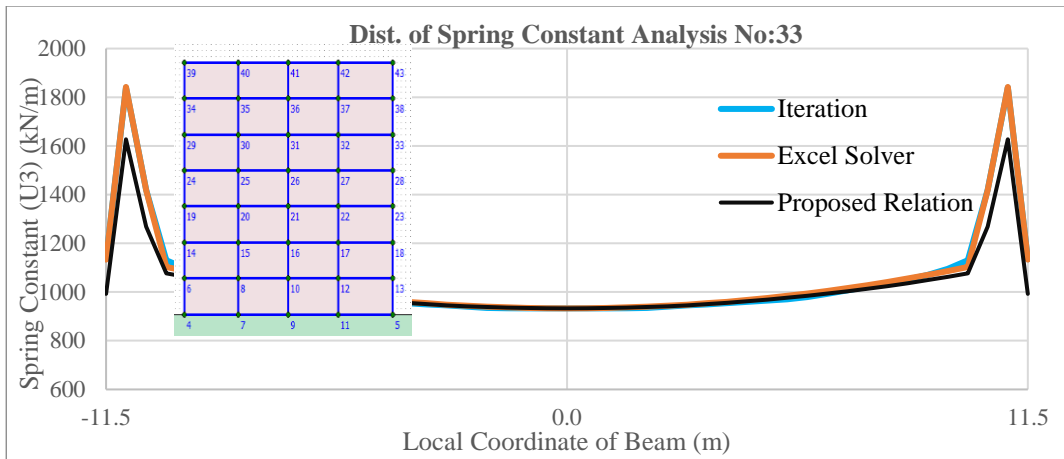


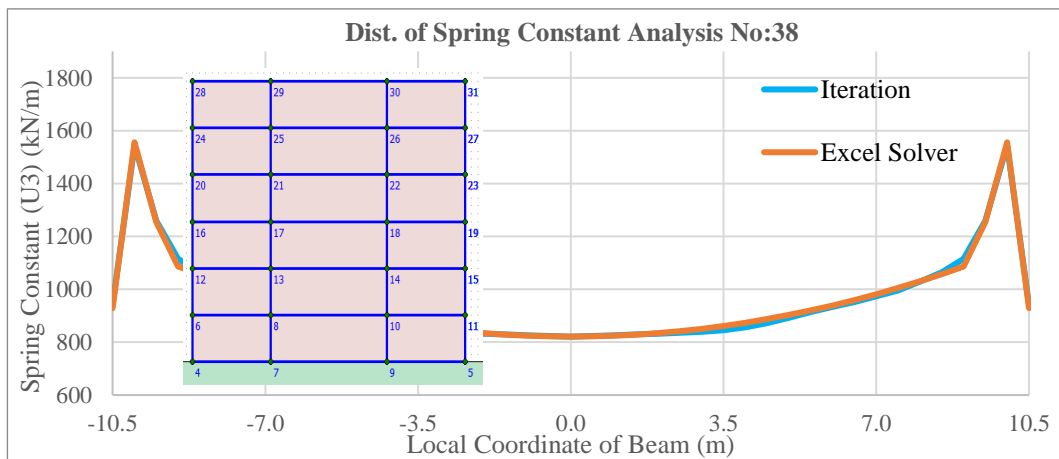
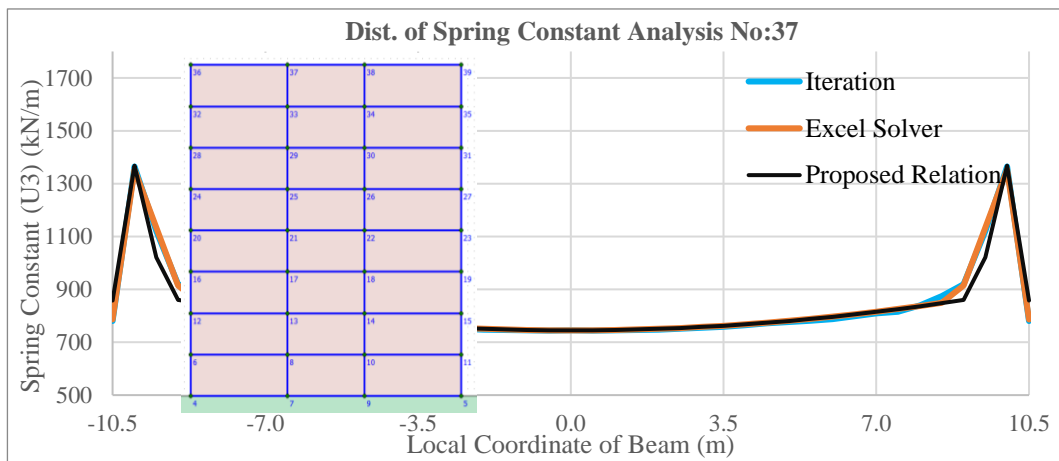
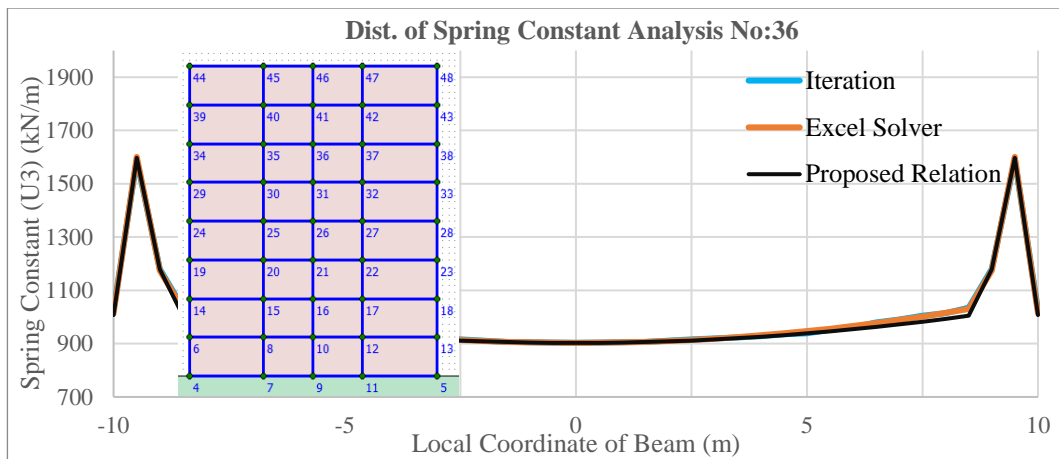


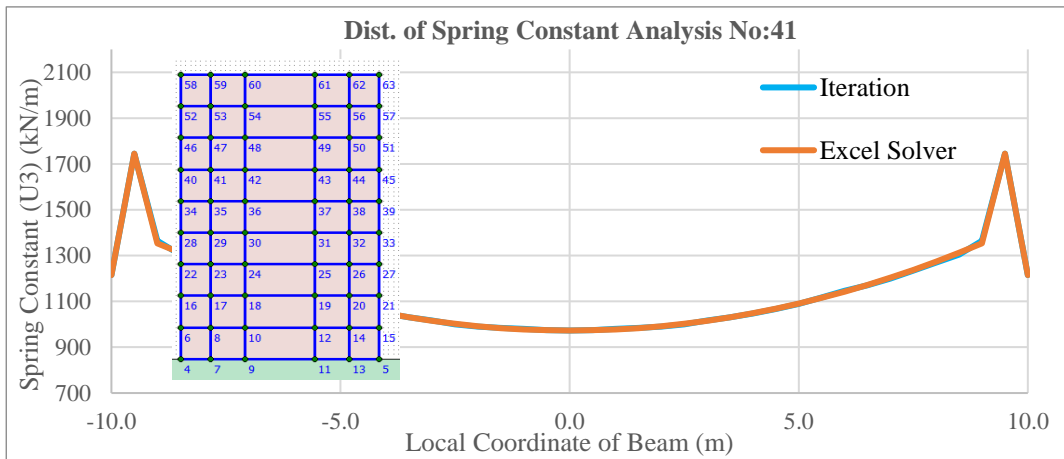
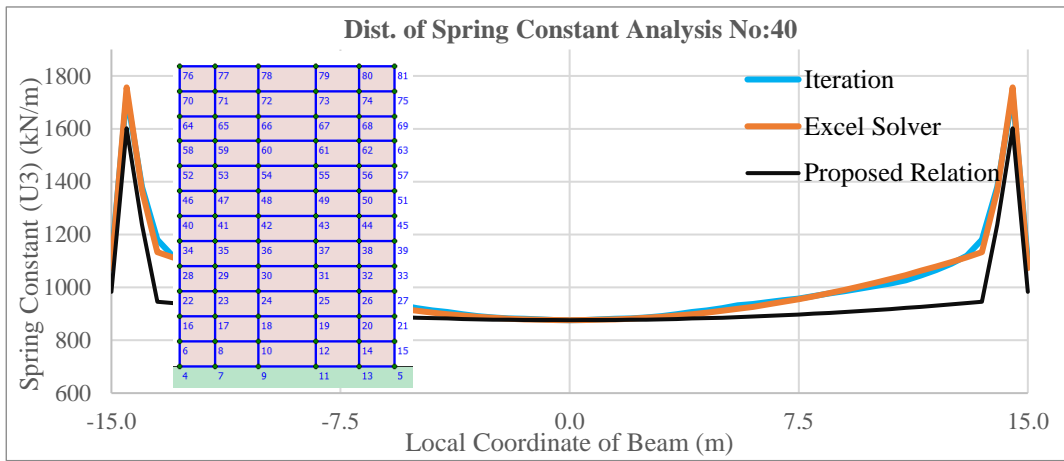
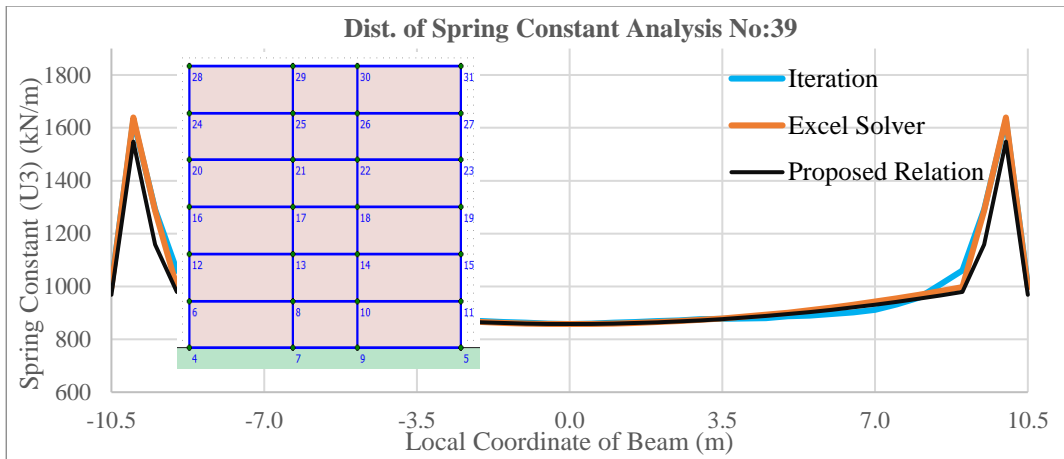


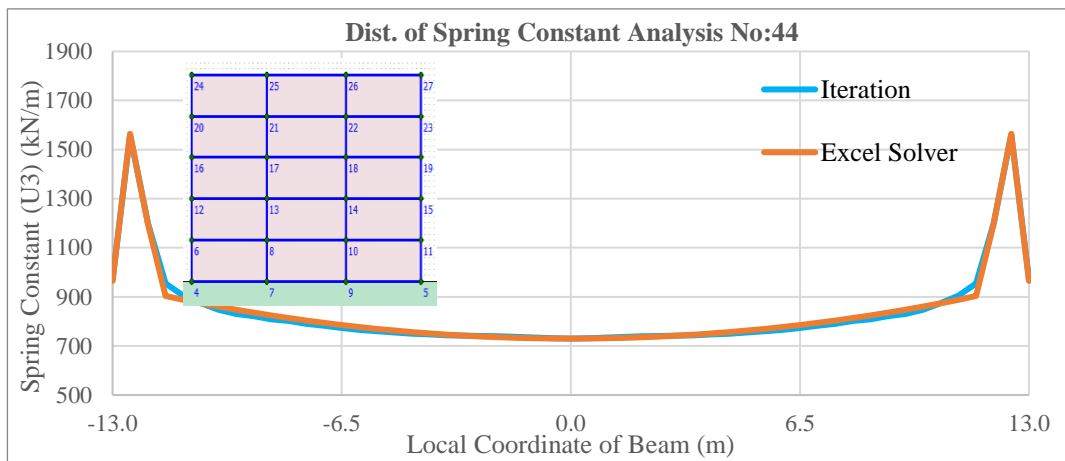
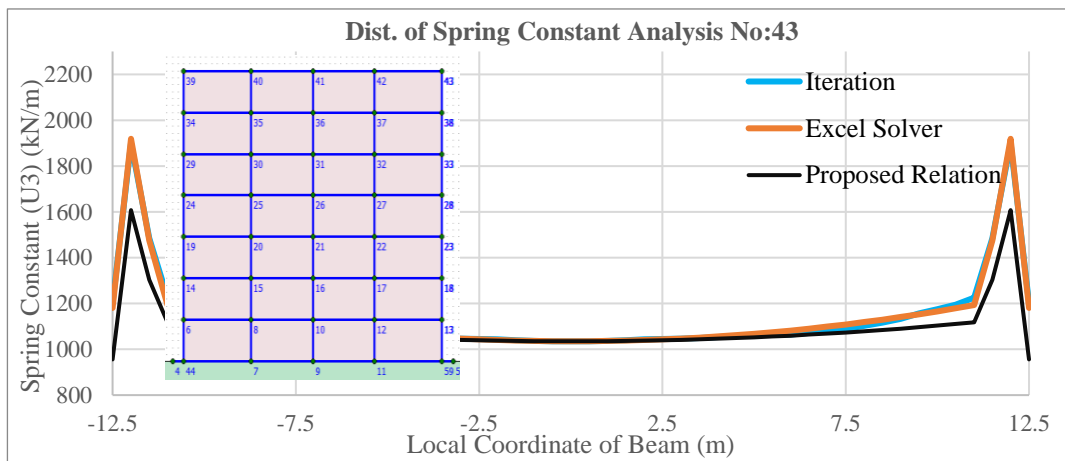
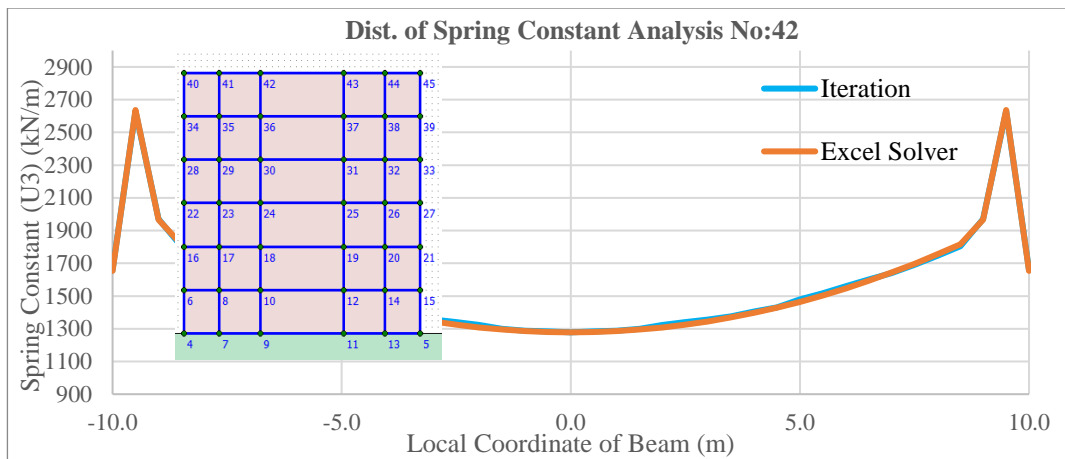


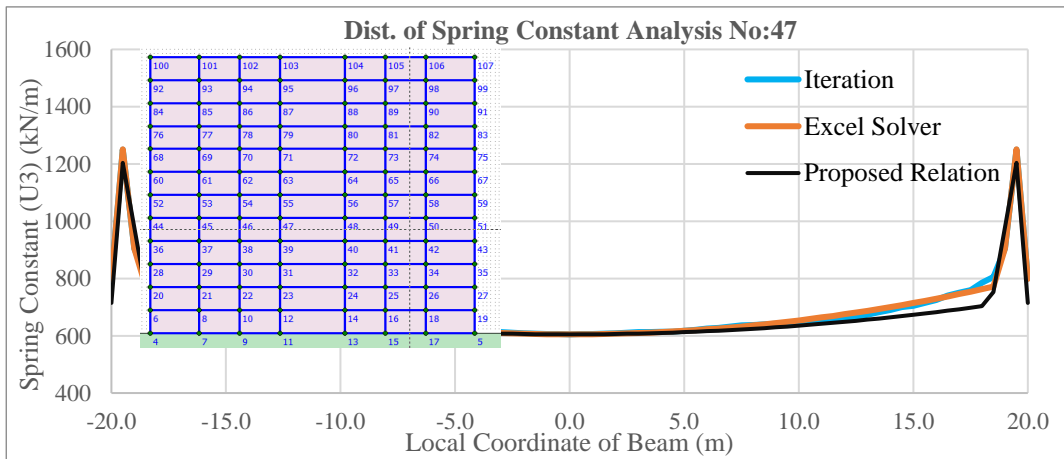
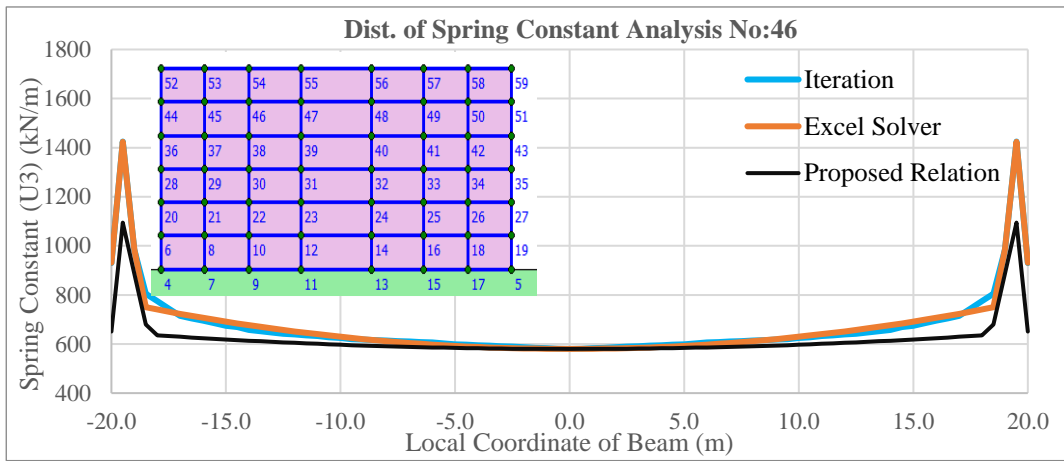
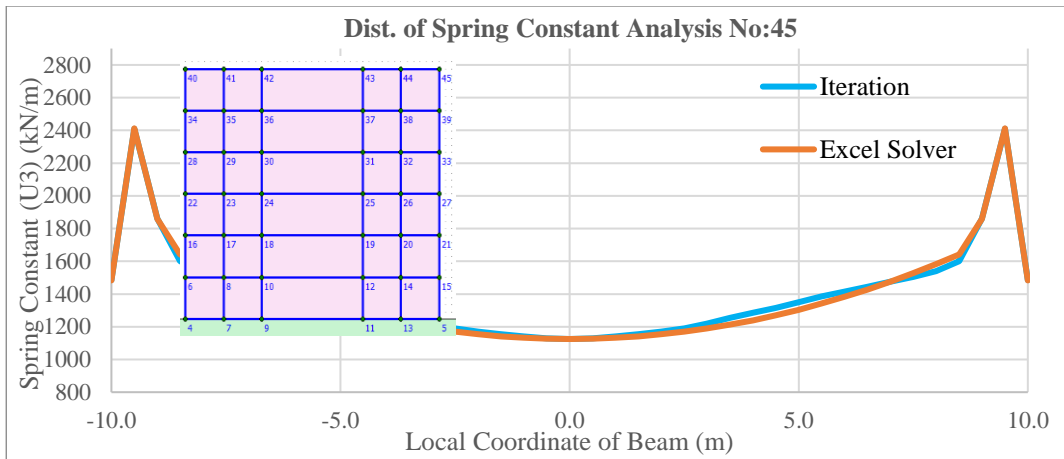


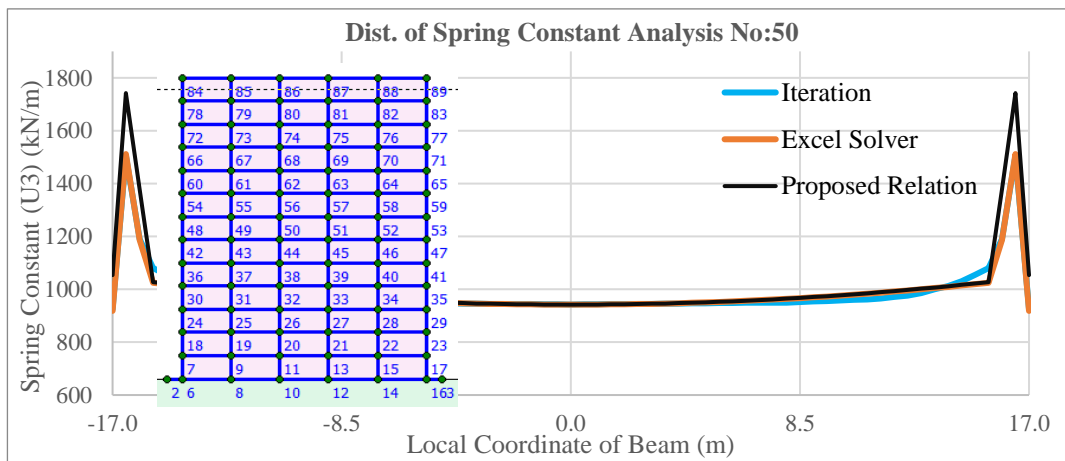
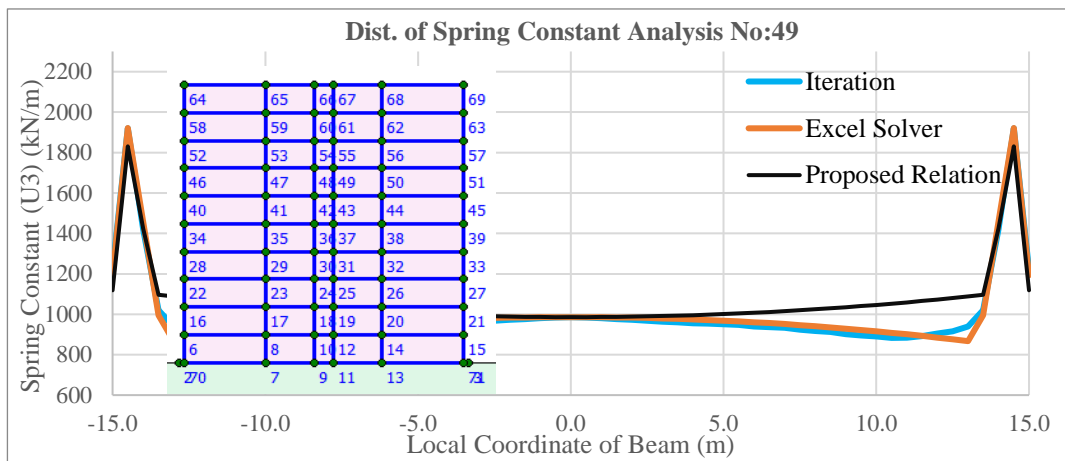
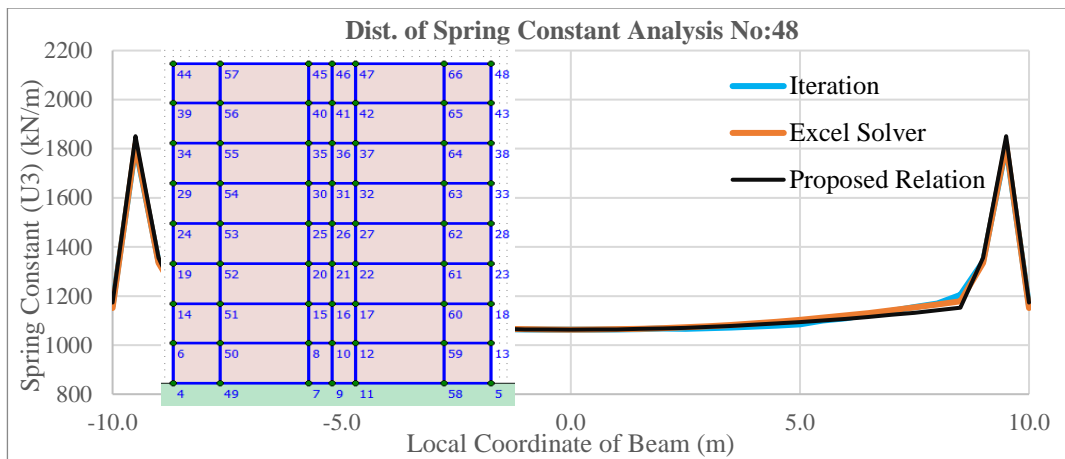


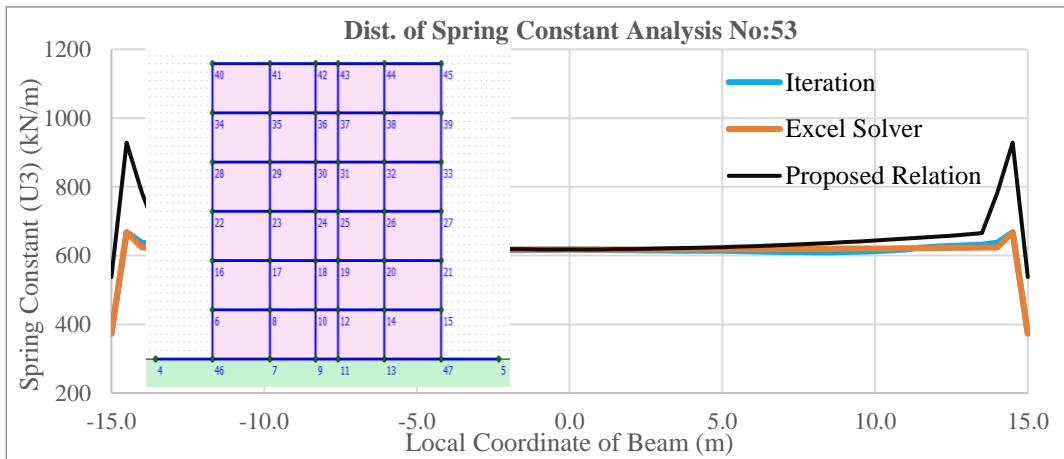
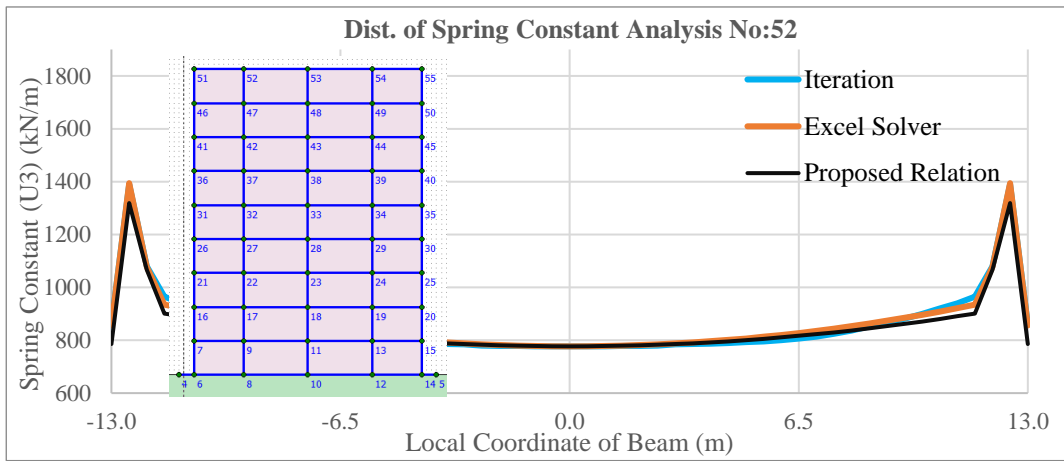
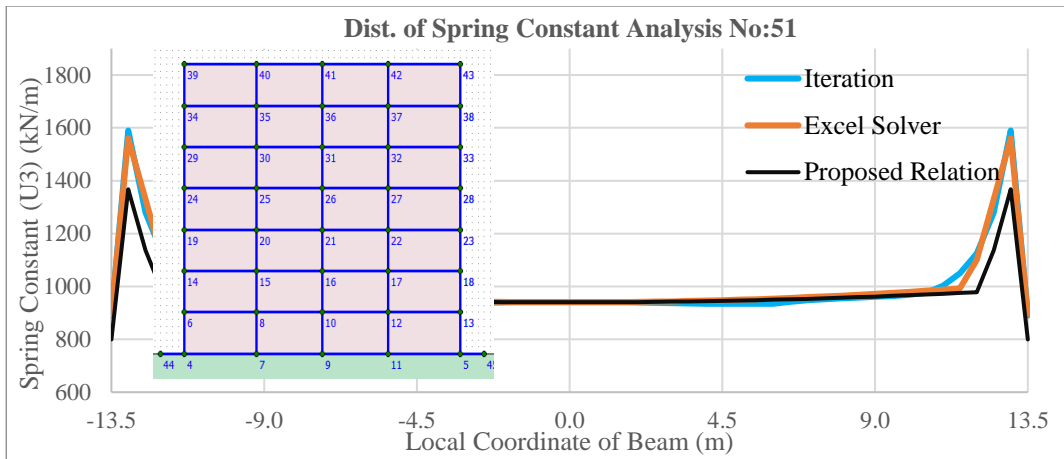












E. Views of Excel Program for Spring Constant Analysis

| | A | B | C | D | E | F | G | H | I | J | K |
|---|-----------------|----------------|----------------|-----------------|------------------|--------------------------------|------------------|-----------|-----------------------------|-----------------------------|-----------------------------|
| 1 | Raft Length (m) | Raft Width (m) | Raft Thickness | Slab Thick. (m) | Number of Floors | Soil Stiffness E_{sof} (MPa) | E_{calc} (MPa) | Mesh Size | Resultant Force Positi on_x | Resultant Force Positi on_y | Resultant Force Positi on_z |
| 2 | 30 | 24 | 0.9 | 0.2 | 5 | 25 | 25000 | 0.5 | 0.66 | 0.61 | 308.00 |

Figure E.1 Excel Workbook Data Entry Page

Sap2000 - Patrix 3D compare (Model 53 + Model 32) - Excel

Gokhan OZVURT

Sap2000 Joint Spring Assignment Results

| TABLE: Joint Coordinates | CoordSys | CoordType | XorR | Y | Z | Specialt | GlobalX | GlobalY | GlobalZ | GUID | Text | |
|--------------------------|----------|-----------|------|-----|---|----------|---------|---------|---------|---|------|-------|
| 1 | 2 | 3 | 4 | 5 | 6 | 7 | 8 | 9 | 10 | 11 | 12 | |
| 1 | GLOBAL | Cartesian | 0 | 0 | 0 | 0 No | 0 | 0 | 0 | 0 ee481105-a118-4ac2-b8ba-bc107d8f647b | 1 | 171.7 |
| 2 | GLOBAL | Cartesian | 0.5 | 0 | 0 | 0 No | 0.5 | 0 | 0 | 0 6cdf0e30-5e8e-423c-b553-1cd46fc8bd4f | 2 | 328.9 |
| 3 | GLOBAL | Cartesian | 0.5 | 0.5 | 0 | 0 No | 0.5 | 0.5 | 0 | 0 bc312bed-85c4-444e-a6fe-e56a0c100d46 | 3 | 582.3 |
| 4 | GLOBAL | Cartesian | 0 | 0.5 | 0 | 0 No | 0 | 0.5 | 0 | 0 4084db4f-dc4d-484b-b83b-4a502c405f17 | 4 | 305.6 |
| 5 | GLOBAL | Cartesian | 1 | 0 | 0 | 0 No | 1 | 0 | 0 | 0 184cb905-248e-4d98-8e64-7af34be224ee | 5 | 314.4 |
| 6 | GLOBAL | Cartesian | 1 | 0.5 | 0 | 0 No | 1 | 0.5 | 0 | 0 63dbdfc9-992e-a644-8a2e-afb191675ec | 6 | 553.3 |
| 7 | GLOBAL | Cartesian | 1.5 | 0 | 0 | 0 No | 1.5 | 0 | 0 | 0 1e289575-5f65-461a-873f-741656a815cc | 7 | 303.3 |
| 8 | GLOBAL | Cartesian | 1.5 | 0.5 | 0 | 0 No | 1.5 | 0.5 | 0 | 0 c317ec09-92ba-47fd-9e4e-82860b024f0 | 8 | 531 |
| 9 | GLOBAL | Cartesian | 2 | 0 | 0 | 0 No | 2 | 0 | 0 | 0 141104fa-be4e-4a92-a6b6-0d310f98814d | 9 | 302.7 |
| 10 | GLOBAL | Cartesian | 2 | 0.5 | 0 | 0 No | 2 | 0.5 | 0 | 0 eb335de4-2891-4c61-93b6-d55054d9b71a | 10 | 529.7 |
| 11 | GLOBAL | Cartesian | 2.5 | 0 | 0 | 0 No | 2.5 | 0 | 0 | 0 be7e7e72-8ccc-48d6-9011-6fc88e376a52 | 11 | 302.1 |
| 12 | GLOBAL | Cartesian | 2.5 | 0.5 | 0 | 0 No | 2.5 | 0.5 | 0 | 0 2f62a201-b957-459f-a35d-d8a1818cadd2 | 12 | 528.5 |
| 13 | GLOBAL | Cartesian | 3 | 0 | 0 | 0 No | 3 | 0 | 0 | 0 e6dd75da-084e-4252-93b1-be70be117ea5 | 13 | 301.5 |
| 14 | GLOBAL | Cartesian | 3 | 0.5 | 0 | 0 No | 3 | 0.5 | 0 | 0 ee442305-7fc5-4d23-9e50-9a74d06dbf6c3 | 14 | 527.4 |
| 15 | GLOBAL | Cartesian | 3.5 | 0 | 0 | 0 No | 3.5 | 0 | 0 | 0 931c9930-39db-47fd-9c18-62b4f9a6768c | 15 | 300.9 |
| 16 | GLOBAL | Cartesian | 3.5 | 0.5 | 0 | 0 No | 3.5 | 0.5 | 0 | 0 ba6fa57e-5c2c-444c-888f-a501618c9697 | 16 | 526.3 |
| 17 | GLOBAL | Cartesian | 4 | 0 | 0 | 0 No | 4 | 0 | 0 | 0 c3fcd794-bba8-4c0d-a7ae-ea1b9b1b80a8 | 17 | 300.4 |
| 18 | GLOBAL | Cartesian | 4 | 0.5 | 0 | 0 No | 4 | 0.5 | 0 | 0 25202f9e-52e0-4ea1-a29d-37c71fe6650e | 18 | 525.2 |
| 19 | GLOBAL | Cartesian | 4.5 | 0 | 0 | 0 No | 4.5 | 0 | 0 | 0 717644e6-0ca5-465a-8589-31780b0b39ca | 19 | 299.9 |
| 20 | GLOBAL | Cartesian | 4.5 | 0.5 | 0 | 0 No | 4.5 | 0.5 | 0 | 0 4ac85f0b-5adb-433a-b7cf-7418a263e289 | 20 | 524.2 |
| 21 | GLOBAL | Cartesian | 5 | 0 | 0 | 0 No | 5 | 0 | 0 | 0 f54e8515-0aa0-45bf-9b38-bfaee35e644e | 21 | 299.4 |
| 22 | GLOBAL | Cartesian | 5 | 0.5 | 0 | 0 No | 5 | 0.5 | 0 | 0 25656b86-d956-4592-9961-946cc-f9650d | 22 | 523.2 |
| 23 | GLOBAL | Cartesian | 5.5 | 0 | 0 | 0 No | 5.5 | 0 | 0 | 0 01e3433d-4444-4646-e1-7d0d2-4-4-382 | 23 | 300 |

Formül Çubuğu: =EGER(A13="",m,A13)

Figure E.2 SAP2000 Coordinate Data Entry and Spring Assignment Results

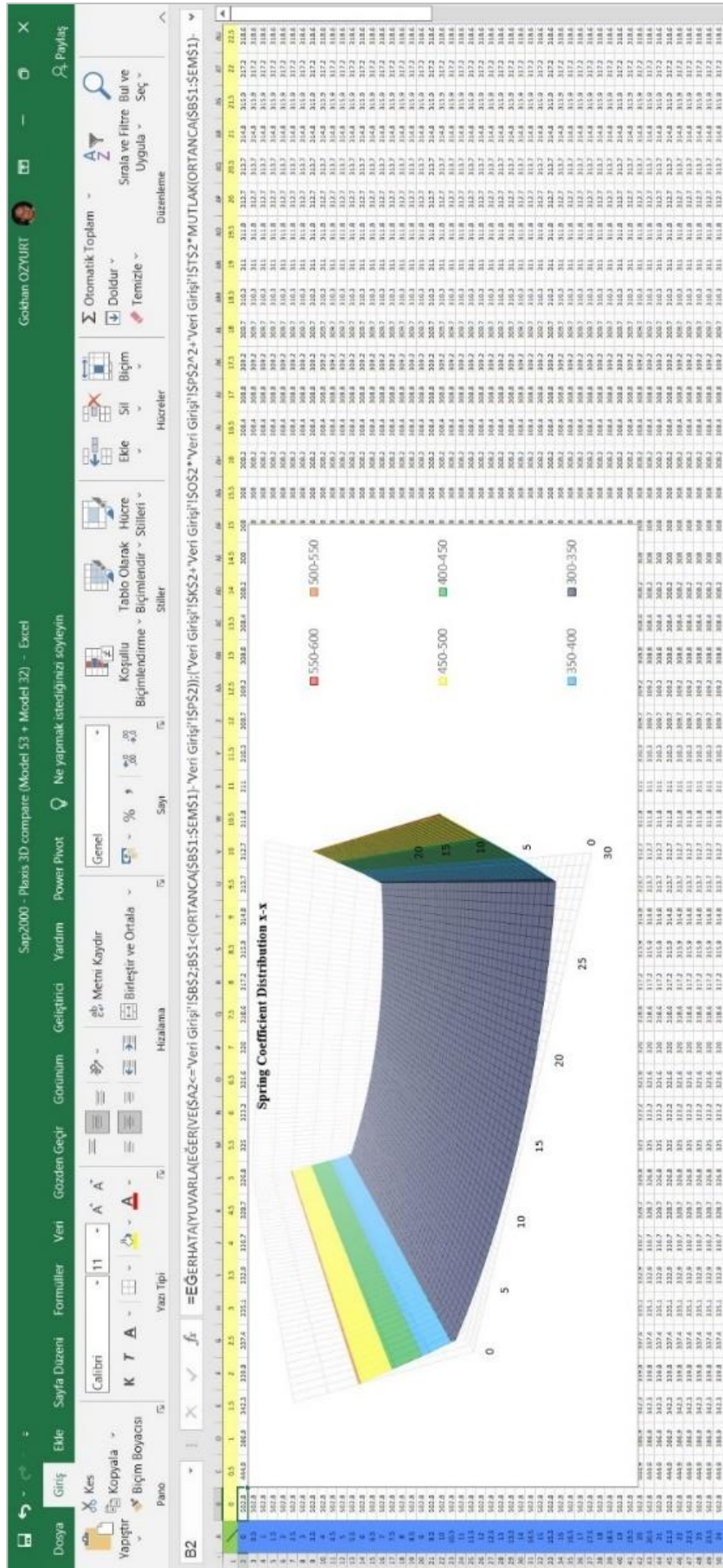


Figure E.3 View of Spring Coefficient Distribution in x-direction

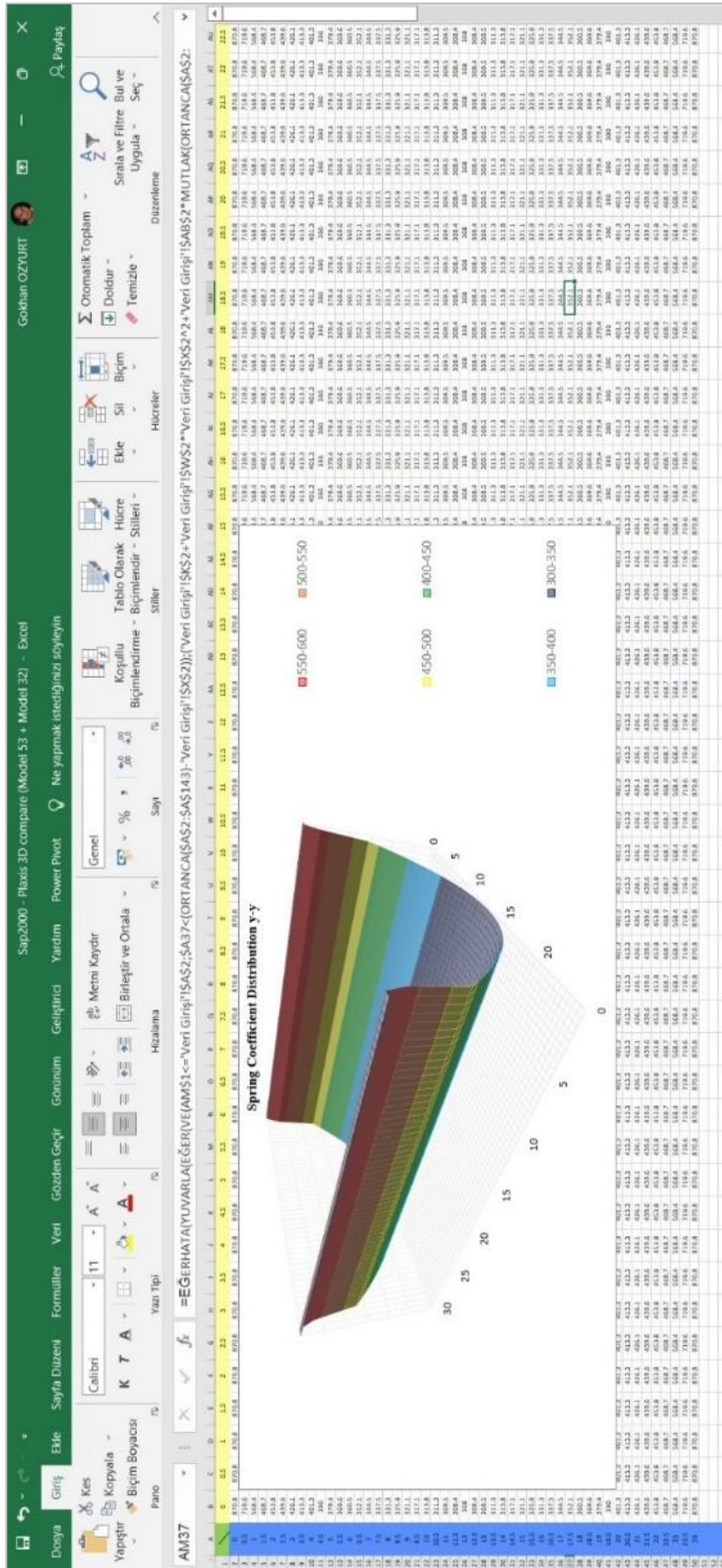


Figure E.4 View of Spring Coefficient Distribution in y-direction

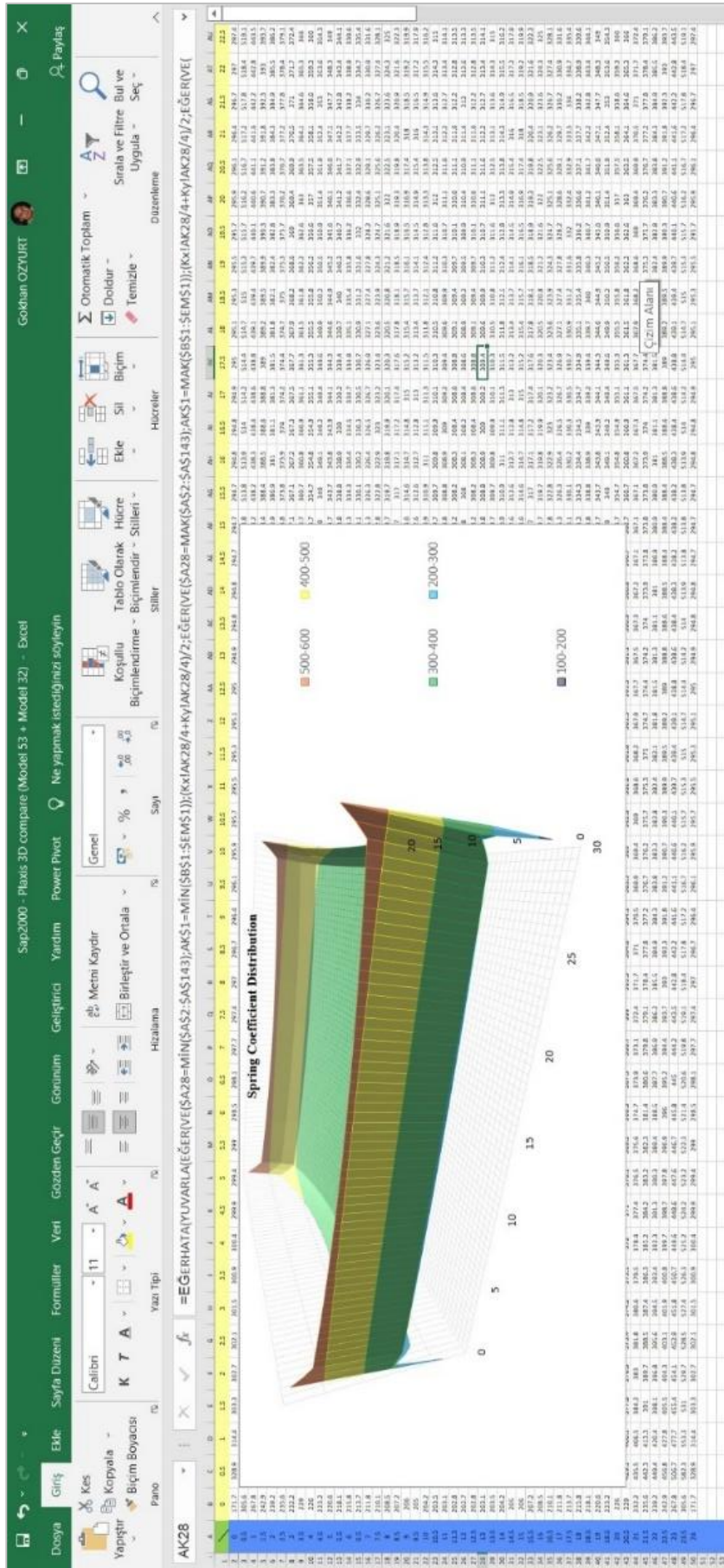


Figure E.5 View of Resultant Spring Coefficient Distribution in 3D

CURRICULUM VITAE

PERSONAL INFORMATION

Surname, Name: Özyurt, Gökhan

Nationality: Turkish (TC)

Date and Place of Birth:

Phone:

email:

EDUCATION

| Degree | Institution | Year of Graduation |
|---------------|-----------------------------|---------------------------|
| MS | METU Civil Engineering | 2012 |
| BS | METU Civil Engineering | 2008 |
| High School | Atatürk High School, Ankara | 2003 |

WORK EXPERIENCE

| Year | Place | Enrollment |
|--------------|--|-------------------------|
| 2010-Present | General Directorate of State Hydraulic Works | Field Control Engineer |
| 2008-2010 | Yüksel Domaniç Engineering Ltd. | Highway Design Engineer |

FOREIGN LANGUAGES

Advanced English

PUBLICATIONS

Thesis

1. Özyurt, G., and Toker, K. (2012). Cataloging and Statistical Evaluation of Common Mistakes in Geotechnical Investigation Reports for Buildings on Shallow Foundations, Master Thesis, METU

National Journal Publications

1. Özyurt, G., and Toker, K. (2013). Geoteknik etüt raporlarındaki yaygın hataların belirlenmesi ve istatistiksel değeriendirilmesi. Türkiye Mühendislik Haberleri, no.476, pp.28-35.